

A Comprehensive Analysis of Fermi Gamma-ray Burst Data: II. E_p -Evolution Patterns and Implications for the Observed Spectrum-Luminosity Relations

Rui-Jing Lu¹, Jun-Jie Wei¹, En-Wei Liang^{1,2,3}, Bin-Bin Zhang⁴, Hou-Jun Lü³, Lian-Zhong, Lü¹, Wei-Hua Lei^{5,3}, and Bing Zhang³

ABSTRACT

We present a time-resolved spectral analysis of 51 long and 11 short bright GRBs observed with the *Fermi*/GBM, paying special attention to E_p evolution within a same burst. Among 8 single-pulse long GRBs, 5 show hard-to-soft evolution, while 3 show intensity-tracking. The multi-pulse long GRBs have more complicated patterns. Statistically, the hard-to-soft evolution pulses tend to be more asymmetric than the intensity-tracking ones, with a steeper rising wing than the falling wing. Short GRBs have E_p tracking intensity exclusively with the 16ms time resolution analysis. We performed a simulation analysis, and suggest that at least for some bursts, the late intensity-tracking pulses could be a consequence of overlapping hard-to-soft pulses. However, the fact that the intensity-tracking pattern exists in the first pulse of multi-pulse long GRBs and some single-pulse GRBs suggest that intensity tracking is an independent component, which may operate in some late pulses as well. For the GRBs with measured redshifts, we present a time-resolved $E_p - L_{\gamma,iso}$ correlation analysis and show that the scatter of the correlation is comparable to that of the global Amati/Yonetoku relation. We discuss the predictions of various radiation models regarding E_p evolution, as well as the possibility of a precessing jet in GRBs. It seems that the data pose great challenge to all these models, and hold the key to unveil the physics of GRB prompt emission.

¹Department of Physics and GXU-NAOC Center for Astrophysics and Space Sciences, Guangxi University, Nanning 530004, China; lew@gxu.edu.cn

²The National Astronomical Observatories, Chinese Academy of Sciences, Beijing 100012, China

³Department of Physics and Astronomy, University of Nevada, Las Vegas, NV 89154; zhang@physics.unlv.edu

⁴Department of Astronomy and Astrophysics, Pennsylvania State University, University Park, PA 16802

⁵School of Physics, Huazhong University of Science and Technology, Wuhan, 430074, China

Subject headings: gamma-rays: bursts – methods: statistics – radiation: non-thermal

1. Introduction

The origin of prompt gamma-ray emission of cosmic gamma-ray bursts (GRBs), the most luminous events in the universe, is still a great puzzle since the discovery of this phenomenon. The GRB spectrum is usually well fit with a smoothly-joint broken power-law with the low- and high-energy photon spectral indices α and β , breaking at E_p in the νf_ν spectrum, the so-called Band function (Band et al. 1993). Broadband observations with the Large Area Telescope (LAT) and Gamma-Ray Burst Monitor (GBM) onboard the *Fermi* mission, which covers an energy band from 8 keV to hundreds of GeV (Atwood et al. 2009), reveal that the spectra of most GRBs are still well fit with the Band function up to the GeV energy band, and only a small fraction of GRBs are detected with LAT (Lü et al. 2010; Goldstein et al. 2012). In the first paper of this series (Zhang et al. 2011, Paper I), we have presented a comprehensive analysis of 17 LAT GRBs. By performing a time-resolved spectral analysis, we identified three elemental spectral components (Band component, thermal component, and power law component) that constitute GRB spectra. We found that except for some cases (e.g. GRB 090902B, GRB 090510, Abdo et al. 2009; Ryde et al. 2010; Ackermann et al. 2010), the Band function spectral component indeed dominates the GRB spectra in most LAT GRBs. In Paper I, we have also studied the evolution of spectral parameters in each burst.

The peak energy of the νf_ν spectrum (E_p) is one of the most interesting parameters of GRBs. It dramatically evolves with time. The physical radiation mechanism that defines E_p and its evolution is unclear (e.g., Zhang & Mészáros 2002, 2004). In general, the spectral properties carry the key to understand the physics of GRBs, such as energy dissipation mechanism, radiation mechanism, jet structure, as well as the properties of the central engine. Some observed energy/luminosity-spectrum relations involving E_p have been widely discussed in the literature. Amati et al. (2002) discovered a relation of the isotropic gamma-ray energy ($E_{\gamma,\text{iso}}$) to E_p in the burst frame. Ghirlanda et al. (2004) replaced $E_{\gamma,\text{iso}}$ with collimation corrected gamma-ray jet energy ($E_{\gamma,j}$), and claimed a tighter correlation between E_p and $E_{\gamma,j}$. Liang & Zhang (2005) introduced the optical temporal break time $t_{\text{b,opt}}$, and discovered a $E_p - E_{\gamma,\text{iso}} - t_{\text{b,opt}}$ “fundamental plane” correlation. These spectrum-energy correlations have been proposed to be plausible probes of cosmological parameters (e.g. Bloom et al. 2003; Schaefer 2003; Dai et al. 2004; Ghirlanda et al. 2004; Liang & Zhang

2005, 2006). Similarly, the isotropic peak luminosity ($L_{p,iso}$) is also found to be correlated with E_p in the burst frame among bursts (Wei & Gao 2003; Yonetoku et al. 2004), and within a same GRB (Liang et al. 2004). This $E_p - L_{\gamma,iso}$ relation is even tighter within a GRB pulse, especially during the decay phase (Lu & Liang 2010; Lu et al. 2010). The tight $E_p - L_{\gamma,iso}$ relation within a GRB and/or a pulse of GRB may be the origin of the global Amati/Yonetoku relation (Lu & Liang 2010; Lu et al. 2010; Ghirlanda et al. 2010; Firmani et al. 2009; Ohno et al. 2009), which suggests that the Amati/Yonetoku relation may not be caused by an observational selection effect (c.f., Nakar & Piran 2005; Band & Preece 2005; Shahmoradi & Nemiroff 2009). The evolution of E_p within a burst would then be a key to reveal the origin of these relations.

Two evolution patterns of E_p have been seen in GRBs, i.e., hard-to-soft evolution and intensity-tracking (Liang & Kargatis 1996; Ford et al. 1995; Kaneko et al. 2006; Lu et al. 2010; Peng et al. 2010). Two-thirds of the smooth GRB pulses in the BATSE sample have E_p showing a hard-to-soft evolution, while in the others a strong intensity-tracking was observed (Lu et al. 2010). In this paper, we focus on the spectral evolution patterns of multiple-pulse GRBs in a selected bright GBM GRB sample, and investigate the possible origins of E_p -evolution and the Amati/Yonetoku-relation. Our sample selection and data reduction are described in Section 2. The time-resolved spectral analysis results are shown in Section 3. In section 4, we present the detailed temporal evolutions in 51 long and 11 short GRBs. A simulation about overlapping hard-to-soft evolution pulses making an intensity-tracking pattern is also presented. In Section 5, we discuss a correlation between flux and E_p and its implications for the Amati/Yonetoku relation. We summarize our findings and discuss the physical implications of our finding in Section 6.

2. Sample Selection and Spectral Fits

GBM has 12 sodium iodide (NaI) detectors covering an energy range from 8 keV to 1 MeV, and two bismuth germanate (BGO) scintillation detectors sensitive to higher energies between 200 keV and 40 MeV (Meegan et al. 2009). The signals from all the 14 GBM detectors are collected by a central Data Processing Unit, which packages the resulting data into three different types: CTIME, CSPEC, and TTE. The TTE event data files contain individual photons with time and energy tags. We download data from the NASA *Fermi* web site¹, and use the TTE data to make spectral fits with the software package RMFIT (version 3.3pr7). User-defined intervals before and after the prompt emission phase are selected to

¹<ftp://legacy.gsfc.nasa.gov/fermi/data/>

obtain the background spectrum. The Band function is adopted for the spectral fits. We make an extensive time-resolved spectral analysis for the GBM GRBs as of 31 August 2011. We make joint fits to the spectra collected by the NaI and BGO detectors. The time slices are normally selected to assure a signal-to-noise ratio of 35. The reduced χ^2 of our fits are normally $\sim 0.9 - 1.1$. In order to present robust analyses for the spectral evolution, our sample includes only those GRBs that at least five time-resolved spectra are obtained from the data. These GRBs are bright, with a fluence in the GBM energy-band larger than 10^{-5} erg cm^{-2} for long bursts and 8×10^{-7} erg cm^{-2} for short bursts. We finally get a sample of 51 long GRBs and 11 short GRBs. We show a comparison of the fluence distribution of the GRBs in our sample with that of the first GBM catalog in Figure 1. It is clearly seen that our sample belongs to the brightest sub-sample of GBM GRBs.

3. Time-Resolved Spectral Results

Temporal evolution of E_p along with the lightcurve of each GRB² are shown in Figs. 2 and 3. We derive the bolometric energy flux (F) in the $1 - 10^4$ KeV band and the spectral parameters for each time slice. The $E_p - F$ plots for all the GRBs are also shown in Figs. 2 and 3. We show the E_p , α , and β distributions of our sample in comparison with those of the bright *CGRO*/BATSE GRBs (8459 time-resolved burst spectra of 350 GRBs; Kaneko et al. 2006) in Figure 4. It is found that the α distributions are well consistent with each other. The E_p of the Fermi/GBM GRBs tends to be lower than that of BATSE GRB sample. This may be due to an instrumental selection effect. At the low-energy end, the GRM energy band extends to 8 keV, being lower than the low end of the BATSE band. The trigger efficiency of X-ray flashes would be higher than BATSE, similar to HETE-2 (e.g., Liang & Dai 2004). The photon indices in the high energy band tends to be shallower than that observed with BATSE. Note that the BGO detector extends the efficient energy band up to 40 MeV. Therefore, the photon indices of the high-energy end may be better constrained.

4. Evolution of E_p in Long and Short GRBs

As shown in Figs. 2 and 3, E_p dramatically evolves with time. Two types of E_p evolution, hard-to-soft evolution and intensity-tracking, are observed, as reported previously by Liang & Kargatis (1996), Ford et al. (1995), Kaneko et al. (2006), Preece et al. (2000), Peng et al. (2010), and Lu et al. (2010) with the *CGRO*/BATSE data.

²The time-resolved spectral data are available in the electronic version only.

4.1. Long GRBs

Our analysis of 51 long GRBs are presented in Fig.2.

There are 8 single-pulse long GRBs. They clearly fall into two categories. The hard-to-soft evolution pattern appears in 5 GRBs: 081224, 090809B, 100612A, 100707A, and 110817A. The intensity tracking pattern appears in 3 GRBs: 081207, 090922A, and 100528A. Inspecting the lightcurves, a general trend is that the hard-to-soft pulses tend to be asymmetric, with the rising wing much steeper than the falling ring (except GRB 100612A), while the intensity-tracking pulses tend to be more symmetric (but see GRB 090922A).

The rest 43 long GRBs have multiple pulses. The E_p evolution patterns become more complicated. In a good fraction of GRBs, the first pulse shows a clear hard-to-soft evolution, while the rest pulses show the tracking behavior. On the other hand, a good fraction of GRBs have all pulses (including the first one) showing the intensity tracking behavior. In one case, i.e. GRB 090131 that shows at least 3 high-spike pulses, it is interesting to see that the *second* pulse shows a clear hard-to-soft evolution, even though the first pulse shows a nice tracking behavior. The general message from such a rough inspection is that mixed E_p evolution patterns can co-exist in a same burst, with a variety of combined patterns. We investigate Fig.2 in detail, and identified following groups:

- Intensity-tracking in all pulses (17/43 GRBs): 080825C, 080916C, 081009, 081222, 090323, 090424, 090804, 090820A, 090828, 090829, 090902B, 090926A, 091020, 091127, 100724B, 110123A, 110301A;
- Hard-to-soft evolution in the first pulse followed by intensity-tracking (11/43 GRBs): 080916A, 081215A, 081221, 090618, 090626, 090718B, 100728A, 100814A, 100906A, 101023A, 110721A;
- The evolution pattern of the first pulse is unclear, while late pulses show intensity-tracking (7/43 GRBs): 090328, 090524, 091003, 091120, 100116A, 100122A, 101014A;
- Clear hard-to-soft evolution throughout the burst (3/43 GRBs): 081125, 090719, 100701B;
- First pulse tracking, second pulse hard-to-soft evolution, third-pulse unclear (1/43 GRBs): 090131;
- First pulse hard-to-soft, second pulse also show hard-to-soft trend (1/43 GRBs): 090530B;
- Data quality not good enough to give clear conclusion (3/43 GRBs): 090516A, 101123A, 110731A.

To investigate whether all hard-to-soft evolution pulses tend to be more asymmetric than the intensity-tracking pulses, we selected 30 pulses (15 hard-to-soft pulses and 15 tracking pulses excluding the pulses from short GRBs) that have clearly identified either pattern, fit each pulse with the function (Kocevski et al. 2003)

$$F(t) = F_m \left(\frac{t + t_0}{t_m + t_0} \right)^r \left[\frac{d}{d+r} + \frac{r}{d+r} \left(\frac{t + t_0}{t_m + t_0} \right)^{(r+1)} \right]^{-\frac{r+d}{r+1}}, \quad (1)$$

and investigate the distribution of the parameter t_r/t_d , the ratio between the rising time scale and the falling time scale (Fig. 5). Indeed such a trend is revealed in the histogram, although some opposite examples also exist.

We have also searched for other possible differences between the GRB samples that have dominant hard-to-soft and intensity-tracking patterns. No statistically significant correlations are found. This may be due to the small sample effect, but it is possible that the two patterns are related to fundamental emission mechanisms that do not depend on the global properties of GRBs. Indeed the fact that both patterns co-exist in a same burst also suggests this.

4.2. Short GRBs

The E_p -evolution of 11 short GRBs in our sample are shown in Fig.3. Interestingly, clear intensity-tracking patterns are observed in all of them whose data quality is good enough. Notice that E_p does not always exactly track the intensity. The maximum E may lag behind or come before the peak of the corresponding pulse (e.g. GRBs 090227B, 090510, and 090228A). We'd like to caution that the time resolution of the light curves is 16 ms in this analysis. The light curves of short GRBs are usually highly variable in shorter time scales. The time bins of our spectral analysis are usually larger than variability time scales of short GRBs. On the other hand, Guiriec et al. (2010) presented a time-resolved spectral analysis for 3 bright short GRBs with a time scale as short as 2 ms. They showed that the E_p still tracks intensity, with significant fluctuation (see also Ghirlanda et al. 2011 for a sample of 13 short GRBs).

4.3. Superposition of adjacent hard-to-soft pulses as the origin of the intensity-tracking?

Since most late time pulses have intensity-tracking, a natural question is whether they can be due to the superposition of hard-to-soft evolution pulses. Hakkila & Preece (2011) argued that all correlated pulse characteristics can be explained by the hard-to-soft E_p evolution, and the intensity-tracking is merely the result of superposition of two or more hard-to-soft pulses. In order to test such an effect, we perform a simulation analysis with the RMFIT package. We take GRBs 081224 and 100707A, both having a single pulse with hard-to-soft evolution, as a template to perform the simulations. The simulation procedure is as follows.

- Extract the TTE data of the brightest NaI and BGO detectors of the GRB (GRB 081224 or GRB 100707A), and shift the arrival time of each photon with a delay timescale of 10 s, 5 s, and 3 s (case A, B, and C, respectively).
- Co-add the original TTE data with the TTE data of Case A, B, and C, respectively.
- Make time-resolved spectral analysis for the co-added TTE data, and report E_p evolution of the mock light curves.

Our results are shown in Figure 6. We take the simulation using GRB 081224 as an example. In case A, since the separation between the two pulses is wide, the E_p evolution of each pulse is not significantly contaminated in the mock GRB, although in the bridge region, the E_p evolution becomes less significant. In case B, the superposition effect becomes more significant around 4.5 ~ 6 second. In case C, the E_p evolution behavior of the second pulse now turns into intensity tracking, due to the close superposition of the two pulses. The simulation using GRB 100707A reached the similar conclusion. From these simulation, one can tentative draw the conclusion that superposing two hard-to-soft evolution patterns could indeed generate an intensity-tracking pattern under certain conditions. Whether or not this is possible depends on the competition between the flux contrast near the transition regions in the overlapping pulses. If the transition has a sharp dip (corresponding to the wide-separation case), then the hard-to-soft evolution pattern is hardly altered. However, if the transition is smooth with a shallow dip, the tracking behavior is more obvious. Some GRBs with complicated lightcurves show fluctuating E_p features. This may be also a consequence of superposition. This effect also potentially explains the irregular spectral variation in some GRBs with highly variable light curves, such as in GRBs 101123A and 110731A.

To examine the superposition effect on the spectral shape, we illustrate a mock spectrum of Case C of GRB 081224 in the time interval [2.473, 3.911] seconds in Figure 7, which

corresponds to the onset time of the second pulse of the mock GRB. The spectrum is roughly the overlapped spectra of GRB 081224 in the time intervals $[-0.51, 1.002]$ seconds and $[2.473, 3.911]$ seconds. It is found that the superposition significantly modifies the spectra in the two time intervals. However, it is still well fit with the Band function. In the low energy end, the spectrum is dominated by the low- E_p component, while it is dominated in the high- E_p component in the high energy end. The E_p of the superimposed spectrum is similar to that of the high- E_p component³.

We do not claim that all the intensity-tracking pulses after the first pulse are due to superposition of hard-to-soft pulses. This is because some single pulse bursts, and the first pulse of about half of the GRBs in our sample (for which superposition effect does not exist) indeed show the intensity-tracking behavior. As shown in Figure 6, the E_p evolution pattern can be changed to tracking from hard-to-soft evolution only when the two pulses are highly overlapped. As a result, if one sees intensity tracking from a pulse that is well separated from the proceeding one, it is very likely intrinsic and is not due to the superposition effect.

5. Time-resolved E_p - F Correlation and Implications for the Amati/Yonetoku Relation

With the time-resolved spectral analysis results, we also show the $E_p - F$ relation for the bursts in our sample in Figures 2 and 3 for the long and short GRBs. For each GRB, we fit the $E_p - F$ correlation with a simple power-law function, $E_p \propto F^\kappa$, for all the time bins, and record the correlation index κ . For comparison, we take the time bins during the decaying wing of each pulse, and perform the same fits, and derive the corresponding index κ_d . In Figure 8, we show the distributions of κ and κ_d for both long and short GRBs, and found that they are consistent with each other, with a mode at 0.55 ± 0.22 for both long and short GRBs. We measure the scatter of the $E_p - F$ relation with the distance of the data points from the best fit line as done by Ghirlanda et al. (2005). As shown in Fig. 8, the scatter of the $E_p - F$ relation in the decay phase is much tighter than that for the entire GRBs, with a dex of 0.070 ± 0.049 comparing to 0.17 ± 0.08 for GRB. The large dispersion of the $E_p - F$ relation in the entire GRB would be due to the variation of κ_d in different pulses, and the rising wing of the pulses during which hard-to-soft spectral evolution may happen. As shown in Lu et al. (2010), the data points of the rising wing of a hard-to-soft

³Note that the composed νf_ν spectrum may show a plateau or a two-hump feature if E_p of the two spectral components are well separated and have comparable energy fluxes. The spectrum may not strictly be a single Band function. This may cause confusion in identifying different emission components in an observed spectrum.

pulse usually deviate from the $E_p - F$ relation observed in the decaying wing. Although the $E_p - F$ relation each pulse is tight, the slope varies among pulses. The mix of different pulses would then enlarge the dispersion of the $E_p - F$ correlation in a burst.

Fifteen GRBs in our sample have redshift measurements. Among them 14 GRBs are long and 1 is short (GRB 090510). We calculate time-resolved isotropic luminosity of these GRBs and correct E_p to the burst rest frame. We show the $E_p^{\text{rest}} - L_{\gamma,\text{iso}}$ correlation of these 15 GRBs in Fig. 9. Also plotted are the GRBs reported by Yonetoku et al. (2010), who reported a correlation between time integrated E_p^{rest} and the peak isotropic luminosity of individual bursts. It is found that the $E_p^{\text{rest}} - L_{\gamma,\text{iso}}$ relation for the time-resolved spectra within a GRB (our sample) is consistent with that for the time-integrated spectra among the GRBs (Yonetoku sample). Our best linear fit to the time-resolved $E_p^{\text{rest}} - L_{\gamma,\text{iso}}$ relation is $\log E_p = -(29.854 \pm 0.178) + (0.621 \pm 0.003) \log L_{\gamma,\text{iso}}$ with a linear coefficient of $r=0.88$ ($N=251$) and chance probability of $p < 10^{-4}$. We measure the scatter of the data points around the best fit and obtain $\text{dex}=0.256$, which is roughly consistent with the intrinsic scatter ($\sigma_{\text{int}}=0.195$) of the time integrated $E_p - L_{\gamma,\text{iso}}$ relation among different GRBs (see also Ghirlanda et al. 2005). Note that the time-resolved $E_p - L_{\gamma,\text{iso}}$ relation of the short GRB 090510 is also consistent with that of the long GRBs, although its E_p is significantly larger than most long GRBs in our sample (see also Ghirlanda et al. 2011). Zhang et al. (2009a) showed that short GRBs do not follow the $E_{\gamma,\text{iso}} - E_p$ relation (the Amati relation) of long GRBs, mostly due to their smaller $E_{\gamma,\text{iso}}$ (by 2 to 3 orders of magnitude). They showed that in terms of $E_p - L_{\gamma,\text{iso}}$ relation, long and short GRBs are similar (see also Ghirlanda et al. 2010 and Zhang et al. 2012). Therefore, despite of different energy reservoirs in long and short GRBs, their radiation physics of both long and short GRBs may be the same (Lü et al. 2010; Ghirlanda et al. 2011).

6. Conclusions and Discussion

We have carried out a detailed time-resolved spectral analysis for a bright sample of Fermi GBM bursts. By studying the E_p evolution within individual GRBs, we confirm the existence of two evolution patterns within certain pulses: a hard-to-soft evolution pattern and an intensity-tracking pattern. Among the 8 single-pulse long GRBs, 5 show hard-to-soft evolution, while the other 3 show intensity-tracking. For multi-pulse long GRBs, the patterns are more complex. For the first pulse, the split between the two patterns is roughly half-half. However, for later pulses the intensity-tracking pattern becomes predominant. Through simulations, we show that some of the late intensity-tracking pulses could be due to the close superposition of pulses with hard-to-soft evolution. However, this cannot account for all the

late pulses, especially those without a preceding overlapping pulse but also show the tracking behavior. Conversely, in two bursts, the hard-to-soft evolution pattern is observed in the second pulse of the burst, when the pulse is well separated from the first pulse. *So overall, it is clear that both patterns are intrinsic, and they can coexist in a same GRB in different pulses.*

The situation of short GRBs is simpler. They are overwhelmingly dominated by the intensity-tracking pattern. One caveat is that the time resolution (16 ms) may not be fine enough to catch the possible hard-to-soft evolution pattern in short GRBs. In any case, an independent study with 2 ms time resolution still did not show evidence of hard-to-soft evolution (Guiriec et al. 2010). So the tracking behavior may be an intrinsic property of short GRBs.

We have presented the correlation between E_p and F within single-pulse and multi-pulse GRBs. This correlation is tighter in the decay phase of the GRBs, suggesting that the decaying phase correlation may be the main source of the global internal $F - E_p$ correlation reported by Liang et al. (2004) (see also Firmani et al. 2009). Fifteen GRBs (14 long GRBs and 1 short GRBs) in our sample have redshift measurements. We shown that the both the slope and the dispersion of the $E_p - L_{\gamma, \text{iso}}$ relation for the time-resolved spectra of these GRBs are well consistent with the global Yonetoku relation derived from the pre-Fermi GRBs.

Our results suggest that the E_p evolution may hold the key to understand the GRB radiation physics, and the origin of various observed spectrum-energy relations (e.g. Amati et al. 2002; Yonetoku et al. 2004; Liang & Dai 2004; Ghirlanda et al. 2004; Liang & Zhang 2005). Any successful physical model of GRB prompt emission has to able to produce two different E_p -evolution patterns. These two patterns not only operate in different bursts, but could also operate within the same burst as well. This is challenging. In the following, we discuss radiation models and geometric models in turn.

6.1. Radiation physics as source of E_p evolution

The prompt emission of GRBs is still a mystery (e.g. Zhang 2011 for a recent review). The main uncertainty is the composition of the outflow (fireball vs. Poynting-flux dominated flow), which determine the energy dissipation mechanism (internal shocks vs. magnetic reconnection), particle acceleration mechanism (1st- or 2nd-order Fermi acceleration), and radiation mechanism (synchrotron vs. inverse Compton scattering). Three emission models are widely discussed: (1) the internal shock synchrotron model; (2) the dissipative photo-

sphere model; and (3) the abrupt magnetic dissipation model. These different models have different predictions regarding E_p evolution within a burst. The data can be then used to constrain these models.

In all the models, E_p is a function of outflow luminosity (which is usually represented by the gamma-ray luminosity $L_{\gamma,\text{iso}}$) and the Lorentz factor Γ . Different models have different dependences on these models (e.g. Zhang & Mészáros 2002; Pe’er et al. 2006). One common feature for all the models is that when emission stops abruptly, the observed emission is the high-latitude emission from the jet due to the curvature of the conical jet (e.g. Fenimore et al. 1996; Kumar & Panaitescu 2000; Dermer 2004; Liang & Zhang 2006; Qin et al. 2008; Zhang et al. 2009b). During this curvature-effect dominated phase, an intensity tracking behavior is expected. Observationally, both hard-to-soft evolution and intensity-tracking show decreasing E_p with decaying flux. This is generally consistent with this “curvature effect” explanation⁴. More specifically, during the decay phase, one has the typical frequency $E_p = DE'_p/(1+z)$, the specific luminosity $L_\nu = D^2L'_{\nu'}$, and the bolometric luminosity $L_{\text{iso}} = D^\varepsilon L'_{\text{iso}}$, where D is the Doppler factor, the prime values are measured in the co-moving frame, and the value of ε takes 3 for a continuous jet and 4 for an impulsive blob (Ghisellini et al. 1993). We have $E_p \propto L_{\text{iso}}^{1/\varepsilon}(1+z)f(E'_p, L'_{\text{iso}})$, where $f(E'_p, L') = E'_p/L_{\text{iso}}^{1/\varepsilon}$. One then expects $E_p \propto L_\nu^{1/2}$ and $E_p \propto L_{\text{iso}}^{1/\varepsilon}$ regardless of the intrinsic relation between the E'_p and $L'_{\gamma,\text{iso}}$. Since what one measures is neither exactly L_ν (since there is a wide band) nor $L_{\gamma,\text{iso}}$ (since the band width is limited), the expected $E_p - F$ relation slope would be roughly between 1/2 and 1/3 (1/4). This is roughly consistent with the data, although 1/4 would be too shallow.

The E_p evolution during the rising phase of a pulse carries the key information to diagnose different prompt emission models. For the standard synchrotron model (valid for internal shocks and internal magnetic dissipation models), one can write down $E_p \propto \gamma_e^2 L^{1/2} R^{-1} (1+z)^{-1}$, where L is the “wind” luminosity of the ejecta, γ_e is the typical electron Lorentz factor in the emission region, and R is the emission radius (Zhang & Mészáros 2002). Naively, this would give a tracking behavior, since $E_p \propto L^{1/2}$. However, considering other factors, the dependence is non-trivial. For internal shocks (e.g. Mészáros et al. 1994; Daigne & Mochkovitch 1998; Daigne et al. 2011), the rising phase is related to crossing of a shock across the colliding shells. The observed light curve can rise even if the wind luminosity

⁴If the instantaneous spectrum at the end of pulse emission is a single power law, then no spectral evolution is expected. On the other hand, if the instantaneous spectrum is curved, the curvature effect naturally gives rise to a spectral evolution. Strong spectral evolution during the steep decay phase of early X-ray afterglow of Swift GRBs has been commonly observed (Zhang et al. 2007). This can be still interpreted within the curvature effect model by assuming a curved instantaneous spectrum at the end of prompt emission (Zhang et al. 2009b).

is constant. The flux is related to the evolution of the strength of the shock during shock crossing (and hence, γ_e), and the number of electrons that are shocked. In general, since shock strength increases as shock propagates, and the number of electrons tend to increase, a rough tracking behavior is expected for the internal shock model, even though detailed modeling is needed to give more precise predictions. On the other hand, the internal shock model has several issues to interpret the available data (see a full discussion in Zhang & Yan 2011), including its inability to account for the Amati/Yonetoku relation in view of the recent finding of $\Gamma - E_{\gamma,iso}$ (Liang et al. 2010) and $\Gamma - L_{\gamma,iso}$ (Lü et al. 2012) correlations.

Zhang & Yan (2011) proposed a GRB prompt emission model invoking a sudden discharge of magnetic energy through turbulent magnetic reconnection triggered by multiple internal collisions among magnetically dominated shells. This ICMART model also attributes GRB prompt emission to synchrotron emission of electrons. However, an extra dependence of γ_e on the magnetization factor σ is invoked. Since during an ICMART event σ is expected to drop with time, the dissipated magnetic energy is expected to be shared by more and more electrons, so that γ_e drops with time as electron number increases with time. As a result, a hard-to-soft evolution during the pulse rising phase is expected, although detailed numerical calculations are needed to validate this prediction.

Finally, the dissipative photosphere model (Rees & Mészáros 2005; Pe’er et al. 2006; Giannios 2008; Beloborodov 2009; Lazzati & Begelman 2009 Ioka 2010; Toma et al. 2011; Ryde et al. 2011) attributes E_p to the temperature of the photosphere. Naively, a quasi-thermal nature of emission generally calls for an intensity-tracking behavior, since a hot temperature tends to be brighter. On the other hand, the temporal evolution of the Lorentz factor, optical depth, and the radius of photosphere may complicate the picture, and detailed modeling is called for (e.g. W. Deng, & B. Zhang, 2012, in preparation).

In general, radiation models can account for both hard-to-soft evolution (ICMART model) and intensity-tracking (internal shocks and probably photosphere), although detailed theoretical modeling in all these cases are desirable. The difficulty for all these models is that both evolutionary trends coexist in different pulses of a same burst. One therefore has to invoke multiple models to interpret different pulses in a same burst. This may happen if the composition of a jet varies with time in a same burst, i.e. the magnetization parameter σ can switch from > 1 to < 1 within a same burst. This is not impossible (Zhang 2011), since given the same magnetic field strength at the central engine, a variation in baryon loading can cause a large fluctuation of the σ value.

6.2. Geometric effect as source of E_p evolution

It was proposed that the broad pulses with a dramatical E_p evolution in GRBs may be due to the precession of GRB jets (Portegies Zwart et al. 1999; Reynoso et al. 2006; Lei et al. 2007; Liu et al. 2010). Fixing the observer’s viewing angle, the precession would result in the jet sweeping in and out the observer’s line of sight. This would result in a rapid evolution of the Doppler factor. Assuming that the rest-frame emission properties remain the same during precession, the observer would record a rapid flux variability and spectral evolution. Since both E_p and luminosity are positively related to the Doppler factor, this model could explain the intensity-tracking behavior of the pulses. Since there is no preference of the precession direction, the pulse tend to be symmetric (Liu et al. 2010).

How can a GRB jet precess? This is a great issue. The progenitors of GRBs are massive stars or compact star binaries. In both scenarios, the new-born central engine object (a black hole or a rapidly rotating, highly magnetized pulsar) is expected to spin rapidly (van Putten 2004). The anisotropic mass fall-back in a collapsar, or the mis-alignment of angular momenta of two merged compact objects may lead to a tilted disc. The fragmentation of the star (King et al. 2005) or disk (Perna et al. 2006) may also lead to a misaligned disc. The Lense-Thirring precession appears for such a Kerr BH with a tilted disc (Lense & Thirring 1918). Current favored jet launching models for GRBs include neutrino-annihilation mechanism (Popham et al. 1999) and Blandford-Znajek process (Blandford & Znajek 1977). For both models, the jet is expected to be perpendicular to the midplane of the disc, so that the precession of the disc would result in precession of the jet (Lei et al. 2007; Liu et al. 2010). It is found that the overall shape and temporal evolution of the GRB light curves can be fit with jet precession if the jet is narrow enough (Lei et al. 2007; Liu et al. 2010). Clear periodic signals are not expected due to the stochastic nature of the process (Liu et al. 2010). One issue is that for long GRBs, the existence of a massive stellar envelope tends to stall and quench a precessing jet, especially when the precession angle is larger than the jet opening angle (Zhang et al. 2004). That simulation did not include magnetic fields, which would enhance collimation of the precessing jet. Further MHD simulations are needed to test whether large-angle precession is allowed for a magnetically dominated jet propagating in a stellar envelope.

The main difficulty of the precession scenario is again the coexistence of both hard-to-soft and intensity-tracking behaviors in a same burst. It is hard to interpret an asymmetric pulse with clear hard-to-soft evolution during the rising wing within the jet precession model. Other issues include the detailed energy dissipation, particle acceleration, and emission processes of a precession jet. When these details are considered, the simple assumption of a constant co-moving emissivity has to be replaced by the more detailed calculation of time-

dependent co-moving spectra. The radiation physics as discussed above (§6.1) has to be considered, which would introduce extra complications. How the precession hypothesis fares with the successful afterglow theory and confronts with the afterglow data is also subject to further intense modeling.

This work is supported by NSFC (Grants No. 11025313, 10873002, 11063001, 11163001, and 10847003), the “973” Program of China (2009CB824800), Special Foundation for Distinguished Expert Program of Guangxi, the Guangxi SHI-BAI-QIAN project (Grant 2007201), the Guangxi Natural Science Foundation (2010GXNSFA013112 and 2010GXNSFC013011, Contract No. 2011-135), and the 3th Innovation Project of Guangxi University. BZ acknowledges support from NASA (NNX10AD48G) and NSF (AST-0908362).

REFERENCES

- Abdo, A. A., Ackermann, M., Ajello, M., et al. 2009, *ApJ*, 706, L138
- Ackermann, M., Asano, K., Atwood, W. B., et al. 2010, *ApJ*, 716, 1178
- Amati, L., Frontera, F., Tavani, M., et al. 2002, *A&A*, 390, 81
- Atwood, W. B., Abdo, A. A., Ackermann, M., et al. 2009, *ApJ*, 697, 1071
- Band, D., Matteson, J., Ford, L. et al. 1993, *ApJ*, 413, 281
- Band, D. L., & Preece, R. D. 2005, *ApJ*, 627, 319
- Beloborodov, A. M. 2009, *ApJ*, 703, 1044
- Blandford, R. D., & Znajek, R. L. 1977, *MNRAS*, 179, 433
- Bloom, J. S., Frail, D. A., & Kulkarni, S. R. 2003, *ApJ*, 594, 674
- Dai, Z. G., Liang, E. W., & Xu, D. 2004, *ApJ*, 612, L101
- Daigne, F., Bošnjak, Ž., & Dubus, G. 2011, *A&A*, 526, A110
- Daigne, F., & Mochkovitch, R. 1998, *MNRAS*, 296, 275
- Dermer, C. D. 2004, *ApJ*, 614, 284
- Firmani, C., Cabrera, J. I., Avila-Reese, V., et al. 2009, *MNRAS*, 393, 1209

- Fenimore, E. E., Madras, C. D., Nayakshin, S. 1996, *ApJ*, 473, 998
- Ford, L. A., Band, D. L., Matteson, J. L., et al. 1995, *ApJ*, 439, 307
- Ghirlanda, G., Ghisellini, G., Firmani, C., Celotti, A., & Bosnjak, Z. 2005, *MNRAS*, 360, L45
- Ghirlanda, G., Ghisellini, G., Nava, L., & Burlon, D. 2011, *MNRAS*, 410, L47
- Ghirlanda, G., Nava, L., & Ghisellini, G. 2010, *A&A*, 511, A43
- Ghirlanda, G., Ghisellini, G., & Lazzati, D. 2004, *ApJ*, 616, 331
- Ghisellini, G., Padovani, P., Celotti, A., & Maraschi, L. 1993, *ApJ*, 407, 65
- Goldstein, A., Burgess, J. M., Preece, R. D., & Fermi/GBM Science Team 2012, *American Astronomical Society Meeting Abstracts*, 219, #149.09
- Guiriec, S., Briggs, M. S., Connaughton, V., et al. 2010, *ApJ*, 725, 225
- Giannios, D. 2008, *A&A*, 480, 305
- Hakkila, J., & Preece, R. D. 2011, *ApJ*, 740, 104
- Ioka, K. 2010, *Progress of Theoretical Physics*, 124, 667
- Kaneko, Y., Preece, R. D., Briggs, M. S., et al. 2006, *ApJS*, 166, 298
- Kocevski, D., Ryde, F., & Liang, E. 2003, *ApJ*, 596, 389
- Kumar, P., & Panaitescu, A. 2000, *ApJ*, 541, L51
- King, A. R., Lubow, S. H., Ogilvie, G. I., & Pringle, J. E. 2005, *MNRAS*, 363, 49
- Lazzati, D., & Begelman, M. C. 2009, *ApJ*, 700, L141
- Lei, W. H., Wang, D. X., Gong, B. P., & Huang, C. Y. 2007, *A&A*, 468, 563
- Lense, J., & Thirring, H. 1918, *Phys. Z.*, 19, 156
- Liang, E. W., & Dai, Z. G. 2004, *ApJ*, 608, L9
- Liang, E. W., Dai, Z. G., & Wu, X. F. 2004, *ApJ*, 606, L29
- Liang, E., & Kargatis, V. 1996, *Nature*, 381, 49
- Liang, E.-W., Yi, S.-X., Zhang, J., et al. 2010, *ApJ*, 725, 2209

- Liang, E.-W., & Zhang, B. 2006, MNRAS, 369, L37
- Liang, E.-W., & Zhang, B. 2005, ApJ, 633, 611
- Liu, T., Liang, E.-W., Gu, W.-M., et al. 2010, A&A, 516, 16
- Lu, R.-J., Hou, S.-J., & Liang, E.-W. 2010, ApJ, 720, 1146
- Lu, R.-J., & Liang, E.-W. 2010, Science in China G: Physics and Astronomy, 53, 163
- Lü, H.-J., Liang, E.-W., & Tong, X. 2010, Science in China G: Physics and Astronomy, 53, 73
- Lü, J., Zou, Y.-C., Lei, W.-H., et al. 2012, ApJin press. arXiv:1109.3757
- Meegan, C., Lichti, G., Bhat, P. N., et al. 2009, ApJ, 702, 791
- Mészáros, P., Rees, M. J., & Papathanassiou, H. 1994, ApJ, 432, 181
- Nakar, E., & Piran, T. 2005, MNRAS, 360, L73
- Ohno, M., Ioka, K., Yamaoka, K., et al. 2009, PASJ, 61, 201
- Peng, Z. Y., Yin, Y., Bi, X. W., et al. 2010, ApJ, 718, 894
- Pe’er, A., Mészáros, P., Rees, M. J. 2006, ApJ, 652, 482
- Popham, R., Woosley, S. E., & Fryer, C. 1999, ApJ, 518, 356
- Portegies Zwart, S. F., Lee, C.-H., & Lee, H. K. 1999, ApJ, 520, 666
- Perna, R., Bozzo, E., & Stella, L. 2006, ApJ, 639, 363
- Preece, R. D., Briggs, M. S., Malozzi, R. S., et al. 2000, ApJS, 126, 19
- Qin, Y.-P. 2008, ApJ, 683, 900
- Reynoso, M. M., Romero, G. E., & Sampayo, O. A. 2006, A&A, 454, 11
- Rees, M. J., & Mészáros, P. 2005, ApJ, 628, 847
- Ryde, F., Axelsson, M., Zhang, B. B., et al. 2010, ApJ, 709, L172
- Ryde, F., Pe’Er, A., Nymark, T., et al. 2011, MNRAS, 415, 3693
- Schaefer, B. E. 2003, ApJ, 583, L67

- Shahmoradi, A., & Nemiroff, R. 2009, American Institute of Physics Conference Series, 1133, 425
- Toma, K., Wu, X.-F., & Mészáros, P. 2011, MNRAS, 415, 1663
- van Putten, M. H. P. M. 2004, ApJ, 611, L81
- Wei, D. M., & Gao, W. H. 2003, MNRAS, 345, 743
- Yonetoku, D., Murakami, T., Nakamura, T., et al. 2004, ApJ, 609, 935
- Yonetoku, D., Murakami, T., Tsutsui, R., et al. 2010, PASJ, 62, 1495
- Zhang, B. 2011, Comptes Rendus Physique, 12, 206
- Zhang, B., & Mészáros, P. 2004, International Journal of Modern Physics A, 19, 2385
- Zhang, B., & Mészáros, P. 2002, ApJ, 581, 1236
- Zhang, B., & Yan, H. 2011, ApJ, 726, 90
- Zhang, B., Zhang, B.-B., Virgili, F. J., et al. 2009a, ApJ, 703, 1696
- Zhang, B.-B., Zhang, B., Liang, E.-W., et al. 2011, ApJ, 730, 141 (Paper I)
- Zhang, B.-B., Liang, E.-W., & Zhang, B. 2007, ApJ, 666, 1002
- Zhang, B.-B., Zhang, B., Liang, E.-W., & Wang, X.-Y. 2009b, ApJ, 690, L10
- Zhang, F.-W., Shao, L., Lan, J.-Z., Wei, D. M. 2012, ApJ, 750, 88
- Zhang, W., Woosley, S. E., Heger, A. 2004, ApJ, 608, 365

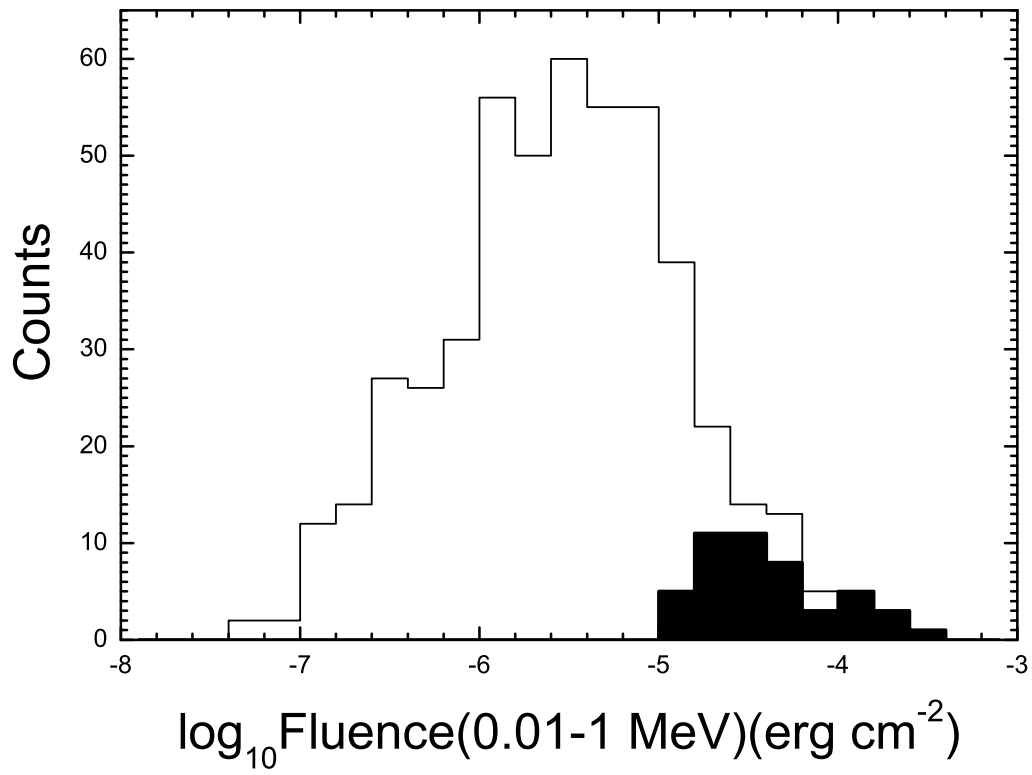


Fig. 1.— Gamma-ray fluence distribution of the GRBs in our sample (solid histogram) in comparison with that of the first 2-year GBM Catalog (open histogram, William et al. 2012).

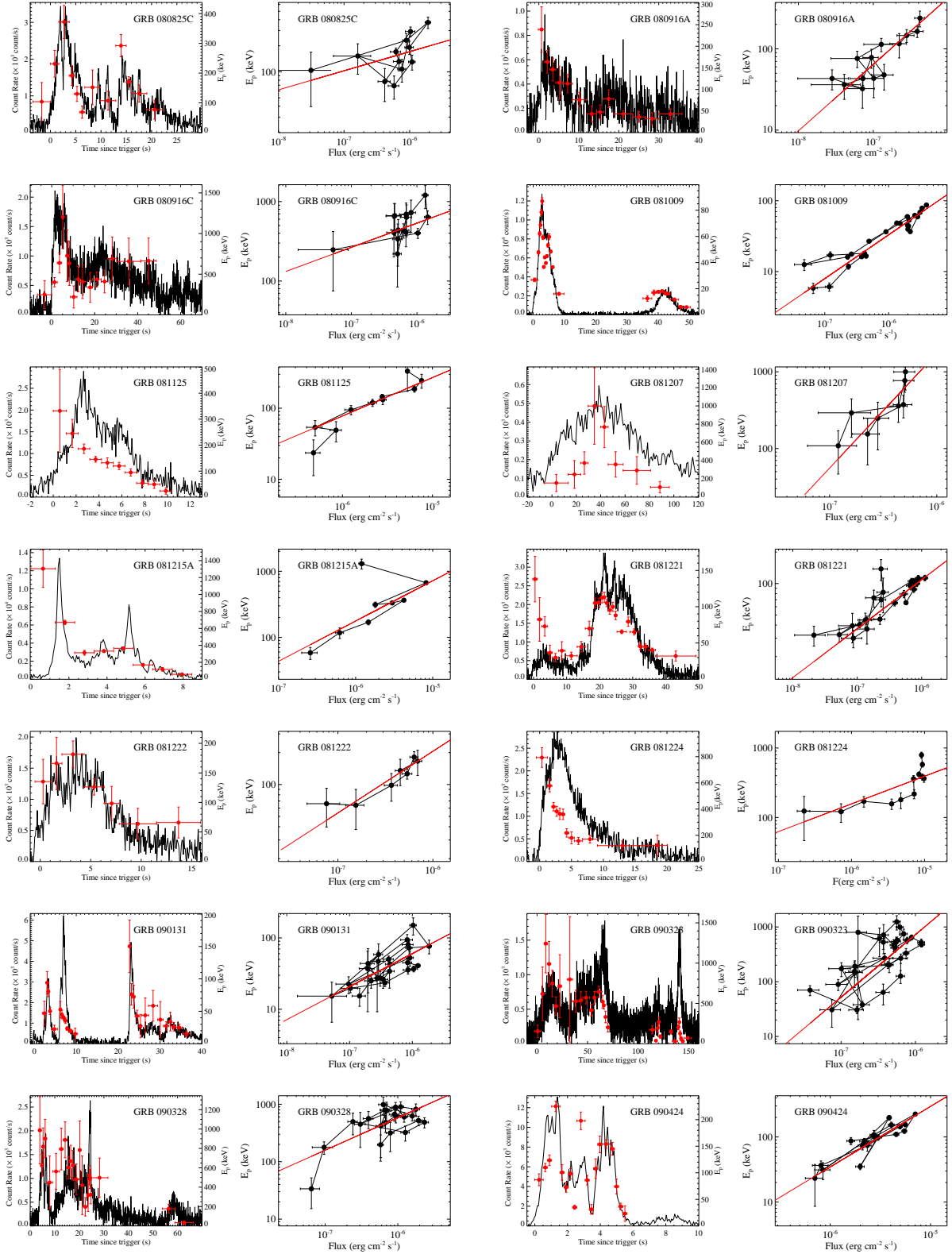


Fig. 2.— *Left:* Light curves (connected lines) along with E_p evolution (circles with error bars) of long GRBs in our sample; *Right:* Time-resolved E_p as a function of flux, along with the best fit line for the $E_p - F$ correlation for the long GRBs in our sample.

Fig. 2.— *-continued.*

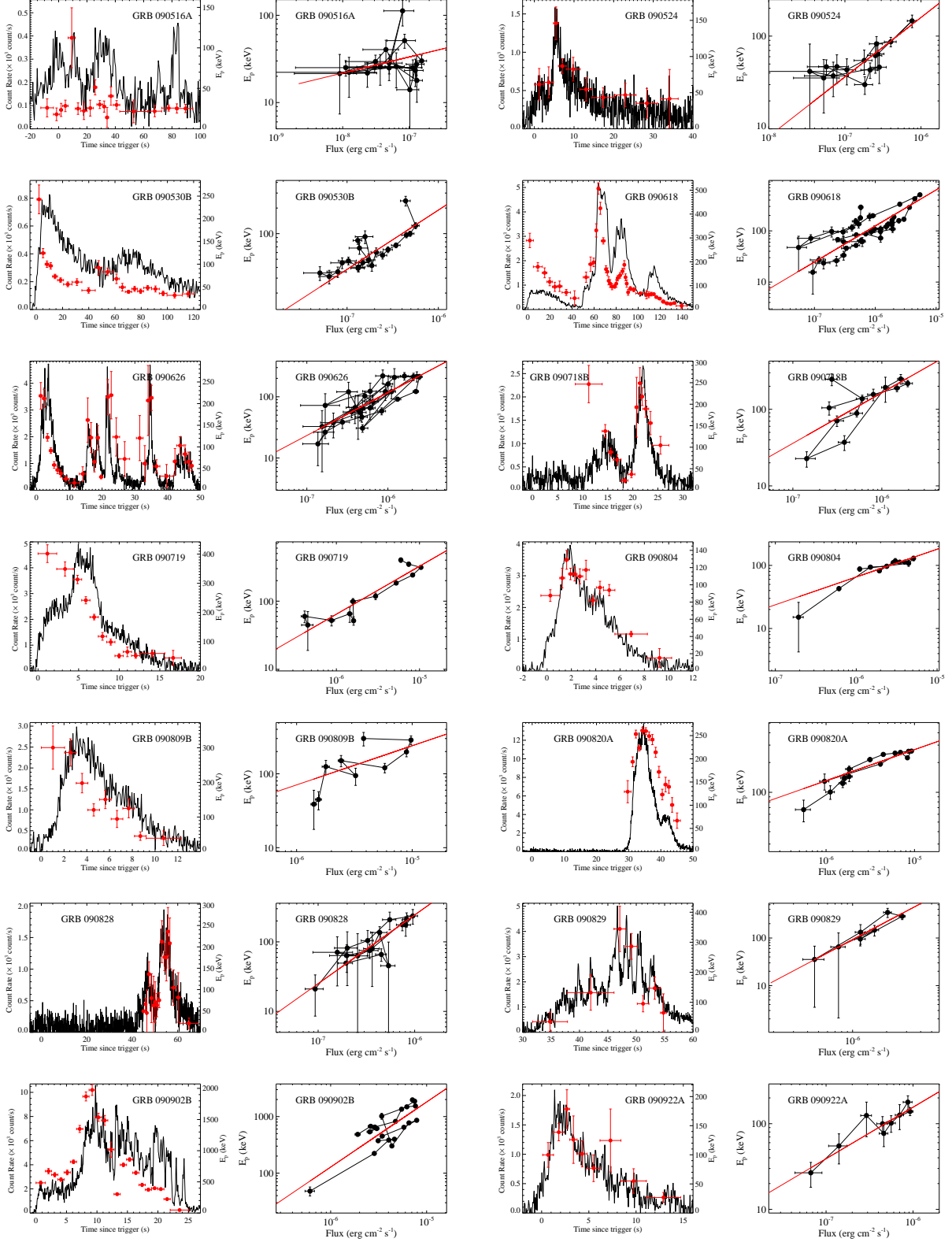


Fig. 2.— *-continued.*

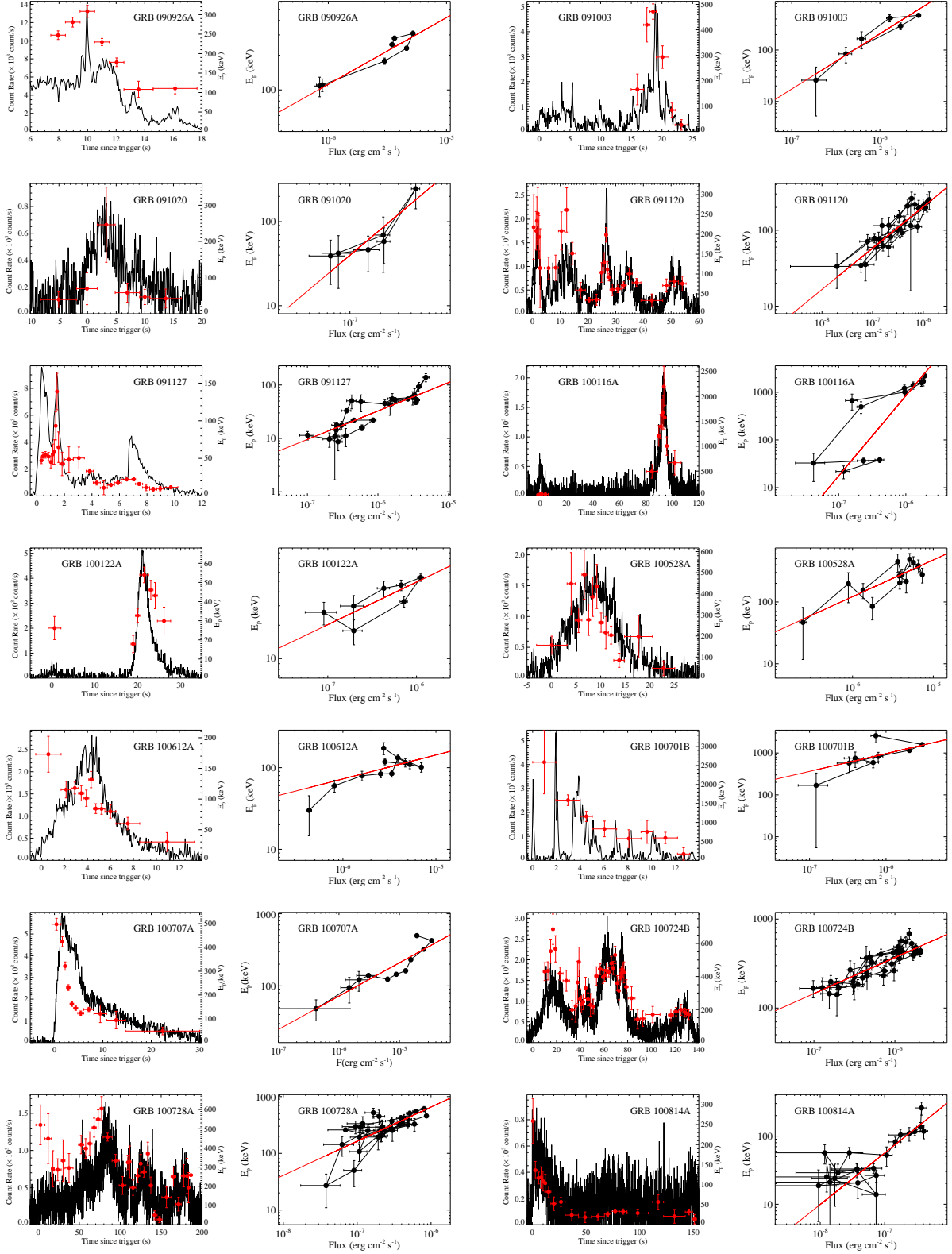
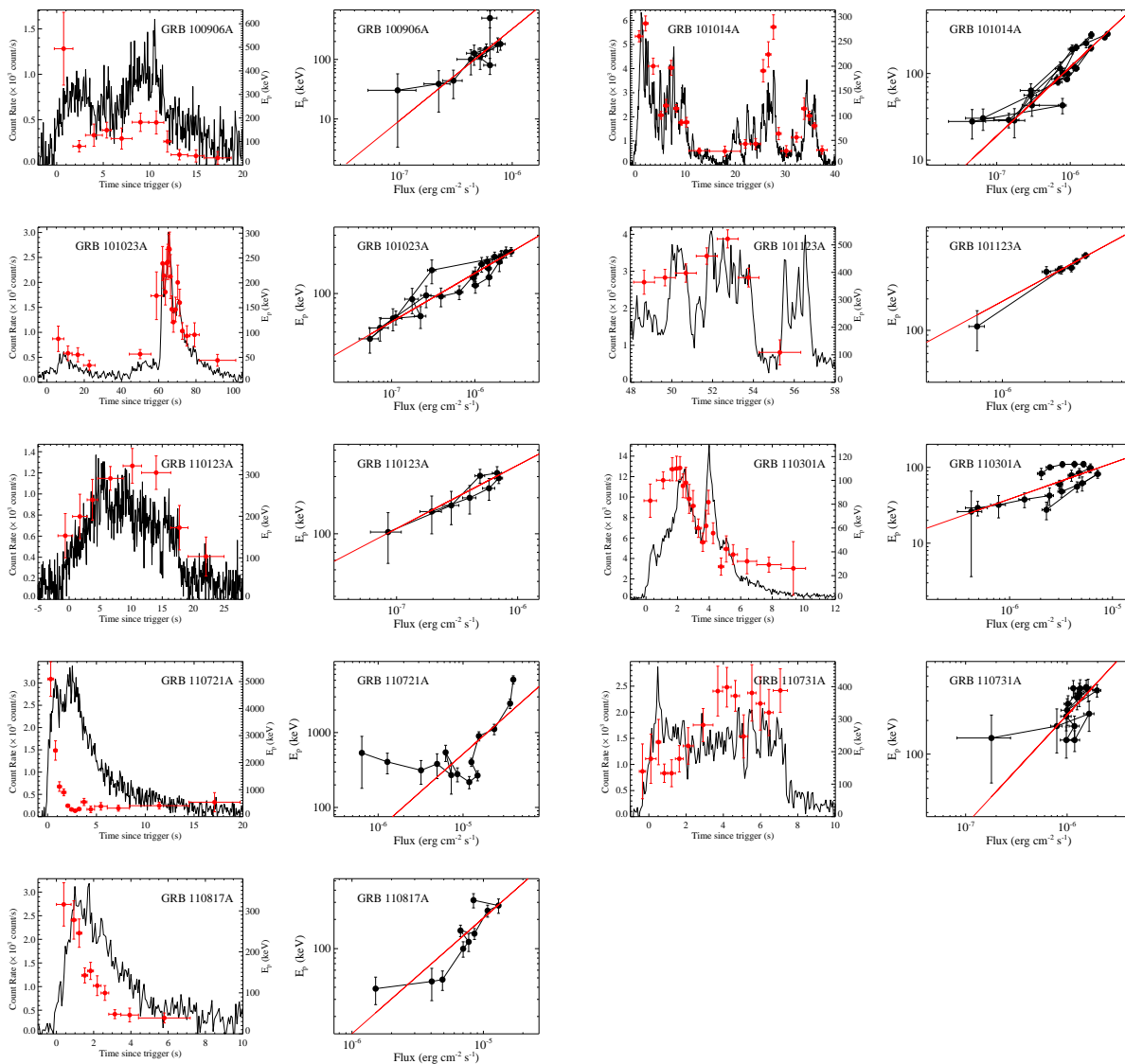


Fig. 2.— *-continued.*



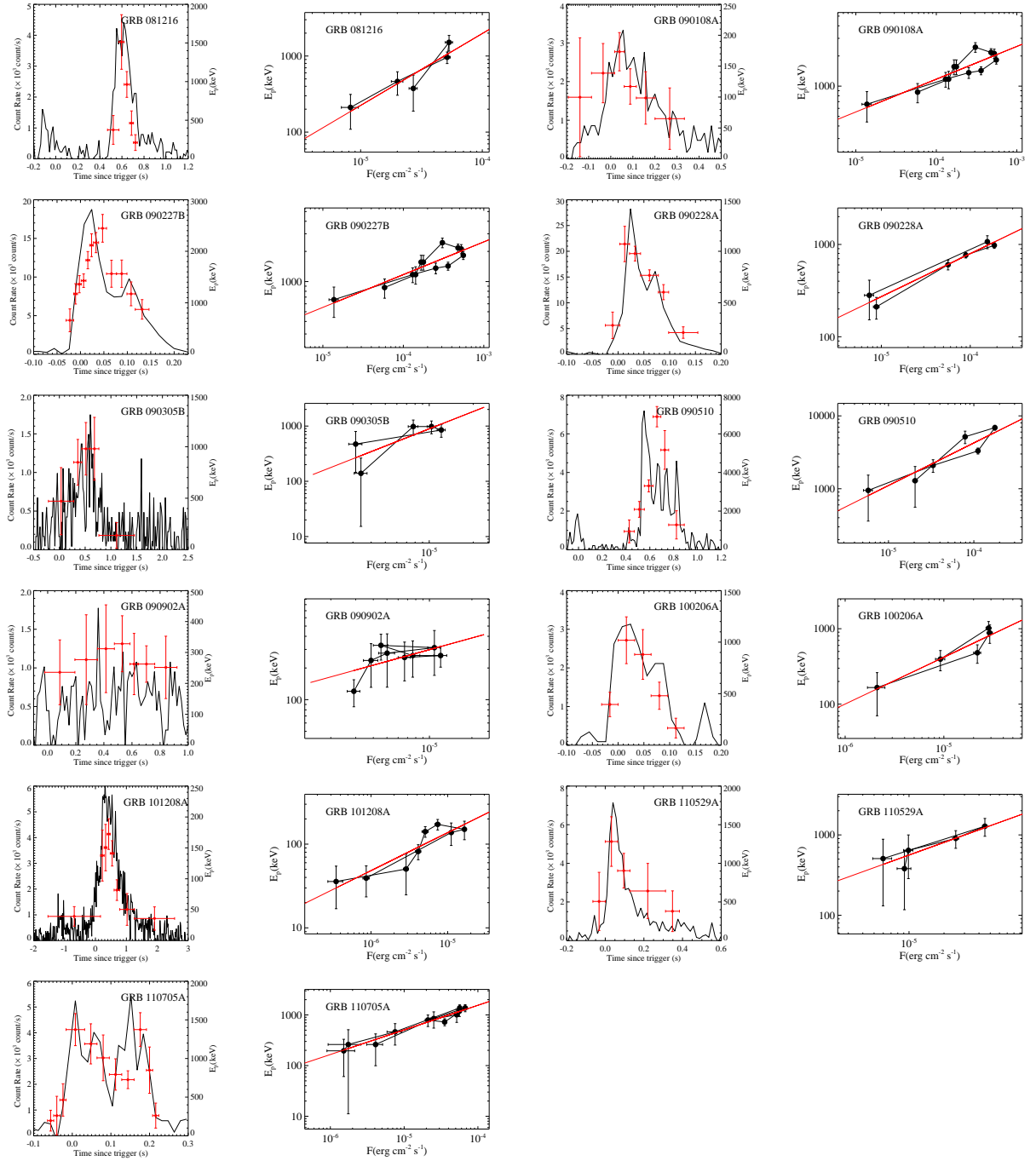


Fig. 3.— The same as Fig. 2, but for the short GRBs in our sample.

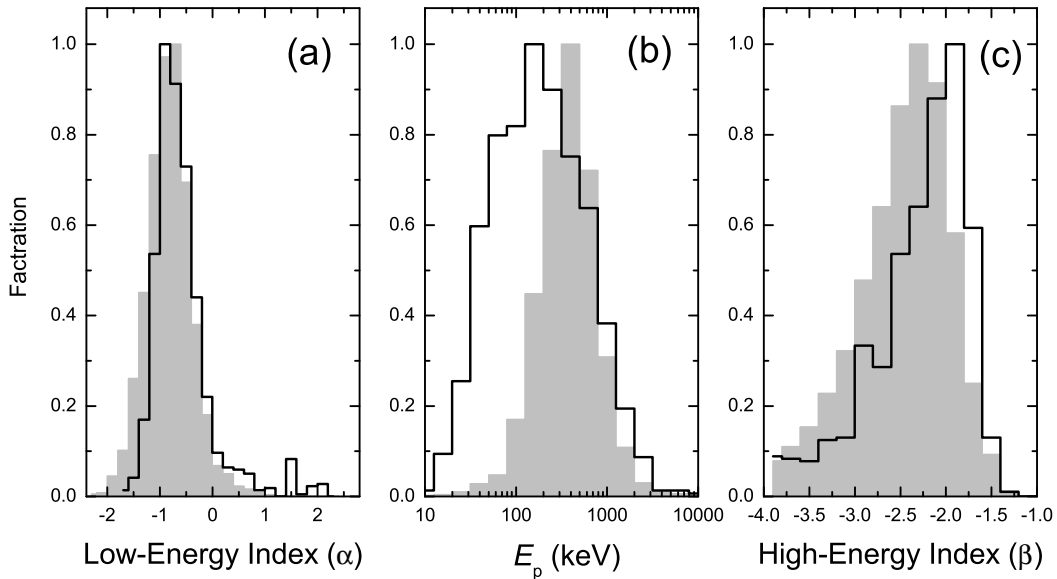


Fig. 4.— A comparison of time-resolved Band spectral parameters, i.e. low-energy spectral index (a), peak energy (b), and high-energy spectral index (c), between the 350 bright *CGRO*/*BATSE* GRBs with 8459 time-resolved burst spectra (gray shapes, Data from Kaneko et al. 2006) and the Fermi GRBs included in our sample (solid lines).

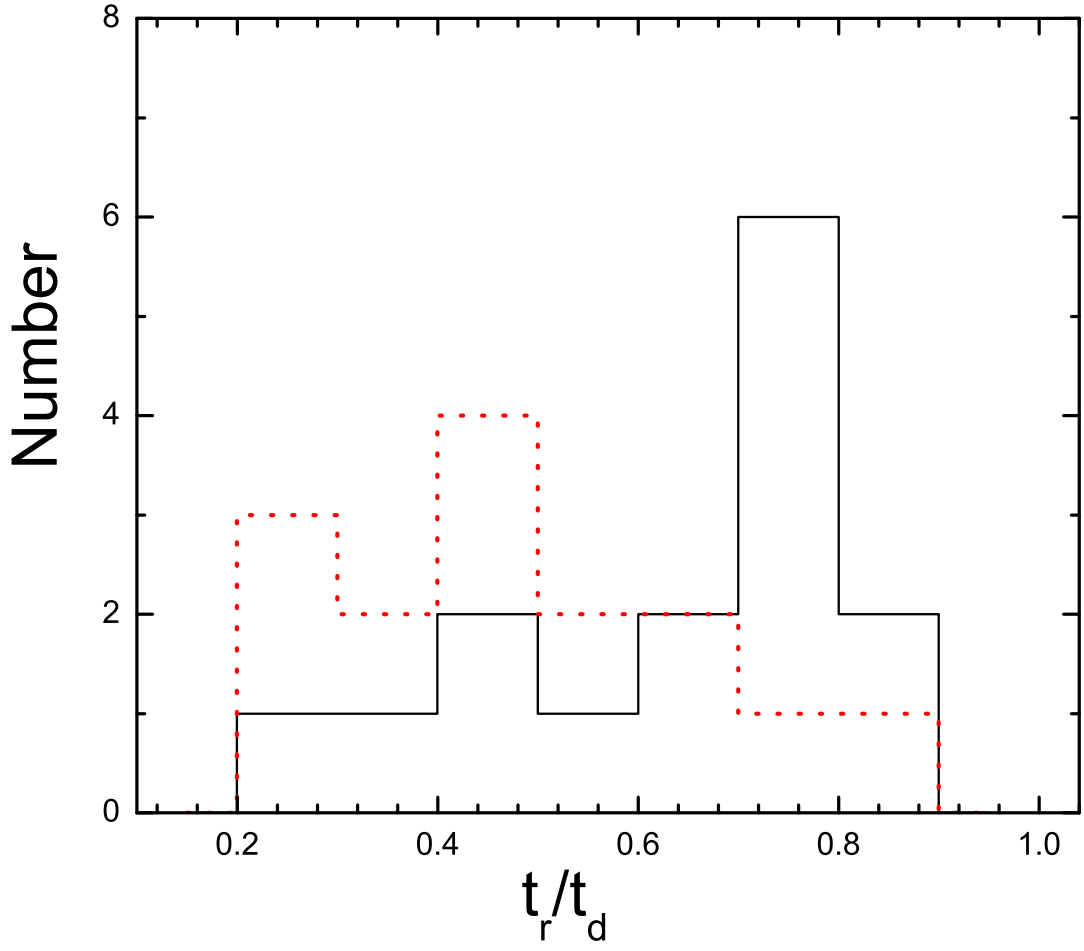


Fig. 5.— Distributions of the ratio between the rising time scale (t_r) and the fall time scale (t_d) for the tracking pulses (the solid line) and hard-to-soft pulses (the dotted line).

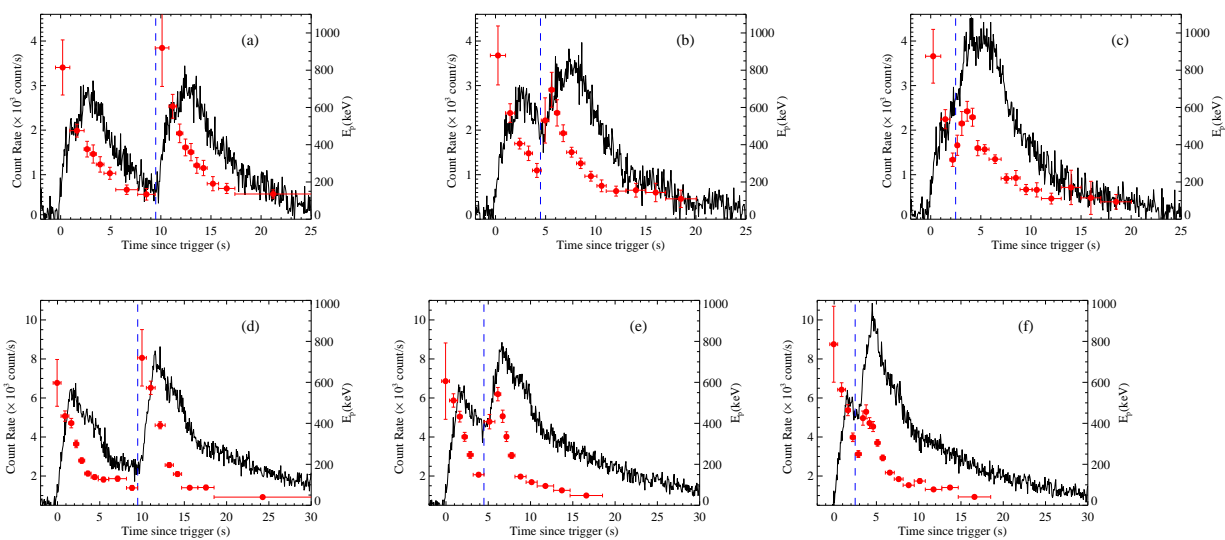


Fig. 6.— A simulation tests of overlapping hard-to-soft pulses for GRBs 081224 (first row) and 100707A (second row) are taken as template. The six panels show the E_p evolution pattern of the simulated GRB with different pulse separations: 10 s (first column), 5 s (second column), 3 s (third column). The vertical dash lines mark the onset of the second pulses. The symbols are the same as Fig. 2.

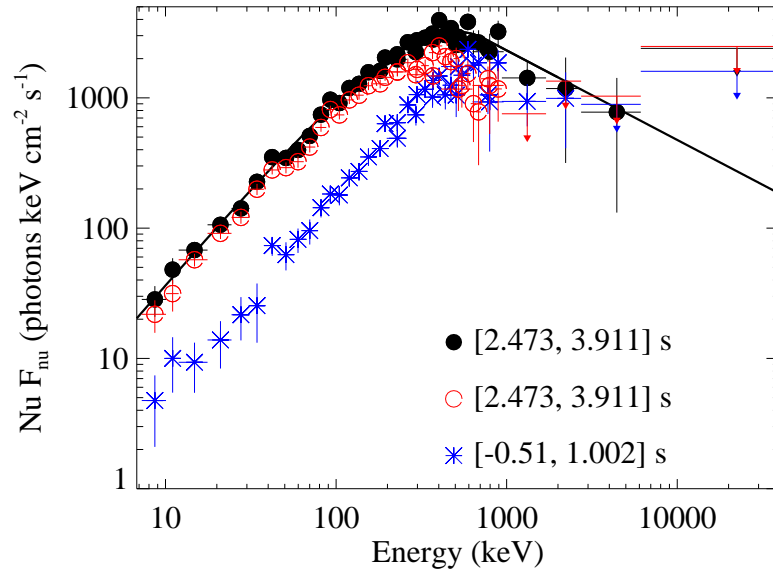


Fig. 7.— Illustrations of the superposition effect on the spectral shape for the simulated GRB 081224. These three mock spectra correspond to that of the onset time bin of the second pulse of the mock GRB as shown in Fig. 6. Every mock spectrum in the onset time bin of the second pulse of the mock GRB (*solid dots*) is roughly the superimposition of the observed GRB 081224 spectra in the two different time bins as marked in the legends.

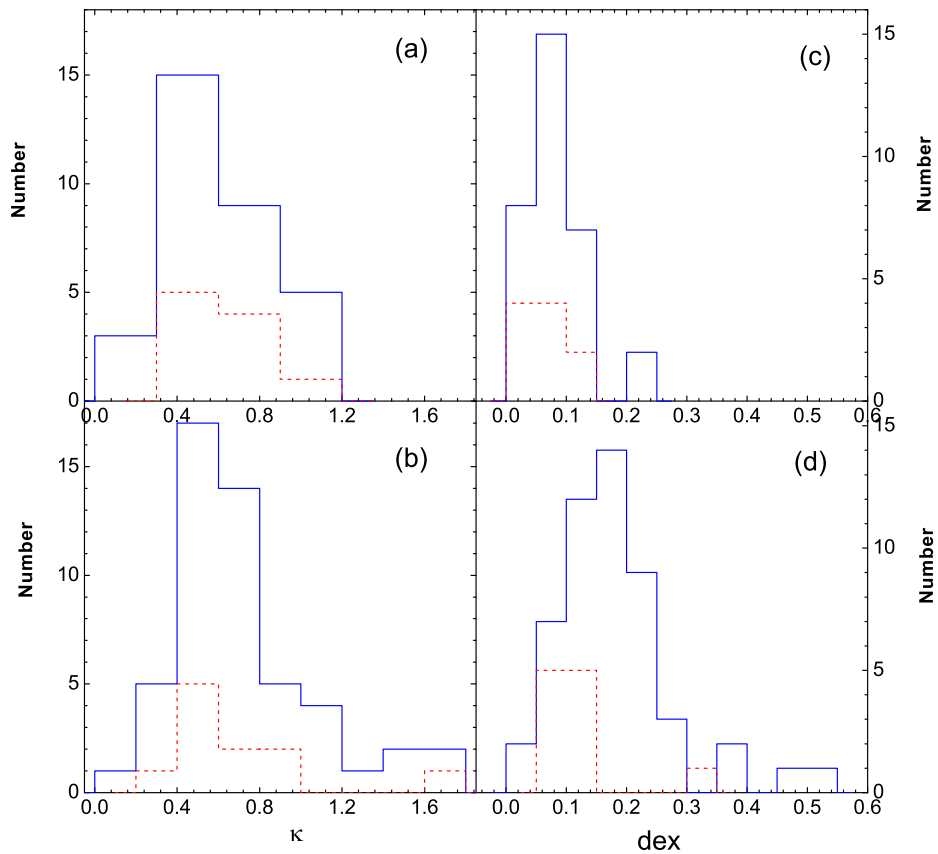


Fig. 8.— Distributions of the correlation power law index κ (a, b) of the $E_p - F$ correlation and the scatter (dex) of data points around the best $E_p - F$ correlation (c, d) in the decay phase of the pulses (the first row panels) and for the entire burst (the second row panels). The solid and dashed lines denote the long and short GRBs in our sample, respectively.

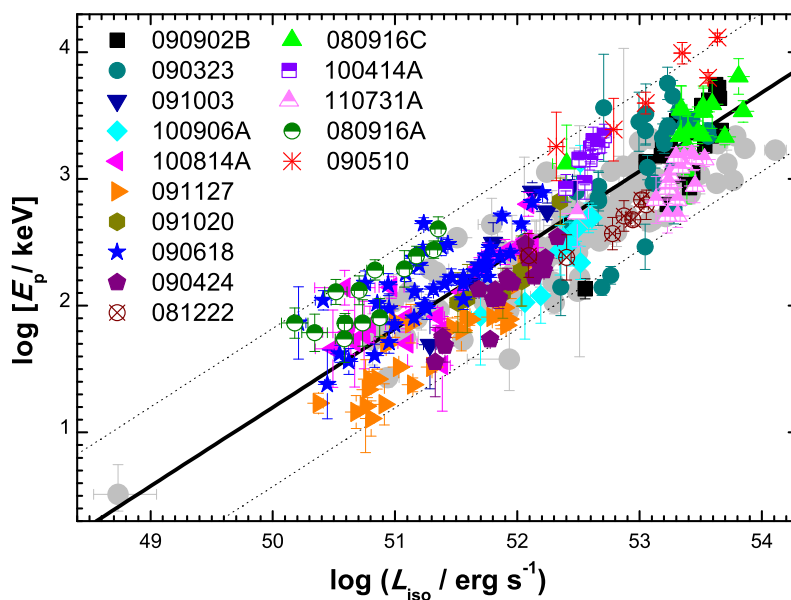


Fig. 9.— A comparison of the time resolved $E_p - L_{\gamma,\text{iso}}$ correlation for 15 Fermi GRBs with known redshifts in our sample (marked in color individually) with the time integrated $E_p - L_{\gamma,\text{iso}}$ correlation for the 101 GRBs in Yonetoku et al. (2010) (gray filled circles). The solid line is the best fit to the time resolved spectra, while the two dot lines represent its 2σ dispersion around the best fit.

Table 1. Time-resolved Spectral fits with the Band function for the GRBs in our sample. The fluence is in the 10-1000 keV band.

GRB	Slice#	t_{start} (s)	t_{end} (s)	E_p (keV)	α	β	fluence ^a	χ_r^2
080825C	1	-3.456	0.004	104.0 ± 64.4	-0.71 ± 1.12	-4.41 ± 0.00	0.29 ± 0.11	0.94
080825C	2	0.004	1.664	231.4 ± 44.9	-0.62 ± 0.15	-2.08 ± 0.17	4.18 ± 0.17	1.12
080825C	3	1.664	3.712	372.0 ± 55.5	-0.83 ± 0.08	-2.26 ± 0.21	14.47 ± 0.37	1.10
080825C	4	3.712	4.736	191.8 ± 33.2	-0.67 ± 0.15	-2.43 ± 0.37	17.15 ± 0.15	0.87
080825C	5	4.736	5.760	130.3 ± 25.6	-0.34 ± 0.26	-1.94 ± 0.09	20.09 ± 0.13	1.32
080825C	6	5.760	6.784	68.9 ± 20.6	0.47 ± 0.94	-1.84 ± 0.09	21.66 ± 0.11	0.92
080825C	7	6.784	9.856	152.3 ± 58.4	-0.87 ± 0.43	-4.41 ± 0.00	22.97 ± 0.29	0.93
080825C	8	9.856	12.928	107.5 ± 31.6	0.02 ± 0.54	-1.76 ± 0.07	29.15 ± 0.33	0.87
080825C	9	12.928	14.976	292.3 ± 37.3	-0.83 ± 0.10	-4.41 ± 0.00	34.73 ± 0.35	1.00
080825C	10	14.976	16.000	170.4 ± 17.5	-0.50 ± 0.16	-4.41 ± 0.00	36.40 ± 0.11	1.05
080825C	11	16.000	19.072	131.6 ± 28.9	-0.04 ± 0.39	-2.04 ± 0.16	41.97 ± 0.38	1.00
080825C	12	19.072	22.144	77.2 ± 31.8	-0.79 ± 0.00	-1.62 ± 0.08	45.35 ± 0.27	0.78
080916A	1	-0.128	1.472	238.8 ± 52.6	0.01 ± 0.28	-1.81 ± 0.12	1.77 ± 0.10	0.95
080916A	2	1.472	2.746	164.0 ± 26.2	0.44 ± 0.35	-2.11 ± 0.21	3.06 ± 0.10	0.84
080916A	3	2.746	4.228	146.0 ± 26.3	-0.11 ± 0.28	-2.25 ± 0.30	4.15 ± 0.11	0.94
080916A	4	4.228	6.011	115.7 ± 38.5	-0.50 ± 0.36	-1.89 ± 0.17	5.19 ± 0.10	0.94
080916A	5	6.011	8.390	113.4 ± 21.1	-0.34 ± 0.30	-2.64 ± 0.68	6.00 ± 0.13	1.11
080916A	6	8.390	11.968	76.1 ± 17.3	-0.11 ± 0.55	-2.61 ± 0.66	6.57 ± 0.12	0.89
080916A	7	12.032	14.487	43.3 ± 18.3	-0.22 ± 0.00	-1.58 ± 0.11	0.66 ± 0.09	0.92
080916A	8	14.487	16.212	47.7 ± 16.6	-0.22 ± 0.00	-1.59 ± 0.10	1.29 ± 0.08	1.08
080916A	9	16.212	18.725	78.2 ± 20.6	-1.01 ± 0.31	-2.39 ± 0.00	1.92 ± 0.06	0.90
080916A	10	18.725	23.502	43.1 ± 7.6	0.39 ± 0.73	-2.32 ± 0.20	2.83 ± 0.11	1.03
080916A	11	23.502	26.628	36.2 ± 12.3	0.19 ± 1.43	-2.36 ± 0.39	3.17 ± 0.08	0.94
080916A	12	26.628	30.031	32.4 ± 13.8	-0.22 ± 0.00	-1.69 ± 0.13	3.81 ± 0.11	1.00
080916A	13	30.031	35.840	43.2 ± 12.0	-0.45 ± 0.82	-2.73 ± 0.77	4.24 ± 0.11	1.03
080916C	1	-6.656	0.004	247.5 ± 172.3	-0.41 ± 0.69	-2.16 ± 0.00	0.92 ± 0.25	1.02
080916C	2	0.004	2.560	401.3 ± 57.1	-0.56 ± 0.08	-2.00 ± 0.12	7.88 ± 0.26	1.02
080916C	3	2.560	4.608	638.5 ± 123.9	-0.74 ± 0.07	-1.86 ± 0.08	15.76 ± 0.32	0.96
080916C	4	4.608	5.632	1203.2 ± 387.7	-1.01 ± 0.05	-1.82 ± 0.10	19.37 ± 0.15	0.99
080916C	5	6.656	7.680	725.9 ± 317.3	-1.14 ± 0.07	-1.88 ± 0.17	24.58 ± 0.14	0.88
080916C	6	7.680	8.704	634.1 ± 273.8	-1.09 ± 0.09	-1.93 ± 0.21	26.45 ± 0.14	0.97
080916C	7	8.704	11.776	220.0 ± 135.8	-0.93 ± 0.23	-1.60 ± 0.07	30.54 ± 0.22	1.10
080916C	8	11.776	12.800	439.2 ± 155.3	-0.90 ± 0.13	-2.16 ± 0.48	31.94 ± 0.12	0.89
080916C	9	12.800	15.872	407.4 ± 206.6	-1.07 ± 0.14	-1.92 ± 0.28	35.55 ± 0.31	0.98
080916C	10	16.896	18.944	338.1 ± 183.6	-0.99 ± 0.16	-1.69 ± 0.11	7.03 ± 0.18	1.07
080916C	11	18.944	23.040	436.0 ± 89.5	-0.88 ± 0.09	-12.14 ± 0.00	13.76 ± 0.54	1.00
080916C	12	23.040	26.112	409.7 ± 139.6	-0.88 ± 0.12	-1.81 ± 0.13	19.27 ± 0.32	0.99
080916C	13	26.112	30.208	691.5 ± 265.5	-0.93 ± 0.10	-1.97 ± 0.23	26.66 ± 0.58	0.96
080916C	14	30.208	41.472	657.8 ± 286.3	-1.09 ± 0.11	-12.14 ± 0.00	40.09 ± 1.30	0.97
080916C	15	41.472	48.641	664.8 ± 279.5	-1.06 ± 0.11	-12.14 ± 0.00	48.76 ± 0.83	1.03
081009	1	-0.640	1.432	26.8 ± 1.4	-0.61 ± 0.24	-2.52 ± 0.05	2.69 ± 0.07	1.00
081009	2	1.432	1.919	47.8 ± 1.3	-0.82 ± 0.08	-3.77 ± 0.39	4.63 ± 0.05	1.08
081009	3	1.919	2.217	62.1 ± 1.6	-0.79 ± 0.07	-4.68 ± 1.43	6.64 ± 0.05	0.92
081009	4	2.217	2.490	68.7 ± 2.5	-0.87 ± 0.07	-3.40 ± 0.32	8.87 ± 0.06	0.96
081009	5	2.490	2.744	78.5 ± 2.3	-0.90 ± 0.06	-4.00 ± 0.00	11.10 ± 0.04	1.04
081009	6	2.744	2.971	87.0 ± 2.6	-0.83 ± 0.06	-4.00 ± 0.00	13.43 ± 0.05	1.02
081009	7	2.971	3.234	59.3 ± 1.7	-0.80 ± 0.07	-3.93 ± 0.53	15.40 ± 0.05	1.14
081009	8	3.234	3.546	36.7 ± 1.1	-0.34 ± 0.14	-3.17 ± 0.11	17.19 ± 0.04	1.00
081009	9	3.546	3.879	44.0 ± 0.9	-0.79 ± 0.08	-4.00 ± 0.00	18.98 ± 0.03	1.01
081009	10	3.879	4.212	39.6 ± 0.9	-0.47 ± 0.11	-3.68 ± 0.22	20.74 ± 0.03	1.04
081009	11	4.212	4.557	44.9 ± 1.1	-0.82 ± 0.08	-3.99 ± 0.46	22.53 ± 0.04	0.92
081009	12	4.557	4.906	53.2 ± 1.5	-0.83 ± 0.08	-3.81 ± 0.44	24.45 ± 0.05	0.90
081009	13	4.906	5.324	59.7 ± 2.2	-1.00 ± 0.07	-3.30 ± 0.30	26.61 ± 0.06	1.04
081009	14	5.324	5.875	48.4 ± 1.1	-0.52 ± 0.09	-4.08 ± 0.45	28.56 ± 0.04	1.03
081009	15	5.875	6.615	36.5 ± 0.7	-0.54 ± 0.09	-4.88 ± 0.93	30.33 ± 0.03	1.11
081009	16	6.615	9.856	16.1 ± 1.1	-1.13 ± 0.17	-3.85 ± 0.32	32.27 ± 0.04	1.04
081009	17	35.136	37.956	12.5 ± 2.2	-1.19 ± 0.00	-3.00 ± 0.35	0.35 ± 0.04	1.03
081009	18	37.956	39.367	17.0 ± 2.0	-0.93 ± 0.40	-3.80 ± 0.00	0.81 ± 0.02	1.09
081009	19	39.367	40.777	17.6 ± 1.2	-0.99 ± 0.19	-4.77 ± 1.19	1.78 ± 0.03	0.98
081009	20	40.777	41.780	18.2 ± 1.0	-0.92 ± 0.21	-3.71 ± 0.26	2.88 ± 0.03	0.93
081009	21	41.780	42.720	16.6 ± 1.0	-0.94 ± 0.22	-3.72 ± 0.24	3.98 ± 0.03	1.06
081009	22	42.720	43.831	16.2 ± 0.8	-0.62 ± 0.30	-3.60 ± 0.18	5.09 ± 0.03	1.09
081009	23	43.831	46.561	11.8 ± 1.0	-0.57 ± 0.40	-3.69 ± 0.14	6.78 ± 0.03	1.02
081009	24	46.561	47.830	6.1 ± 0.8	-1.19 ± 0.00	-3.35 ± 0.17	7.17 ± 0.02	1.04
081009	25	47.830	50.368	5.8 ± 1.0	-1.19 ± 0.00	-3.31 ± 0.18	7.61 ± 0.03	1.05
081107	1	-0.640	1.432	26.8 ± 1.4	-0.61 ± 0.24	-2.52 ± 0.05	2.69 ± 0.07	1.00
081107	2	1.432	1.919	47.8 ± 1.3	-0.82 ± 0.08	-3.77 ± 0.39	4.63 ± 0.05	1.08

Table 1—Continued

GRB	Slice#	t_{start} (s)	t_{end} (s)	E_p (keV)	α	β	fluence ^a	χ_r^2
081107	3	1.919	2.217	62.1 ± 1.6	-0.79 ± 0.07	-4.68 ± 1.43	6.64 ± 0.05	0.92
081107	4	2.217	2.490	68.7 ± 2.5	-0.87 ± 0.07	-3.40 ± 0.32	8.87 ± 0.06	0.96
081107	5	2.490	2.744	78.5 ± 2.3	-0.90 ± 0.06	-4.00 ± 0.00	11.10 ± 0.04	1.04
081107	6	2.744	2.971	87.0 ± 2.6	-0.83 ± 0.06	-4.00 ± 0.00	13.43 ± 0.05	1.02
081107	7	2.971	3.234	59.3 ± 1.7	-0.80 ± 0.07	-3.93 ± 0.53	15.40 ± 0.05	1.14
081107	8	3.234	3.546	36.7 ± 1.1	-0.34 ± 0.14	-3.17 ± 0.11	17.19 ± 0.04	1.00
081107	9	3.546	3.879	44.0 ± 0.9	-0.79 ± 0.08	-4.00 ± 0.00	18.98 ± 0.03	1.01
081107	10	3.879	4.212	39.6 ± 0.9	-0.47 ± 0.11	-3.68 ± 0.22	20.74 ± 0.03	1.04
081107	11	4.212	4.557	44.9 ± 1.1	-0.82 ± 0.08	-3.99 ± 0.46	22.53 ± 0.04	0.92
081107	12	4.557	4.906	53.2 ± 1.5	-0.83 ± 0.08	-3.81 ± 0.44	24.45 ± 0.05	0.90
081107	13	4.906	5.324	59.7 ± 2.2	-1.00 ± 0.07	-3.30 ± 0.30	26.61 ± 0.06	1.04
081107	14	5.324	5.875	48.4 ± 1.1	-0.52 ± 0.09	-4.08 ± 0.45	28.56 ± 0.04	1.03
081107	15	5.875	6.615	36.5 ± 0.7	-0.54 ± 0.09	-4.88 ± 0.93	30.33 ± 0.03	1.11
081107	16	6.615	9.856	16.1 ± 1.1	-1.13 ± 0.17	-3.85 ± 0.32	32.27 ± 0.04	1.04
081107	17	35.136	37.956	12.5 ± 2.2	-1.19 ± 0.00	-3.00 ± 0.35	0.35 ± 0.04	1.03
081107	18	37.956	39.367	17.0 ± 2.0	-0.93 ± 0.40	-3.80 ± 0.00	0.81 ± 0.02	1.09
081107	19	39.367	40.777	17.6 ± 1.2	-0.99 ± 0.19	-4.77 ± 1.19	1.78 ± 0.03	0.98
081107	20	40.777	41.780	18.2 ± 1.0	-0.92 ± 0.21	-3.71 ± 0.26	2.88 ± 0.03	0.93
081107	21	41.780	42.720	16.6 ± 1.0	-0.94 ± 0.22	-3.72 ± 0.24	3.98 ± 0.03	1.06
081107	22	42.720	43.831	16.2 ± 0.8	-0.62 ± 0.30	-3.60 ± 0.18	5.09 ± 0.03	1.09
081107	23	43.831	46.561	11.8 ± 1.0	-0.57 ± 0.40	-3.69 ± 0.14	6.78 ± 0.03	1.02
081107	24	46.561	47.830	6.1 ± 0.8	-1.19 ± 0.00	-3.35 ± 0.17	7.17 ± 0.02	1.04
081107	25	47.830	50.368	5.8 ± 1.0	-1.19 ± 0.00	-3.31 ± 0.18	7.61 ± 0.03	1.05
081125	1	0.003	1.152	332.0 ± 159.5	-0.57 ± 0.23	-1.82 ± 0.64	2.56 ± 0.30	0.92
081125	2	1.152	2.176	245.1 ± 54.4	-0.32 ± 0.18	-1.94 ± 0.34	6.42 ± 0.33	1.13
081125	3	2.176	3.200	186.2 ± 18.1	-0.02 ± 0.13	-2.44 ± 0.35	11.34 ± 0.36	0.93
081125	4	3.200	4.224	145.4 ± 11.2	-0.20 ± 0.14	-3.11 ± 0.00	13.99 ± 0.13	1.11
081125	5	4.224	5.248	132.0 ± 19.2	-0.36 ± 0.19	-2.43 ± 0.43	16.27 ± 0.26	1.03
081125	6	5.248	6.272	119.7 ± 13.8	-0.26 ± 0.19	-2.79 ± 0.64	18.25 ± 0.24	0.89
081125	7	6.272	7.296	94.9 ± 14.0	-0.46 ± 0.25	-2.85 ± 0.86	19.40 ± 0.19	0.84
081125	8	7.296	8.320	53.8 ± 13.1	-0.32 ± 0.70	-2.71 ± 0.72	19.85 ± 0.10	0.84
081125	9	8.320	9.344	49.1 ± 15.6	-0.51 ± 0.00	-1.97 ± 0.29	20.38 ± 0.13	1.10
081125	10	9.344	10.368	23.5 ± 12.3	-0.51 ± 0.00	-2.06 ± 0.27	20.69 ± 0.09	0.80
081207	1	-6.144	13.312	154.6 ± 93.5	0.39 ± 1.12	-1.51 ± 0.11	11.60 ± 1.24	1.05
081207	2	13.312	23.552	248.4 ± 152.5	-0.01 ± 0.68	-1.48 ± 0.10	19.20 ± 0.76	1.00
081207	3	23.552	29.696	373.5 ± 122.4	-0.39 ± 0.23	-1.76 ± 0.15	27.11 ± 0.59	0.93
081207	4	29.696	39.937	998.6 ± 419.2	-0.77 ± 0.13	-2.16 ± 0.48	40.88 ± 1.16	0.95
081207	5	39.937	46.081	768.4 ± 225.7	-0.58 ± 0.16	-2.36 ± 0.00	49.03 ± 0.67	1.01
081207	6	46.081	58.369	358.2 ± 138.9	-0.49 ± 0.24	-1.72 ± 0.14	63.22 ± 1.12	0.95
081207	7	58.369	80.897	292.1 ± 152.0	-0.79 ± 0.31	-2.36 ± 0.00	72.71 ± 1.84	0.90
081207	8	80.897	96.257	108.7 ± 62.1	-0.60 ± 0.00	-1.56 ± 0.19	77.59 ± 0.89	1.06
081215A	1	0.004	1.280	1304.4 ± 221.0	-0.78 ± 0.06	-2.52 ± 0.32	4.02 ± 0.12	1.05
081215A	2	1.280	2.304	670.7 ± 25.8	-0.56 ± 0.02	-2.31 ± 0.05	26.17 ± 0.26	1.01
081215A	3	2.304	3.328	312.7 ± 28.8	-0.80 ± 0.05	-2.28 ± 0.14	31.03 ± 0.12	1.04
081215A	4	3.328	4.352	332.7 ± 17.0	-0.60 ± 0.04	-2.66 ± 0.18	39.07 ± 0.15	1.17
081215A	5	4.352	5.376	365.3 ± 15.6	-0.52 ± 0.03	-2.54 ± 0.11	50.48 ± 0.17	1.09
081215A	6	5.376	6.400	169.5 ± 14.8	-0.52 ± 0.08	-2.18 ± 0.09	54.43 ± 0.10	0.89
081215A	7	6.400	7.424	117.4 ± 21.5	-0.77 ± 0.17	-2.06 ± 0.11	56.11 ± 0.08	0.87
081215A	8	7.424	8.448	58.4 ± 12.0	-0.22 ± 0.49	-2.22 ± 0.16	56.80 ± 0.06	1.00
081216	1	0.159	0.573	178.2 ± 27.7	0.67 ± 0.00	-1.50 ± 0.07	1.80 ± 0.05	0.89
081216	2	0.573	0.620	1740.4 ± 280.2	-0.54 ± 0.08	-3.15 ± 0.81	2.80 ± 0.06	0.84
081216	3	0.620	0.669	1176.6 ± 189.4	-0.34 ± 0.11	-2.73 ± 0.42	3.91 ± 0.06	1.00
081216	4	0.669	0.705	626.5 ± 169.4	-0.45 ± 0.19	-2.02 ± 0.00	4.38 ± 0.04	0.72
081216	5	0.705	0.742	469.9 ± 206.4	-0.80 ± 0.21	-2.02 ± 0.00	4.65 ± 0.03	0.77
081221	1	-0.256	1.131	138.0 ± 31.3	0.72 ± 0.68	-2.09 ± 0.24	0.86 ± 0.08	1.01
081221	2	1.131	2.518	82.5 ± 30.1	-0.22 ± 0.60	-1.84 ± 0.11	1.78 ± 0.07	0.95
081221	3	2.518	4.223	73.0 ± 13.5	-0.48 ± 0.35	-2.41 ± 0.27	2.59 ± 0.08	1.11
081221	4	4.223	5.674	36.7 ± 10.3	0.61 ± 1.34	-2.08 ± 0.14	3.14 ± 0.06	0.92
081221	5	5.674	7.582	29.9 ± 5.7	-0.54 ± 0.00	-2.30 ± 0.20	3.57 ± 0.06	0.95
081221	6	7.582	9.531	39.4 ± 12.4	-0.43 ± 0.91	-2.33 ± 0.27	4.01 ± 0.06	1.03
081221	7	9.531	13.194	32.4 ± 4.9	-0.32 ± 0.71	-2.88 ± 0.44	4.55 ± 0.06	1.02
081221	8	13.194	15.634	44.8 ± 7.3	-0.64 ± 0.40	-2.49 ± 0.22	5.41 ± 0.08	1.04
081221	9	15.634	18.075	70.0 ± 10.1	-1.04 ± 0.17	-2.46 ± 0.23	6.93 ± 0.10	1.09
081221	10	18.075	19.210	105.2 ± 6.8	-0.30 ± 0.12	-2.83 ± 0.24	9.01 ± 0.09	1.10
081221	11	19.210	20.261	105.7 ± 6.1	-0.26 ± 0.11	-3.03 ± 0.30	11.07 ± 0.09	1.04
081221	12	20.261	21.098	112.4 ± 7.2	-0.35 ± 0.11	-2.96 ± 0.29	13.03 ± 0.08	1.11
081221	13	21.098	21.741	113.1 ± 6.9	-0.24 ± 0.11	-2.96 ± 0.26	14.93 ± 0.07	0.94

Table 1—Continued

GRB	Slice#	t_{start} (s)	t_{end} (s)	E_p (keV)	α	β	fluence ^a	χ_r^2
081221	14	21.741	22.523	105.0 ± 4.9	-0.28 ± 0.10	-4.06 ± 1.09	16.61 ± 0.07	1.15
081221	15	22.523	23.565	95.5 ± 5.9	-0.52 ± 0.11	-3.09 ± 0.36	18.42 ± 0.08	0.89
081221	16	23.565	24.408	99.8 ± 6.3	-0.40 ± 0.11	-2.92 ± 0.26	20.29 ± 0.08	0.99
081221	17	24.408	25.271	88.0 ± 5.9	-0.50 ± 0.12	-2.85 ± 0.24	22.01 ± 0.07	1.04
081221	18	25.271	28.101	65.5 ± 2.6	-0.68 ± 0.08	-2.87 ± 0.14	26.27 ± 0.11	1.08
081221	19	28.101	29.188	79.5 ± 6.4	-1.00 ± 0.11	-2.98 ± 0.42	27.80 ± 0.08	1.08
081221	20	29.188	31.681	65.2 ± 4.3	-0.96 ± 0.10	-2.80 ± 0.22	30.30 ± 0.10	1.22
081221	21	31.681	32.845	45.6 ± 4.9	-0.14 ± 0.39	-2.69 ± 0.22	30.99 ± 0.05	0.80
081221	22	32.845	34.883	44.8 ± 4.0	-0.78 ± 0.26	-3.18 ± 0.58	31.74 ± 0.06	1.04
081221	23	34.883	36.921	40.3 ± 2.7	-0.17 ± 0.36	-3.32 ± 0.00	32.32 ± 0.03	1.01
081221	24	36.921	49.152	32.0 ± 6.9	-1.15 ± 0.59	-2.99 ± 1.04	33.01 ± 0.13	1.09
081222	1	-0.512	1.076	135.3 ± 37.6	-0.20 ± 0.34	-1.63 ± 0.06	1.90 ± 0.08	1.01
081222	2	1.076	2.150	166.1 ± 44.3	-0.79 ± 0.16	-1.77 ± 0.07	3.86 ± 0.08	1.04
081222	3	2.150	4.349	181.4 ± 22.7	-0.81 ± 0.08	-2.21 ± 0.17	7.54 ± 0.14	1.03
081222	4	4.349	6.334	126.3 ± 13.8	-0.71 ± 0.11	-2.28 ± 0.16	10.35 ± 0.13	0.98
081222	5	6.334	7.823	98.3 ± 28.8	-0.58 ± 0.31	-1.83 ± 0.09	11.79 ± 0.09	1.16
081222	6	7.823	11.522	63.8 ± 26.2	-0.60 ± 0.54	-1.85 ± 0.11	13.29 ± 0.12	0.87
081222	7	11.522	15.872	66.0 ± 26.2	-0.79 ± 0.00	-1.74 ± 0.16	14.16 ± 0.12	1.02
081224	1	-0.512	1.203	795.1 ± 73.1	-0.28 ± 0.07	-2.43 ± 0.18	7.23 ± 0.20	1.15
081224	2	1.203	1.889	565.9 ± 38.8	-0.17 ± 0.07	-3.41 ± 1.00	12.04 ± 0.16	0.86
081224	3	1.889	2.404	429.1 ± 25.2	-0.29 ± 0.06	-4.57 ± 0.00	15.59 ± 0.11	0.97
081224	4	2.404	2.874	465.6 ± 38.3	-0.42 ± 0.06	-3.10 ± 0.77	19.00 ± 0.12	0.93
081224	5	2.874	3.371	385.5 ± 36.8	-0.45 ± 0.07	-2.51 ± 0.28	22.11 ± 0.10	0.91
081224	6	3.371	3.899	355.4 ± 36.3	-0.57 ± 0.07	-2.57 ± 0.36	24.93 ± 0.09	0.96
081224	7	3.899	4.517	249.1 ± 29.2	-0.48 ± 0.10	-2.10 ± 0.13	27.49 ± 0.08	0.98
081224	8	4.517	5.325	268.7 ± 37.0	-0.73 ± 0.08	-2.21 ± 0.21	29.92 ± 0.08	1.07
081224	9	5.325	6.552	181.1 ± 21.3	-0.45 ± 0.12	-2.11 ± 0.13	32.56 ± 0.09	1.00
081224	10	6.552	8.623	172.2 ± 23.6	-0.70 ± 0.11	-2.22 ± 0.20	35.19 ± 0.12	0.90
081224	11	8.623	13.557	123.1 ± 22.0	-0.74 ± 0.16	-2.09 ± 0.16	38.08 ± 0.16	0.97
081224	12	13.557	19.456	167.2 ± 39.8	-1.16 ± 0.15	-4.57 ± 0.00	39.40 ± 0.15	0.95
090108	1	-0.192	-0.087	99.7 ± 96.1	-0.95 ± 0.82	-2.00 ± 0.00	0.08 ± 0.01	0.79
090108	2	-0.087	0.017	138.7 ± 47.9	-0.49 ± 0.37	-2.11 ± 0.31	0.32 ± 0.03	0.82
090108	3	0.017	0.061	173.4 ± 30.9	-0.37 ± 0.24	-3.13 ± 1.28	0.54 ± 0.03	0.80
090108	4	0.061	0.116	117.1 ± 28.6	-0.27 ± 0.35	-2.15 ± 0.21	0.83 ± 0.03	0.91
090108	5	0.116	0.200	98.6 ± 42.4	-0.37 ± 0.56	-1.88 ± 0.15	1.06 ± 0.02	0.87
090108	6	0.200	0.333	65.1 ± 49.7	-0.46 ± 1.05	-1.75 ± 0.13	1.27 ± 0.03	0.85
090131	1	1.906	2.877	47.0 ± 18.6	-0.54 ± 0.71	-1.96 ± 0.12	1.49 ± 0.07	0.99
090131	2	2.877	3.227	94.1 ± 17.2	-0.99 ± 0.20	-2.62 ± 0.42	2.26 ± 0.06	0.92
090131	3	3.227	3.435	80.5 ± 8.0	-0.71 ± 0.16	-2.97 ± 0.50	2.73 ± 0.04	0.89
090131	4	3.435	4.042	50.3 ± 5.3	-0.71 ± 0.26	-2.77 ± 0.29	3.40 ± 0.05	1.08
090131	5	4.042	5.504	22.5 ± 6.0	-1.00 ± 0.00	-2.32 ± 0.20	3.77 ± 0.05	1.07
090131	6	5.964	6.424	52.7 ± 12.6	-0.26 ± 0.48	-1.89 ± 0.06	1.38 ± 0.06	1.00
090131	7	6.424	6.731	45.1 ± 6.8	-0.22 ± 0.43	-2.27 ± 0.11	2.06 ± 0.04	0.93
090131	8	6.731	7.150	40.9 ± 2.1	0.20 ± 0.24	-2.71 ± 0.09	3.42 ± 0.04	1.22
090131	9	7.150	7.316	36.8 ± 3.4	0.16 ± 0.46	-2.66 ± 0.15	3.88 ± 0.03	0.86
090131	10	7.316	7.551	35.5 ± 4.3	-0.10 ± 0.50	-2.44 ± 0.12	4.41 ± 0.03	0.99
090131	11	7.551	8.114	23.5 ± 2.7	-0.27 ± 0.78	-2.53 ± 0.12	4.95 ± 0.03	1.01
090131	12	8.114	9.209	19.7 ± 2.7	-0.49 ± 1.21	-2.79 ± 0.29	5.25 ± 0.03	0.91
090131	13	9.209	10.304	15.3 ± 8.7	-0.31 ± 0.00	-2.24 ± 0.27	5.40 ± 0.04	0.93
090131	14	22.465	22.978	150.3 ± 40.5	-0.88 ± 0.17	-1.91 ± 0.11	1.58 ± 0.06	1.03
090131	15	22.978	23.347	76.3 ± 16.6	-0.71 ± 0.24	-1.87 ± 0.05	3.38 ± 0.06	1.09
090131	16	23.347	24.037	72.4 ± 17.8	-1.07 ± 0.21	-2.01 ± 0.08	4.99 ± 0.07	1.00
090131	17	24.037	25.000	42.8 ± 9.0	-0.95 ± 0.00	-1.84 ± 0.06	6.11 ± 0.07	1.04
090131	18	25.000	25.664	27.2 ± 18.0	-0.95 ± 0.00	-1.75 ± 0.08	6.60 ± 0.05	1.02
090131	19	25.664	27.256	43.8 ± 26.8	-1.01 ± 0.72	-1.96 ± 0.12	0.83 ± 0.08	0.98
090131	20	27.256	29.400	58.5 ± 23.7	-0.95 ± 0.40	-1.91 ± 0.08	2.46 ± 0.10	0.90
090131	21	29.400	30.720	37.1 ± 27.9	-1.14 ± 0.00	-1.72 ± 0.08	3.14 ± 0.07	0.96
090131	22	30.720	32.101	27.4 ± 6.4	-0.09 ± 0.00	-1.69 ± 0.05	1.07 ± 0.07	0.96
090131	23	32.101	32.802	34.1 ± 14.3	0.07 ± 1.34	-1.81 ± 0.07	1.87 ± 0.06	1.03
090131	24	32.802	33.785	26.2 ± 6.6	-0.09 ± 0.00	-1.70 ± 0.05	2.76 ± 0.06	0.93
090131	25	33.785	35.343	25.0 ± 5.3	-0.09 ± 0.00	-1.83 ± 0.07	3.66 ± 0.07	0.93
090131	26	35.343	37.281	15.3 ± 4.3	-0.09 ± 0.00	-2.05 ± 0.07	4.40 ± 0.07	0.94
090227B	1	-0.031	-0.014	659.9 ± 221.2	-0.26 ± 0.30	-2.89 ± 0.00	0.15 ± 0.02	0.55
090227B	2	-0.014	-0.006	1173.1 ± 197.2	-0.36 ± 0.11	-2.89 ± 0.00	0.63 ± 0.03	0.81
090227B	3	-0.006	0.002	1361.1 ± 166.9	-0.19 ± 0.10	-2.89 ± 0.00	1.41 ± 0.04	0.86
090227B	4	0.002	0.012	1429.4 ± 131.2	0.08 ± 0.10	-2.89 ± 0.00	2.63 ± 0.06	0.91
090227B	5	0.012	0.020	1827.3 ± 167.5	0.09 ± 0.10	-2.89 ± 0.00	3.75 ± 0.05	0.81

Table 1—Continued

GRB	Slice#	t_{start} (s)	t_{end} (s)	E_p (keV)	α	β	fluence ^a	χ_r^2
090227B	6	0.020	0.028	2117.2 ± 221.5	-0.28 ± 0.07	-2.89 ± 0.00	4.78 ± 0.05	0.84
090227B	7	0.028	0.039	2169.0 ± 196.4	-0.08 ± 0.08	-2.89 ± 0.00	5.94 ± 0.05	0.90
090227B	8	0.039	0.056	2445.9 ± 268.9	-0.37 ± 0.06	-3.13 ± 0.51	7.12 ± 0.05	1.05
090227B	9	0.056	0.077	1564.1 ± 262.7	-0.38 ± 0.08	-2.17 ± 0.18	8.20 ± 0.05	0.86
090227B	10	0.077	0.099	1564.1 ± 265.4	-0.40 ± 0.08	-2.17 ± 0.18	9.28 ± 0.05	0.88
090227B	11	0.099	0.117	1173.1 ± 231.3	-0.46 ± 0.09	-2.08 ± 0.17	10.15 ± 0.04	0.86
090227B	12	0.117	0.146	871.7 ± 189.8	-0.67 ± 0.09	-2.14 ± 0.22	10.92 ± 0.04	0.80
090228	1	-0.008	0.013	546.8 ± 202.7	-0.89 ± 0.13	-2.03 ± 0.27	1.01 ± 0.03	0.82
090228	2	0.013	0.026	1410.4 ± 128.4	-0.39 ± 0.06	-2.98 ± 0.00	2.60 ± 0.06	0.86
090228	3	0.026	0.044	1215.2 ± 118.2	-0.52 ± 0.05	-3.72 ± 1.01	4.20 ± 0.05	0.99
090228	4	0.044	0.069	637.5 ± 52.0	-0.15 ± 0.09	-2.98 ± 0.00	5.60 ± 0.05	0.81
090228	5	0.069	0.104	643.7 ± 51.0	-0.13 ± 0.09	-2.98 ± 0.00	7.13 ± 0.05	0.94
090228	6	0.104	0.468	144.4 ± 39.0	-1.11 ± 0.16	-2.59 ± 0.88	7.55 ± 0.05	0.94
090305	1	-0.212	0.279	471.4 ± 325.7	-0.76 ± 0.28	-1.71 ± 0.21	0.54 ± 0.06	0.94
090305	2	0.279	0.436	848.6 ± 222.2	-0.11 ± 0.26	-2.01 ± 0.00	1.22 ± 0.04	0.81
090305	3	0.436	0.594	980.0 ± 254.9	-0.42 ± 0.17	-2.51 ± 0.55	1.99 ± 0.05	0.88
090305	4	0.594	0.767	980.0 ± 305.3	-0.42 ± 0.20	-2.51 ± 0.67	2.63 ± 0.05	0.80
090305	5	0.767	1.457	139.3 ± 124.0	-0.56 ± 0.00	-1.25 ± 0.06	3.03 ± 0.04	1.01
090308	1	-0.212	0.279	471.4 ± 325.7	-0.76 ± 0.28	-1.71 ± 0.21	0.54 ± 0.06	0.94
090308	2	0.279	0.436	848.6 ± 222.2	-0.11 ± 0.26	-2.01 ± 0.00	1.22 ± 0.04	0.81
090308	3	0.436	0.594	980.0 ± 254.9	-0.42 ± 0.17	-2.51 ± 0.55	1.99 ± 0.05	0.88
090308	4	0.594	0.767	980.0 ± 305.3	-0.42 ± 0.20	-2.51 ± 0.67	2.63 ± 0.05	0.80
090308	5	0.767	1.457	139.3 ± 124.0	-0.56 ± 0.00	-1.25 ± 0.06	3.03 ± 0.04	1.01
090323	1	-2.560	3.803	154.5 ± 76.2	-0.15 ± 0.59	-1.54 ± 0.07	2.54 ± 0.16	0.94
090323	2	3.803	6.984	619.1 ± 332.6	-0.84 ± 0.16	-1.60 ± 0.09	5.30 ± 0.20	0.97
090323	3	6.984	10.165	1242.5 ± 363.4	-0.96 ± 0.06	-2.53 ± 0.57	10.00 ± 0.18	1.04
090323	4	10.165	13.593	990.8 ± 278.8	-0.98 ± 0.06	-1.97 ± 0.15	15.60 ± 0.24	0.98
090323	5	13.593	16.534	747.0 ± 163.8	-0.92 ± 0.06	-2.06 ± 0.17	21.00 ± 0.24	0.90
090323	6	16.534	20.685	466.7 ± 112.4	-0.89 ± 0.08	-1.81 ± 0.09	26.58 ± 0.22	1.03
090323	7	20.685	24.298	714.2 ± 390.6	-1.11 ± 0.09	-1.70 ± 0.11	30.13 ± 0.22	1.03
090323	8	29.717	35.136	798.3 ± 778.0	-1.34 ± 0.11	-2.00 ± 0.54	36.35 ± 0.28	0.86
090323	9	35.008	41.875	527.1 ± 137.6	-1.03 ± 0.07	-1.96 ± 0.16	6.72 ± 0.31	1.10
090323	10	41.875	45.060	539.0 ± 111.0	-0.98 ± 0.06	-2.32 ± 0.40	11.37 ± 0.24	1.00
090323	11	45.060	51.926	572.1 ± 78.0	-0.97 ± 0.04	-2.56 ± 0.50	21.63 ± 0.39	1.07
090323	12	51.926	55.509	415.5 ± 71.5	-0.83 ± 0.07	-2.23 ± 0.29	26.62 ± 0.22	1.09
090323	13	55.509	57.873	572.1 ± 76.8	-0.83 ± 0.06	-2.90 ± 0.00	31.45 ± 0.20	1.11
090323	14	57.873	64.212	644.6 ± 69.1	-0.87 ± 0.04	-2.15 ± 0.12	46.31 ± 0.37	1.10
090323	15	64.212	65.477	522.3 ± 79.0	-0.70 ± 0.07	-2.16 ± 0.18	50.31 ± 0.16	0.91
090323	16	65.477	66.781	476.8 ± 47.1	-0.63 ± 0.06	-2.90 ± 0.00	54.47 ± 0.16	0.92
090323	17	66.781	68.637	331.8 ± 71.8	-0.90 ± 0.08	-1.86 ± 0.10	58.13 ± 0.13	0.88
090323	18	68.637	71.560	202.6 ± 56.3	-1.01 ± 0.12	-1.83 ± 0.10	61.56 ± 0.13	0.98
090323	19	111.232	116.789	172.8 ± 49.3	-1.30 ± 0.13	-12.99 ± 0.00	1.48 ± 0.18	1.07
090323	20	116.789	118.461	38.0 ± 6.1	0.33 ± 0.00	-1.76 ± 0.09	2.33 ± 0.08	1.03
090323	21	118.461	120.191	192.2 ± 48.3	-1.34 ± 0.00	-12.99 ± 0.00	3.03 ± 0.09	1.07
090323	22	120.191	120.973	269.6 ± 59.6	-0.87 ± 0.14	-12.99 ± 0.0	3.83 ± 0.09	0.88
090323	23	120.973	123.054	89.3 ± 20.3	-1.23 ± 0.22	-12.99 ± 0.0	4.33 ± 0.06	1.01
090323	24	131.272	133.739	147.2 ± 27.0	-1.04 ± 0.14	-11.03 ± 0.0	2.08 ± 0.10	0.99
090323	25	133.739	139.003	30.7 ± 16.0	-0.75 ± 1.17	-2.03 ± 0.13	3.12 ± 0.12	1.07
090323	26	139.003	140.451	203.7 ± 29.0	-1.12 ± 0.08	-11.03 ± 0.0	4.76 ± 0.11	0.94
090323	27	140.451	141.016	267.9 ± 52.5	-1.06 ± 0.10	-11.03 ± 0.0	5.70 ± 0.08	1.15
090323	28	141.016	142.021	126.4 ± 33.6	-0.89 ± 0.18	-1.90 ± 0.10	7.38 ± 0.08	1.17
090323	29	142.021	142.929	63.9 ± 26.3	-0.80 ± 0.46	-1.90 ± 0.11	8.26 ± 0.07	1.08
090323	30	142.929	145.480	30.5 ± 4.4	0.09 ± 0.00	-1.86 ± 0.08	9.36 ± 0.09	1.25
090323	31	145.480	152.512	70.2 ± 14.6	-1.20 ± 0.26	-11.03 ± 0.0	10.07 ± 0.09	1.14
090328	1	3.267	4.491	987.4 ± 346.3	-1.03 ± 0.08	-2.35 ± 0.59	2.04 ± 0.11	1.09
090328	2	4.491	4.974	623.8 ± 113.8	-0.68 ± 0.09	-2.29 ± 0.30	4.05 ± 0.10	1.03
090328	3	4.974	5.390	818.8 ± 192.9	-0.68 ± 0.10	-1.94 ± 0.14	6.00 ± 0.09	0.93
090328	4	5.390	6.683	901.0 ± 198.3	-0.86 ± 0.07	-1.95 ± 0.13	9.75 ± 0.14	0.96
090328	5	6.683	9.088	449.1 ± 272.2	-0.96 ± 0.18	-1.66 ± 0.12	11.68 ± 0.12	1.09
090328	6	9.152	11.861	562.6 ± 185.2	-0.62 ± 0.16	-1.75 ± 0.12	2.82 ± 0.17	1.10
090328	7	11.861	13.385	793.6 ± 215.4	-0.71 ± 0.11	-1.94 ± 0.17	5.50 ± 0.15	0.95
090328	8	13.385	14.983	888.6 ± 186.0	-0.84 ± 0.07	-2.05 ± 0.17	9.43 ± 0.15	1.03
090328	9	14.983	16.067	602.0 ± 115.7	-0.75 ± 0.08	-1.91 ± 0.11	12.92 ± 0.13	1.02
090328	10	16.067	16.892	668.7 ± 164.2	-0.90 ± 0.09	-2.33 ± 0.46	14.89 ± 0.12	1.07
090328	11	16.892	17.719	625.9 ± 153.3	-0.85 ± 0.09	-2.14 ± 0.27	16.94 ± 0.11	1.11
090328	12	17.719	19.712	480.6 ± 158.5	-0.99 ± 0.09	-1.70 ± 0.07	20.50 ± 0.13	0.97
090328	13	19.648	20.634	783.5 ± 300.4	-0.96 ± 0.10	-1.90 ± 0.20	1.82 ± 0.12	0.93

Table 1—Continued

GRB	Slice#	t_{start} (s)	t_{end} (s)	E_p (keV)	α	β	fluence ^a	χ_r^2
090328	14	20.634	21.621	419.3 ± 301.8	-1.17 ± 0.14	-1.67 ± 0.10	3.34 ± 0.08	1.09
090328	15	21.621	23.175	197.3 ± 95.0	-0.98 ± 0.19	-1.64 ± 0.05	5.71 ± 0.08	1.06
090328	16	23.175	23.937	316.5 ± 166.7	-0.93 ± 0.18	-1.60 ± 0.07	7.30 ± 0.07	0.99
090328	17	23.937	24.213	521.3 ± 98.2	-0.79 ± 0.10	-2.12 ± 0.00	8.71 ± 0.07	0.86
090328	18	24.213	24.442	485.1 ± 97.7	-0.78 ± 0.10	-2.22 ± 0.26	10.12 ± 0.07	0.92
090328	19	24.442	24.805	322.7 ± 94.3	-0.92 ± 0.13	-1.97 ± 0.18	11.33 ± 0.06	0.97
090328	20	24.805	31.636	497.4 ± 203.5	-1.26 ± 0.08	-2.05 ± 0.34	15.67 ± 0.25	1.03
090328	21	53.824	58.898	177.6 ± 43.6	-1.15 ± 0.16	-7.77 ± 0.00	1.29 ± 0.15	1.01
090328	22	58.898	66.368	33.7 ± 18.5	-0.93 ± 1.06	-2.08 ± 0.15	2.56 ± 0.14	1.03
090330	1	3.267	4.491	987.4 ± 346.3	-1.03 ± 0.08	-2.35 ± 0.59	2.04 ± 0.11	1.09
090330	2	4.491	4.974	623.8 ± 113.8	-0.68 ± 0.09	-2.29 ± 0.30	4.05 ± 0.10	1.03
090330	3	4.974	5.390	818.8 ± 192.9	-0.68 ± 0.10	-1.94 ± 0.14	6.00 ± 0.09	0.93
090330	4	5.390	6.683	901.0 ± 198.3	-0.86 ± 0.07	-1.95 ± 0.13	9.75 ± 0.14	0.96
090330	5	6.683	9.088	449.1 ± 272.2	-0.96 ± 0.18	-1.66 ± 0.12	11.68 ± 0.12	1.09
090330	6	9.152	11.861	562.6 ± 185.2	-0.62 ± 0.16	-1.75 ± 0.12	2.82 ± 0.17	1.10
090330	7	11.861	13.385	793.6 ± 215.4	-0.71 ± 0.11	-1.94 ± 0.17	5.50 ± 0.15	0.95
090330	8	13.385	14.983	888.6 ± 186.0	-0.84 ± 0.07	-2.05 ± 0.17	9.43 ± 0.15	1.03
090330	9	14.983	16.067	602.0 ± 115.7	-0.75 ± 0.08	-1.91 ± 0.11	12.92 ± 0.13	1.02
090330	10	16.067	16.892	668.7 ± 164.2	-0.90 ± 0.09	-2.33 ± 0.46	14.89 ± 0.12	1.07
090330	11	16.892	17.719	625.9 ± 153.3	-0.85 ± 0.09	-2.14 ± 0.27	16.94 ± 0.11	1.11
090330	12	17.719	19.712	480.6 ± 158.5	-0.99 ± 0.09	-1.70 ± 0.07	20.50 ± 0.13	0.97
090330	13	19.648	20.634	783.5 ± 300.4	-0.96 ± 0.10	-1.90 ± 0.20	1.82 ± 0.12	0.93
090330	14	20.634	21.621	419.3 ± 301.8	-1.17 ± 0.14	-1.67 ± 0.10	3.34 ± 0.08	1.09
090330	15	21.621	23.175	197.3 ± 95.0	-0.98 ± 0.19	-1.64 ± 0.05	5.71 ± 0.08	1.06
090330	16	23.175	23.937	316.5 ± 166.7	-0.93 ± 0.18	-1.60 ± 0.07	7.30 ± 0.07	0.99
090330	17	23.937	24.213	521.3 ± 98.2	-0.79 ± 0.10	-2.12 ± 0.00	8.71 ± 0.07	0.86
090330	18	24.213	24.442	485.1 ± 97.7	-0.78 ± 0.10	-2.22 ± 0.26	10.12 ± 0.07	0.92
090330	19	24.442	24.805	322.7 ± 94.3	-0.92 ± 0.13	-1.97 ± 0.18	11.33 ± 0.06	0.97
090330	20	24.805	31.636	497.4 ± 203.5	-1.26 ± 0.08	-2.05 ± 0.34	15.67 ± 0.25	1.03
090330	21	53.824	58.898	177.6 ± 43.6	-1.15 ± 0.16	-7.77 ± 0.00	1.29 ± 0.15	1.01
090330	22	58.898	66.368	33.7 ± 18.5	-0.93 ± 1.06	-2.08 ± 0.15	2.56 ± 0.14	1.03
090424	1	0	0.512	86.9 ± 11.2	-0.75 ± 0.15	-2.12 ± 0.07	2.70 ± 0.07	1.13
090424	2	0.512	0.768	109.9 ± 7.7	-0.56 ± 0.09	-2.36 ± 0.08	5.78 ± 0.07	1.08
090424	3	0.768	1.024	123.5 ± 10.1	-0.67 ± 0.08	-2.18 ± 0.06	9.48 ± 0.08	1.08
090424	4	1.024	1.536	225.0 ± 9.9	-0.73 ± 0.03	-2.52 ± 0.09	18.98 ± 0.13	1.05
090424	5	1.536	1.792	100.6 ± 14.6	-0.76 ± 0.15	-2.06 ± 0.07	20.86 ± 0.06	0.99
090424	6	1.792	2.048	72.8 ± 9.5	-0.35 ± 0.24	-2.11 ± 0.07	22.27 ± 0.05	1.10
090424	7	2.048	2.304	98.3 ± 9.5	-0.38 ± 0.15	-2.20 ± 0.08	24.30 ± 0.06	0.97
090424	8	2.304	2.560	35.1 ± 3.6	1.77 ± 0.78	-1.97 ± 0.04	25.64 ± 0.05	0.99
090424	9	2.560	3.072	197.8 ± 16.5	-0.76 ± 0.06	-2.17 ± 0.07	30.86 ± 0.10	1.06
090424	10	3.072	3.328	86.0 ± 9.1	-0.41 ± 0.18	-2.27 ± 0.10	32.34 ± 0.06	1.09
090424	11	3.328	3.584	31.2 ± 9.1	-0.65 ± 0.00	-1.76 ± 0.06	32.91 ± 0.04	0.96
090424	12	3.584	3.840	107.7 ± 18.5	-0.58 ± 0.18	-1.90 ± 0.05	34.75 ± 0.06	1.00
090424	13	3.840	4.096	153.5 ± 15.7	-0.58 ± 0.10	-2.13 ± 0.08	37.49 ± 0.07	1.02
090424	14	4.096	4.608	154.2 ± 8.0	-0.40 ± 0.06	-2.22 ± 0.05	45.08 ± 0.12	0.97
090424	15	4.608	4.864	145.1 ± 12.0	-0.56 ± 0.09	-2.21 ± 0.07	48.42 ± 0.08	1.26
090424	16	4.864	5.120	74.1 ± 13.9	-0.47 ± 0.27	-1.90 ± 0.05	50.00 ± 0.05	1.16
090424	17	5.120	5.376	36.5 ± 6.2	0.60 ± 0.84	-2.14 ± 0.09	50.55 ± 0.04	0.95
090424	18	5.376	5.632	23.2 ± 14.6	-0.65 ± 0.00	-1.69 ± 0.05	51.02 ± 0.04	1.04
090510	1	0.384	0.469	949.4 ± 589.5	-0.83 ± 0.23	-2.46 ± 0.00	0.25 ± 0.03	0.72
090510	2	0.469	0.554	2089.7 ± 409.3	-0.76 ± 0.07	-2.46 ± 0.00	1.11 ± 0.05	0.85
090510	3	0.554	0.627	3306.3 ± 310.9	-0.60 ± 0.05	-3.05 ± 0.39	2.68 ± 0.06	0.96
090510	4	0.627	0.693	6888.2 ± 526.0	-0.45 ± 0.05	-3.85 ± 1.00	3.61 ± 0.04	1.02
090510	5	0.693	0.758	5166.2 ± 1003.0	-0.75 ± 0.06	-2.26 ± 0.27	4.38 ± 0.04	0.96
090510	6	0.758	0.889	1288.3 ± 730.3	-0.97 ± 0.11	-1.70 ± 0.11	5.20 ± 0.05	0.90
090516A	1	-12.579	-3.654	25.9 ± 11.2	1.49 ± 0.00	-1.51 ± 0.09	1.77 ± 0.18	1.13
090516A	2	-3.654	0.718	17.9 ± 7.8	1.49 ± 0.00	-1.55 ± 0.05	3.27 ± 0.12	1.02
090516A	3	0.718	2.836	23.4 ± 8.1	1.49 ± 0.00	-1.59 ± 0.09	3.96 ± 0.08	1.03
090516A	4	2.836	6.690	28.3 ± 7.1	1.49 ± 0.00	-1.93 ± 0.20	4.47 ± 0.11	0.99
090516A	5	6.690	11.772	112.4 ± 37.0	-0.87 ± 0.32	-2.53 ± 0.88	5.54 ± 0.19	1.00
090516A	6	11.772	15.625	25.0 ± 7.1	1.49 ± 0.00	-1.89 ± 0.18	6.04 ± 0.11	1.10
090516A	7	15.625	20.100	22.2 ± 10.8	1.49 ± 0.00	-2.33 ± 0.69	6.19 ± 0.09	0.95
090516A	8	20.100	24.574	25.6 ± 9.8	1.49 ± 0.00	-1.85 ± 0.23	6.62 ± 0.12	1.01
090516A	9	24.574	26.989	51.2 ± 9.4	1.49 ± 0.00	-1.90 ± 0.20	7.17 ± 0.09	1.05
090516A	10	26.989	31.114	30.0 ± 5.0	1.49 ± 0.00	-1.59 ± 0.06	8.84 ± 0.12	1.01
090516A	11	31.114	33.176	27.5 ± 6.9	1.49 ± 0.00	-1.64 ± 0.09	9.54 ± 0.08	1.02
090516A	12	33.176	35.239	14.0 ± 12.4	1.49 ± 0.00	-1.70 ± 0.09	10.10 ± 0.08	1.07

Table 1—Continued

GRB	Slice#	t_{start} (s)	t_{end} (s)	E_p (keV)	α	β	fluence ^a	χ_r^2
090516A	13	35.239	38.656	40.5 ± 11.3	0.31 ± 1.34	-2.53 ± 0.44	10.50 ± 0.08	1.02
090516A	14	38.656	43.162	29.5 ± 5.4	1.49 ± 0.00	-2.37 ± 0.34	10.87 ± 0.09	1.13
090516A	15	43.162	62.892	21.5 ± 14.1	1.49 ± 0.00	-1.94 ± 0.00	11.34 ± 0.14	1.06
090516A	16	62.892	72.757	21.8 ± 6.8	1.49 ± 0.00	-1.94 ± 0.00	11.95 ± 0.09	1.13
090516A	17	72.757	82.622	25.6 ± 3.8	1.49 ± 0.00	-2.26 ± 0.20	12.74 ± 0.14	0.86
090516A	18	82.622	84.327	25.2 ± 5.7	1.49 ± 0.00	-1.79 ± 0.11	13.25 ± 0.07	1.02
090516A	19	84.327	94.720	25.1 ± 5.1	1.49 ± 0.00	-2.85 ± 0.72	13.55 ± 0.10	1.03
090524	1	0.020	2.409	61.6 ± 21.8	0.42 ± 1.02	-1.73 ± 0.09	2.41 ± 0.13	1.08
090524	2	2.409	4.824	64.3 ± 21.4	0.00 ± 0.73	-1.78 ± 0.09	4.13 ± 0.13	0.96
090524	3	4.824	6.057	146.0 ± 22.6	-0.59 ± 0.15	-2.09 ± 0.14	6.61 ± 0.13	0.97
090524	4	6.057	8.030	86.8 ± 10.1	-0.15 ± 0.24	-2.29 ± 0.16	8.70 ± 0.14	0.97
090524	5	8.030	11.559	82.5 ± 16.4	-0.68 ± 0.25	-2.11 ± 0.15	11.12 ± 0.18	1.03
090524	6	11.559	14.525	54.6 ± 16.1	-0.31 ± 0.63	-2.02 ± 0.14	12.52 ± 0.14	1.04
090524	7	14.525	20.207	43.3 ± 13.6	0.30 ± 1.12	-1.96 ± 0.14	14.11 ± 0.19	1.12
090524	8	20.207	25.647	46.8 ± 16.0	-0.39 ± 0.00	-1.78 ± 0.16	15.23 ± 0.18	1.00
090524	9	25.647	31.087	35.4 ± 20.6	-0.39 ± 0.00	-1.76 ± 0.19	15.99 ± 0.17	0.92
090524	10	31.936	36.283	41.6 ± 40.4	-0.66 ± 0.00	-1.81 ± 0.37	0.40 ± 0.15	1.05
090530B	1	0.487	3.578	242.9 ± 31.7	-0.22 ± 0.18	-2.42 ± 0.33	5.02 ± 0.17	1.07
090530B	2	3.578	6.670	124.3 ± 10.2	0.48 ± 0.24	-2.26 ± 0.10	9.61 ± 0.16	1.08
090530B	3	6.670	9.564	99.9 ± 7.1	0.67 ± 0.26	-2.45 ± 0.12	13.35 ± 0.15	1.01
090530B	4	9.564	12.322	96.3 ± 7.0	0.20 ± 0.22	-2.58 ± 0.16	16.60 ± 0.14	0.98
090530B	5	12.322	16.167	73.0 ± 4.9	0.70 ± 0.30	-2.55 ± 0.12	20.08 ± 0.14	1.08
090530B	6	16.167	20.764	64.8 ± 5.1	0.49 ± 0.34	-2.48 ± 0.11	23.48 ± 0.15	0.96
090530B	7	20.764	27.206	55.6 ± 5.3	0.59 ± 0.44	-2.27 ± 0.08	27.64 ± 0.18	1.18
090530B	8	27.206	34.745	60.5 ± 7.4	0.10 ± 0.40	-2.23 ± 0.09	31.78 ± 0.19	0.99
090530B	9	34.745	44.960	42.1 ± 6.0	0.74 ± 0.74	-2.01 ± 0.06	36.81 ± 0.22	0.97
090530B	10	44.960	50.048	92.1 ± 15.7	-0.69 ± 0.27	-2.53 ± 0.34	38.92 ± 0.18	0.92
090530B	11	49.984	58.915	83.1 ± 8.2	-0.74 ± 0.20	-2.67 ± 0.00	3.08 ± 0.13	0.97
090530B	12	58.915	63.380	67.7 ± 10.5	-0.59 ± 0.35	-2.62 ± 0.33	4.69 ± 0.14	0.93
090530B	13	63.380	67.845	49.1 ± 8.4	0.02 ± 0.62	-2.25 ± 0.12	6.71 ± 0.13	1.08
090530B	14	67.845	72.769	39.1 ± 3.5	1.19 ± 0.75	-2.65 ± 0.15	8.43 ± 0.11	0.90
090530B	15	72.769	77.171	45.6 ± 5.5	-0.46 ± 0.42	-2.64 ± 0.21	10.15 ± 0.12	0.96
090530B	16	77.171	81.924	40.4 ± 4.8	-0.02 ± 0.58	-2.58 ± 0.17	11.83 ± 0.11	1.13
090530B	17	81.924	87.950	47.9 ± 4.9	-1.03 ± 0.27	-3.16 ± 0.71	13.47 ± 0.14	0.99
090530B	18	87.950	93.807	45.3 ± 6.6	-0.87 ± 0.43	-2.83 ± 0.43	14.84 ± 0.13	1.06
090530B	19	93.807	99.664	35.5 ± 4.9	-0.47 ± 0.65	-2.77 ± 0.30	16.06 ± 0.11	1.03
090530B	20	99.664	111.377	31.3 ± 5.7	-0.37 ± 0.88	-2.48 ± 0.18	18.03 ± 0.17	0.90
090530B	21	111.377	120.256	34.4 ± 6.3	-0.54 ± 0.00	-2.48 ± 0.26	19.21 ± 0.15	1.01
090618	1	-1.536	4.929	289.3 ± 30.1	-0.26 ± 0.13	-2.23 ± 0.15	9.85 ± 0.32	0.98
090618	2	4.929	13.033	179.1 ± 17.8	-0.42 ± 0.12	-2.16 ± 0.10	22.02 ± 0.35	1.13
090618	3	13.033	17.224	153.8 ± 20.7	-0.59 ± 0.15	-2.32 ± 0.19	27.28 ± 0.24	1.11
090618	4	17.224	22.217	116.2 ± 16.5	-0.44 ± 0.20	-2.13 ± 0.11	32.72 ± 0.25	1.07
090618	5	22.217	26.584	95.2 ± 19.2	-0.57 ± 0.29	-2.14 ± 0.14	36.13 ± 0.22	1.06
090618	6	26.584	30.951	97.5 ± 21.8	-0.87 ± 0.27	-2.46 ± 0.38	38.34 ± 0.23	1.11
090618	7	30.951	38.515	71.6 ± 12.7	-0.46 ± 0.43	-2.89 ± 0.73	40.08 ± 0.26	1.01
090618	8	38.515	46.080	47.4 ± 31.2	-1.00 ± 1.18	-2.18 ± 0.00	41.17 ± 0.15	1.06
090618	9	50.176	55.296	135.3 ± 21.6	-0.98 ± 0.11	-2.13 ± 0.12	7.19 ± 0.28	1.21
090618	10	55.296	58.368	189.8 ± 30.5	-0.94 ± 0.10	-2.11 ± 0.12	13.73 ± 0.22	1.00
090618	11	58.368	60.928	197.6 ± 17.9	-0.97 ± 0.07	-3.15 ± 0.91	19.89 ± 0.25	1.06
090618	12	60.928	62.976	331.6 ± 27.7	-0.89 ± 0.04	-2.20 ± 0.09	33.53 ± 0.26	0.96
090618	13	62.976	64.768	507.0 ± 23.9	-0.94 ± 0.02	-2.87 ± 0.23	59.11 ± 0.37	1.29
090618	14	64.768	66.560	424.2 ± 25.1	-1.04 ± 0.03	-2.55 ± 0.15	80.18 ± 0.33	1.35
090618	15	66.560	70.144	287.7 ± 13.1	-1.05 ± 0.02	-2.43 ± 0.08	114.58 ± 0.37	1.38
090618	16	70.144	71.424	168.9 ± 14.4	-0.90 ± 0.06	-2.21 ± 0.07	124.56 ± 0.19	1.14
090618	17	71.424	72.704	158.5 ± 15.9	-0.98 ± 0.07	-2.21 ± 0.08	132.79 ± 0.18	1.09
090618	18	72.704	73.728	120.5 ± 17.0	-1.01 ± 0.11	-2.23 ± 0.11	136.87 ± 0.14	1.02
090618	19	73.728	75.264	109.1 ± 16.2	-1.15 ± 0.11	-2.32 ± 0.16	140.81 ± 0.16	1.09
090618	20	75.264	77.312	95.8 ± 12.9	-1.03 ± 0.13	-2.26 ± 0.12	145.44 ± 0.18	1.01
090618	21	77.312	79.872	97.1 ± 8.0	-0.92 ± 0.09	-2.32 ± 0.08	153.68 ± 0.22	1.01
090618	22	79.872	80.384	108.5 ± 15.7	-0.67 ± 0.17	-2.19 ± 0.11	156.28 ± 0.11	0.94
090618	23	80.384	82.496	131.4 ± 11.2	-1.03 ± 0.06	-2.26 ± 0.08	166.78 ± 0.22	1.06
090618	24	82.496	84.608	143.3 ± 11.8	-0.99 ± 0.06	-2.30 ± 0.09	177.36 ± 0.22	0.99
090618	25	84.608	86.848	160.5 ± 12.2	-1.07 ± 0.05	-2.46 ± 0.13	188.50 ± 0.23	1.03
090618	26	86.848	87.968	187.4 ± 17.6	-1.11 ± 0.06	-2.69 ± 0.32	194.46 ± 0.17	1.06
090618	27	87.968	89.088	135.0 ± 14.3	-0.99 ± 0.09	-2.46 ± 0.17	199.29 ± 0.16	0.84
090618	28	89.088	90.112	108.6 ± 15.3	-0.98 ± 0.13	-2.30 ± 0.14	202.58 ± 0.14	0.92
090618	29	90.112	91.648	72.2 ± 12.4	-0.68 ± 0.23	-1.96 ± 0.05	207.54 ± 0.15	1.09

Table 1—Continued

GRB	Slice#	t_{start} (s)	t_{end} (s)	E_p (keV)	α	β	fluence ^a	χ_r^2
090618	30	91.648	94.208	87.7 ± 8.4	-0.93 ± 0.12	-2.49 ± 0.16	212.23 ± 0.20	0.90
090618	31	94.208	97.792	83.4 ± 8.7	-1.01 ± 0.12	-2.53 ± 0.20	216.84 ± 0.22	0.97
090618	32	97.792	106.496	67.7 ± 5.4	-1.28 ± 0.10	-3.09 ± 0.64	222.38 ± 0.34	1.00
090618	33	106.496	108.544	61.5 ± 16.7	-1.06 ± 0.34	-2.27 ± 0.21	224.01 ± 0.14	0.96
090618	34	108.544	110.592	61.7 ± 12.2	-0.90 ± 0.26	-2.12 ± 0.09	227.31 ± 0.16	0.92
090618	35	110.592	113.152	64.6 ± 7.8	-1.35 ± 0.12	-2.48 ± 0.18	231.24 ± 0.18	1.02
090618	36	113.152	115.200	64.4 ± 4.5	-1.27 ± 0.10	-3.29 ± 0.72	234.44 ± 0.17	0.89
090618	37	115.200	117.760	52.0 ± 3.6	-1.47 ± 0.10	-3.48 ± 1.21	237.70 ± 0.18	1.07
090618	38	117.760	121.088	45.9 ± 4.2	-1.48 ± 0.13	-2.90 ± 0.47	240.63 ± 0.19	1.12
090618	39	121.088	124.416	33.3 ± 6.5	-1.52 ± 0.33	-2.24 ± 0.00	243.28 ± 0.10	1.10
090618	40	124.416	127.744	26.2 ± 5.6	-1.12 ± 0.71	-2.24 ± 0.00	245.30 ± 0.09	1.07
090618	41	127.744	131.072	23.6 ± 5.5	-1.49 ± 0.52	-2.57 ± 0.29	246.54 ± 0.13	1.03
090618	42	131.072	134.400	27.1 ± 4.2	-1.31 ± 0.41	-3.08 ± 0.69	247.58 ± 0.11	1.17
090618	43	134.400	144.384	15.5 ± 9.7	-1.63 ± 1.31	-2.24 ± 0.00	250.06 ± 0.13	0.96
090626	1	0.768	1.792	218.0 ± 30.7	-0.36 ± 0.11	-1.89 ± 0.15	4.31 ± 0.18	1.10
090626	2	1.792	2.816	211.8 ± 20.6	-0.41 ± 0.08	-1.98 ± 0.12	10.92 ± 0.21	1.07
090626	3	2.816	3.840	122.0 ± 8.6	-0.26 ± 0.09	-2.06 ± 0.07	16.90 ± 0.18	1.16
090626	4	3.840	4.864	91.5 ± 6.4	-0.37 ± 0.11	-2.30 ± 0.10	20.45 ± 0.13	0.95
090626	5	4.864	5.888	58.3 ± 7.6	-0.35 ± 0.25	-2.04 ± 0.07	22.71 ± 0.10	0.99
090626	6	5.888	6.912	46.7 ± 8.4	-0.03 ± 0.50	-2.01 ± 0.09	24.00 ± 0.08	1.09
090626	7	6.912	7.936	38.5 ± 8.2	-0.54 ± 0.55	-2.23 ± 0.14	24.74 ± 0.06	1.04
090626	8	7.936	9.984	26.4 ± 5.6	0.48 ± 1.45	-2.30 ± 0.15	25.65 ± 0.10	0.99
090626	9	9.984	13.056	17.0 ± 9.5	-1.04 ± 0.00	-2.07 ± 0.12	26.76 ± 0.15	0.97
090626	10	13.056	15.104	37.7 ± 16.4	-0.51 ± 1.00	-2.01 ± 0.14	27.90 ± 0.13	0.98
090626	11	15.104	16.128	162.1 ± 51.2	-1.12 ± 0.12	-1.84 ± 0.13	30.62 ± 0.14	0.96
090626	12	16.128	17.152	121.5 ± 34.7	-1.05 ± 0.15	-1.86 ± 0.11	33.13 ± 0.13	0.97
090626	13	17.152	18.176	65.7 ± 23.3	-0.88 ± 0.34	-1.86 ± 0.08	34.75 ± 0.10	0.87
090626	14	18.176	19.200	121.2 ± 28.5	-0.95 ± 0.14	-1.85 ± 0.09	37.74 ± 0.14	1.07
090626	15	19.200	20.224	30.6 ± 4.4	-0.05 ± 0.00	-1.76 ± 0.05	39.05 ± 0.08	0.92
090626	16	21.248	22.272	215.0 ± 40.7	-0.77 ± 0.09	-1.67 ± 0.08	47.24 ± 0.18	0.85
090626	17	22.272	23.296	219.5 ± 54.7	-1.05 ± 0.10	-2.15 ± 0.42	49.57 ± 0.16	1.07
090626	18	23.296	25.344	123.0 ± 44.1	-1.02 ± 0.20	-1.88 ± 0.15	52.83 ± 0.24	1.01
090626	19	25.344	28.416	72.2 ± 40.0	-1.35 ± 0.38	-2.24 ± 0.52	54.20 ± 0.26	0.89
090626	20	30.465	32.513	120.4 ± 52.0	-1.04 ± 0.00	-1.62 ± 0.14	56.99 ± 0.19	0.98
090626	21	32.513	33.536	61.6 ± 41.4	-0.63 ± 0.74	-1.66 ± 0.09	58.14 ± 0.09	0.97
090626	22	33.536	34.561	207.2 ± 80.9	-0.98 ± 0.13	-1.64 ± 0.10	61.39 ± 0.14	1.08
090626	23	34.561	35.585	213.4 ± 29.1	-0.68 ± 0.08	-1.89 ± 0.12	66.98 ± 0.19	1.12
090626	24	35.585	37.633	55.4 ± 15.1	-0.70 ± 0.39	-1.99 ± 0.10	69.43 ± 0.17	1.09
090626	25	37.633	41.729	32.7 ± 26.7	-1.04 ± 0.00	-1.77 ± 0.13	71.09 ± 0.26	0.80
090626	26	41.729	42.753	66.4 ± 30.0	-1.12 ± 0.35	-1.97 ± 0.13	72.15 ± 0.09	1.17
090626	27	42.753	44.801	103.1 ± 20.3	-1.18 ± 0.13	-2.36 ± 0.36	74.95 ± 0.25	1.01
090626	28	44.801	45.825	83.5 ± 21.0	-0.89 ± 0.22	-1.96 ± 0.11	76.72 ± 0.11	1.00
090626	29	45.825	46.849	65.7 ± 22.5	-1.09 ± 0.29	-2.00 ± 0.12	78.03 ± 0.09	0.95
090626	30	46.849	47.873	56.4 ± 11.1	-0.76 ± 0.32	-2.24 ± 0.17	78.99 ± 0.08	1.08
090718B	1	8.512	13.888	246.8 ± 43.4	-1.17 ± 0.07	-2.83 ± 1.40	7.49 ± 0.22	1.02
090718B	2	13.888	15.104	137.4 ± 15.2	-0.59 ± 0.13	-2.39 ± 0.22	9.42 ± 0.10	1.00
090718B	3	15.104	16.064	88.6 ± 9.2	-0.53 ± 0.17	-2.44 ± 0.19	10.74 ± 0.08	0.94
090718B	4	16.064	17.664	70.8 ± 11.2	-1.13 ± 0.17	-2.37 ± 0.21	12.06 ± 0.09	1.11
090718B	5	17.664	19.040	22.7 ± 5.2	-0.39 ± 1.49	-2.32 ± 0.13	12.58 ± 0.05	1.13
090718B	6	19.040	20.416	37.1 ± 8.1	-1.05 ± 0.00	-1.86 ± 0.05	13.96 ± 0.08	1.03
090718B	7	20.416	21.088	192.9 ± 69.5	-1.17 ± 0.12	-1.79 ± 0.07	15.90 ± 0.07	0.90
090718B	8	21.088	21.760	248.9 ± 36.1	-0.96 ± 0.07	-2.07 ± 0.13	18.79 ± 0.09	0.94
090718B	9	21.760	22.016	217.8 ± 21.0	-0.61 ± 0.09	-2.94 ± 0.63	20.11 ± 0.06	0.91
090718B	10	22.016	23.168	189.1 ± 19.5	-0.83 ± 0.07	-2.07 ± 0.09	24.60 ± 0.11	1.09
090718B	11	23.168	23.872	156.2 ± 27.0	-0.84 ± 0.13	-2.16 ± 0.18	26.09 ± 0.08	0.92
090718B	12	23.872	27.200	104.5 ± 20.6	-1.04 ± 0.16	-2.14 ± 0.17	28.34 ± 0.15	1.06
090719	1	0.003	2.304	401.6 ± 30.4	-0.10 ± 0.10	-2.82 ± 0.38	10.50 ± 0.34	0.82
090719	2	2.304	4.352	349.1 ± 24.3	-0.48 ± 0.06	-2.90 ± 0.40	22.85 ± 0.35	0.95
090719	3	4.352	5.376	313.1 ± 14.3	-0.32 ± 0.05	-3.05 ± 0.30	31.97 ± 0.19	1.00
090719	4	5.376	6.400	241.9 ± 12.2	-0.37 ± 0.06	-2.90 ± 0.24	39.27 ± 0.17	0.77
090719	5	6.400	7.424	184.3 ± 9.5	-0.36 ± 0.07	-3.23 ± 0.40	44.26 ± 0.15	0.88
090719	6	7.424	8.448	118.3 ± 13.1	-0.51 ± 0.14	-2.42 ± 0.18	46.68 ± 0.12	0.98
090719	7	8.448	9.472	98.9 ± 10.4	-0.67 ± 0.15	-2.98 ± 0.54	48.15 ± 0.11	1.07
090719	8	9.472	10.496	51.6 ± 7.2	-0.07 ± 0.41	-2.29 ± 0.13	49.45 ± 0.09	1.04
090719	9	10.496	11.520	65.3 ± 16.5	-0.90 ± 0.32	-2.22 ± 0.18	50.52 ± 0.09	0.91
090719	10	11.520	12.544	52.1 ± 8.9	-0.46 ± 0.42	-2.52 ± 0.27	51.27 ± 0.08	0.99
090719	11	12.544	15.616	59.9 ± 11.7	-1.14 ± 0.34	-3.36 ± 0.00	52.34 ± 0.12	0.84

Table 1—Continued

GRB	Slice#	t_{start} (s)	t_{end} (s)	E_p (keV)	α	β	fluence ^a	χ_r^2
090719	12	15.616	17.664	44.6 ± 25.7	-0.70 ± 0.00	-1.93 ± 0.31	52.87 ± 0.15	0.94
090804	1	-0.512	1.039	87.5 ± 6.8	-0.19 ± 0.18	-2.78 ± 0.27	1.55 ± 0.09	0.95
090804	2	1.039	1.445	107.9 ± 11.4	-0.46 ± 0.15	-2.38 ± 0.15	2.97 ± 0.06	1.05
090804	3	1.445	1.766	129.0 ± 10.9	-0.36 ± 0.13	-2.71 ± 0.25	4.41 ± 0.06	1.00
090804	4	1.766	2.078	112.6 ± 6.7	-0.17 ± 0.13	-3.45 ± 0.55	5.60 ± 0.06	1.12
090804	5	2.078	2.461	112.4 ± 7.9	-0.53 ± 0.11	-3.29 ± 0.59	6.85 ± 0.06	1.01
090804	6	2.461	2.932	109.9 ± 8.7	-0.56 ± 0.12	-3.06 ± 0.47	8.09 ± 0.07	0.91
090804	7	2.932	3.464	117.3 ± 11.2	-0.59 ± 0.13	-2.69 ± 0.29	9.50 ± 0.07	0.98
090804	8	3.464	4.052	82.0 ± 5.0	-0.36 ± 0.15	-3.34 ± 0.51	10.57 ± 0.06	0.99
090804	9	4.052	4.643	96.8 ± 7.3	-0.35 ± 0.15	-2.88 ± 0.30	11.86 ± 0.07	1.12
090804	10	4.643	5.574	93.8 ± 6.5	-0.53 ± 0.13	-3.32 ± 0.65	13.17 ± 0.08	0.92
090804	11	5.574	8.248	42.9 ± 3.1	-0.34 ± 0.28	-2.86 ± 0.22	14.47 ± 0.07	1.02
090804	12	8.248	10.240	15.1 ± 10.8	-0.57 ± 0.00	-2.17 ± 0.20	14.72 ± 0.06	0.97
090809B	1	0.003	2.048	300.5 ± 62.4	-0.43 ± 0.16	-1.90 ± 0.12	3.61 ± 0.18	0.99
090809B	2	2.048	3.072	286.4 ± 39.4	-0.54 ± 0.10	-1.94 ± 0.08	8.52 ± 0.16	1.10
090809B	3	3.072	4.096	197.9 ± 28.1	-0.51 ± 0.12	-1.91 ± 0.07	13.14 ± 0.14	0.87
090809B	4	4.096	5.120	120.6 ± 17.6	-0.41 ± 0.17	-1.96 ± 0.08	16.48 ± 0.13	1.06
090809B	5	5.120	6.144	150.6 ± 26.2	-0.85 ± 0.13	-2.52 ± 0.45	18.48 ± 0.14	0.95
090809B	6	6.144	7.168	94.3 ± 24.6	-0.61 ± 0.29	-1.92 ± 0.10	20.31 ± 0.11	1.00
090809B	7	7.168	8.192	124.9 ± 27.1	-0.90 ± 0.18	-2.41 ± 0.41	21.74 ± 0.13	0.96
090809B	8	8.192	9.216	44.9 ± 12.3	-0.04 ± 0.78	-2.01 ± 0.12	22.74 ± 0.09	1.02
090809B	9	9.216	12.288	38.7 ± 21.1	-0.74 ± 0.00	-1.70 ± 0.11	24.55 ± 0.24	1.03
090820A	1	28.672	30.720	129.2 ± 23.9	-0.30 ± 0.23	-1.87 ± 0.07	5.19 ± 0.24	0.90
090820A	2	30.720	31.744	193.6 ± 10.5	-0.24 ± 0.06	-2.20 ± 0.05	16.31 ± 0.20	1.18
090820A	3	31.744	32.769	253.4 ± 8.4	-0.46 ± 0.03	-2.58 ± 0.08	35.05 ± 0.25	1.16
090820A	4	32.769	33.792	223.3 ± 6.3	-0.38 ± 0.03	-2.59 ± 0.06	57.51 ± 0.27	1.15
090820A	5	33.792	34.816	260.9 ± 7.3	-0.52 ± 0.03	-2.64 ± 0.07	82.48 ± 0.28	1.31
090820A	6	34.816	35.840	259.7 ± 7.3	-0.53 ± 0.03	-2.72 ± 0.09	105.62 ± 0.27	1.34
090820A	7	35.840	36.865	249.0 ± 9.2	-0.65 ± 0.03	-2.69 ± 0.11	121.91 ± 0.24	1.21
090820A	8	36.865	37.889	241.5 ± 10.9	-0.72 ± 0.04	-2.71 ± 0.15	133.89 ± 0.21	0.99
090820A	9	37.889	38.913	214.1 ± 10.8	-0.69 ± 0.04	-2.87 ± 0.24	142.37 ± 0.19	1.22
090820A	10	38.913	39.937	171.8 ± 12.1	-0.71 ± 0.06	-2.86 ± 0.31	147.29 ± 0.16	0.86
090820A	11	39.937	40.961	123.0 ± 11.4	-0.77 ± 0.09	-2.39 ± 0.13	151.46 ± 0.15	0.99
090820A	12	40.961	41.985	144.5 ± 15.8	-0.90 ± 0.08	-2.25 ± 0.11	156.40 ± 0.15	1.14
090820A	13	41.985	43.009	139.7 ± 13.8	-0.87 ± 0.08	-2.44 ± 0.16	160.75 ± 0.15	0.93
090820A	14	43.009	44.033	100.6 ± 15.7	-0.77 ± 0.16	-2.07 ± 0.09	163.76 ± 0.13	0.95
090820A	15	44.033	46.081	66.8 ± 16.5	-0.92 ± 0.29	-2.12 ± 0.13	166.77 ± 0.22	1.10
090828	1	44.289	45.534	49.4 ± 0	-0.81 ± 0.28	-1.89 ± 0.21	1.37 ± 0.12	1.00
090828	2	45.534	46.112	65.9 ± 13.5	-0.63 ± 0.00	-1.67 ± 0.13	2.06 ± 0.07	0.94
090828	3	46.112	46.691	45.4 ± 53.9	-0.81 ± 0.91	-1.49 ± 0.08	2.88 ± 0.05	0.92
090828	4	46.691	47.948	136.3 ± 28.9	-1.03 ± 0.00	-1.84 ± 0.04	4.31 ± 0.05	1.05
090828	5	47.948	48.890	80.0 ± 57.2	-0.81 ± 0.23	-1.67 ± 0.11	5.21 ± 0.08	1.14
090828	6	48.890	49.832	62.9 ± 68.4	-0.77 ± 0.70	-1.81 ± 0.08	5.85 ± 0.06	0.98
090828	7	49.832	50.304	70.8 ± 47.5	-0.81 ± 0.84	-2.10 ± 0.12	6.05 ± 0.07	0.90
090828	8	50.368	51.351	63.5 ± 27.1	-1.18 ± 0.00	-1.87 ± 0.16	0.51 ± 0.07	0.93
090828	9	51.351	52.334	75.1 ± 17.5	-0.86 ± 0.29	-2.22 ± 0.19	1.40 ± 0.07	0.97
090828	10	52.334	53.754	212.2 ± 49.1	-1.05 ± 0.10	-1.89 ± 0.09	4.49 ± 0.10	1.00
090828	11	53.754	54.613	176.0 ± 31.7	-0.72 ± 0.14	-2.13 ± 0.18	6.17 ± 0.09	0.92
090828	12	54.613	55.366	175.3 ± 54.9	-0.92 ± 0.17	-1.83 ± 0.09	7.78 ± 0.07	1.06
090828	13	55.366	56.021	235.9 ± 56.2	-0.92 ± 0.12	-1.99 ± 0.15	9.43 ± 0.08	0.88
090828	14	56.021	57.022	208.3 ± 59.4	-1.15 ± 0.12	-2.16 ± 0.29	10.88 ± 0.09	0.95
090828	15	57.022	59.362	104.4 ± 41.5	-0.97 ± 0.26	-1.82 ± 0.08	12.89 ± 0.11	0.98
090828	16	59.362	61.044	81.5 ± 58.0	-1.01 ± 0.53	-1.86 ± 0.14	13.78 ± 0.09	1.00
090828	17	61.044	68.864	21.0 ± 12.5	-1.18 ± 0.00	-1.89 ± 0.06	15.70 ± 0.15	0.95
090829	1	31.744	37.889	35.5 ± 32.0	-1.35 ± 0.00	-1.81 ± 0.07	7.46 ± 0.60	1.03
090829	2	37.889	46.081	132.3 ± 58.7	-1.24 ± 0.19	-1.88 ± 0.07	32.84 ± 0.99	1.08
090829	3	46.081	48.129	344.4 ± 75.5	-1.26 ± 0.06	-2.05 ± 0.11	43.85 ± 0.33	0.94
090829	4	48.129	50.177	286.2 ± 42.8	-1.10 ± 0.06	-2.03 ± 0.07	58.67 ± 0.35	0.91
090829	5	50.177	52.225	95.3 ± 27.1	-1.02 ± 0.23	-1.97 ± 0.07	64.99 ± 0.25	1.04
090829	6	52.225	54.273	147.0 ± 36.8	-1.26 ± 0.11	-2.06 ± 0.10	73.42 ± 0.28	1.02
090829	7	54.273	55.297	65.1 ± 63.0	-1.36 ± 0.51	-1.88 ± 0.07	75.44 ± 0.11	0.95
090902	1	-0.650	-0.021	120.1 ± 34.5	1.05 ± 0.00	-1.42 ± 0.09	0.42 ± 0.04	1.06
090902	2	-0.021	0.194	235.8 ± 104.8	0.63 ± 1.01	-1.81 ± 0.26	0.76 ± 0.04	0.92
090902	3	0.194	0.355	276.6 ± 145.3	0.59 ± 1.10	-1.73 ± 0.24	1.04 ± 0.04	0.95
090902	4	0.355	0.475	312.0 ± 141.9	0.59 ± 0.88	-1.61 ± 0.13	1.42 ± 0.04	0.75
090902	5	0.475	0.586	328.2 ± 90.6	0.93 ± 0.78	-2.50 ± 0.87	1.76 ± 0.04	0.85
090902	6	0.586	0.644	262.5 ± 99.1	0.79 ± 0.93	-2.00 ± 0.38	1.98 ± 0.03	0.79

Table 1—Continued

GRB	Slice#	t_{start} (s)	t_{end} (s)	E_p (keV)	α	β	fluence ^a	χ_r^2
090902	7	0.644	0.762	262.5 ± 58.9	1.05 ± 0.00	-1.45 ± 0.10	2.30 ± 0.03	0.89
090902	8	0.762	0.920	251.6 ± 100.9	0.62 ± 0.86	-1.73 ± 0.18	2.68 ± 0.04	0.84
090902B	1	0.002	1.536	484.4 ± 27.5	-0.35 ± 0.05	-2.94 ± 0.36	7.73 ± 0.18	0.94
090902B	2	1.536	2.560	672.2 ± 41.8	-0.22 ± 0.06	-2.83 ± 0.25	14.78 ± 0.16	1.02
090902B	3	2.560	3.584	614.3 ± 33.6	-0.26 ± 0.05	-2.75 ± 0.20	22.94 ± 0.17	1.01
090902B	4	3.584	4.608	537.4 ± 29.2	-0.19 ± 0.06	-3.08 ± 0.41	29.83 ± 0.17	0.95
090902B	5	4.608	5.632	651.0 ± 37.4	-0.27 ± 0.06	-2.82 ± 0.23	37.61 ± 0.16	1.14
090902B	6	5.632	6.656	821.2 ± 29.9	-0.03 ± 0.05	-3.61 ± 0.42	50.41 ± 0.18	1.08
090902B	7	6.656	7.680	1348.9 ± 56.5	-0.62 ± 0.02	-3.53 ± 0.32	65.22 ± 0.18	1.66
090902B	8	7.680	8.704	1870.3 ± 72.5	-1.00 ± 0.01	-3.61 ± 0.36	85.47 ± 0.19	3.07
090902B	9	8.704	9.728	1973.6 ± 87.3	-1.14 ± 0.01	-3.77 ± 0.58	104.66 ± 0.18	3.05
090902B	10	9.728	10.752	1534.9 ± 64.7	-1.07 ± 0.01	-3.78 ± 0.49	125.30 ± 0.19	3.18
090902B	11	10.752	11.776	1486.3 ± 78.9	-1.06 ± 0.01	-3.27 ± 0.29	142.10 ± 0.17	2.54
090902B	12	11.776	12.800	1017.5 ± 121.8	-1.30 ± 0.02	-2.56 ± 0.20	151.28 ± 0.13	1.11
090902B	13	12.800	13.824	302.5 ± 12.8	-0.81 ± 0.03	-2.55 ± 0.10	163.01 ± 0.15	1.04
090902B	14	13.824	14.848	772.8 ± 28.5	-0.80 ± 0.02	-3.61 ± 0.46	180.66 ± 0.18	1.13
090902B	15	14.848	15.872	858.9 ± 27.4	-0.65 ± 0.02	-3.23 ± 0.19	201.94 ± 0.20	1.22
090902B	16	15.872	16.896	645.8 ± 25.9	-0.75 ± 0.02	-2.87 ± 0.16	217.58 ± 0.19	1.13
090902B	17	16.896	17.920	451.1 ± 26.3	-0.82 ± 0.03	-2.50 ± 0.13	226.88 ± 0.16	1.06
090902B	18	17.920	18.944	373.6 ± 24.0	-0.87 ± 0.03	-2.36 ± 0.10	235.31 ± 0.14	0.93
090902B	19	18.944	19.968	397.9 ± 17.5	-0.73 ± 0.03	-2.48 ± 0.09	247.78 ± 0.16	1.06
090902B	20	19.968	20.992	383.4 ± 19.8	-0.85 ± 0.03	-2.44 ± 0.10	258.65 ± 0.15	1.09
090902B	21	20.992	22.016	223.2 ± 14.5	-0.72 ± 0.05	-2.17 ± 0.06	266.35 ± 0.12	1.05
090902B	22	22.016	25.088	48.1 ± 8.7	-0.51 ± 0.37	-2.02 ± 0.06	271.28 ± 0.21	0.99
090922A	1	0.116	1.256	99.8 ± 21.2	-0.49 ± 0.28	-1.96 ± 0.10	2.09 ± 0.07	0.87
090922A	2	1.256	2.373	138.8 ± 14.7	-0.34 ± 0.14	-2.06 ± 0.08	4.81 ± 0.08	0.99
090922A	3	2.373	2.979	178.6 ± 33.1	-0.72 ± 0.14	-2.10 ± 0.16	6.20 ± 0.06	0.92
090922A	4	2.979	3.756	126.0 ± 40.7	-0.93 ± 0.21	-1.83 ± 0.08	7.64 ± 0.06	0.98
090922A	5	3.756	4.821	101.6 ± 22.4	-0.54 ± 0.26	-1.88 ± 0.08	9.21 ± 0.07	1.01
090922A	6	4.821	6.181	77.0 ± 22.9	-0.47 ± 0.41	-1.77 ± 0.06	10.87 ± 0.07	0.98
090922A	7	6.181	8.397	124.6 ± 54.1	-1.07 ± 0.24	-1.84 ± 0.10	12.57 ± 0.09	0.91
090922A	8	8.397	11.087	55.0 ± 21.1	-0.74 ± 0.60	-2.02 ± 0.14	13.57 ± 0.09	0.96
090922A	9	11.087	14.720	26.7 ± 8.6	-0.91 ± 0.00	-2.10 ± 0.15	14.20 ± 0.08	1.03
090926A	1	7.424	8.448	247.2 ± 11.1	-0.63 ± 0.04	-2.58 ± 0.13	9.35 ± 0.15	0.98
090926A	2	8.448	9.472	280.7 ± 12.6	-0.72 ± 0.03	-2.76 ± 0.20	19.15 ± 0.16	1.13
090926A	3	9.472	10.496	308.5 ± 15.6	-0.95 ± 0.02	-2.32 ± 0.07	33.22 ± 0.18	1.27
090926A	4	10.496	11.520	229.7 ± 9.1	-0.64 ± 0.03	-2.43 ± 0.08	45.62 ± 0.16	1.20
090926A	5	11.520	12.544	177.8 ± 11.0	-0.84 ± 0.04	-2.25 ± 0.07	53.71 ± 0.13	0.98
090926A	6	12.544	14.592	108.1 ± 20.8	-0.89 ± 0.15	-1.95 ± 0.07	58.27 ± 0.18	0.93
090926A	7	14.592	17.664	110.6 ± 13.9	-0.76 ± 0.12	-2.14 ± 0.10	65.47 ± 0.29	1.07
091003	1	14.976	17.024	165.7 ± 60.6	-0.79 ± 0.25	-1.78 ± 0.07	3.35 ± 0.14	0.95
091003	2	17.024	18.048	419.5 ± 67.4	-1.01 ± 0.07	-2.13 ± 0.13	6.83 ± 0.10	1.06
091003	3	18.048	19.072	471.7 ± 30.2	-0.79 ± 0.04	-2.56 ± 0.16	14.27 ± 0.14	0.96
091003	4	19.072	21.120	292.6 ± 44.2	-0.81 ± 0.08	-1.83 ± 0.04	23.53 ± 0.21	1.02
091003	5	21.120	22.144	84.2 ± 27.9	-0.69 ± 0.41	-1.98 ± 0.11	24.64 ± 0.07	0.96
091003	6	22.144	24.192	25.9 ± 20.7	-1.08 ± 0.00	-1.87 ± 0.10	25.65 ± 0.12	0.94
091020	1	-8.192	-1.919	39.0 ± 21.2	-0.33 ± 0.00	-1.68 ± 0.13	1.07 ± 0.16	1.05
091020	2	-1.919	1.710	69.2 ± 44.3	-0.57 ± 0.77	-1.68 ± 0.07	3.10 ± 0.12	1.00
091020	3	1.710	4.819	246.0 ± 103.9	-1.02 ± 0.15	-1.67 ± 0.06	6.74 ± 0.13	1.07
091020	4	4.819	9.079	58.0 ± 26.4	-0.35 ± 0.77	-1.72 ± 0.06	9.17 ± 0.13	1.05
091020	5	9.079	10.905	46.3 ± 21.0	-0.33 ± 0.00	-1.60 ± 0.09	9.90 ± 0.08	0.98
091020	6	10.905	16.384	42.1 ± 26.0	-0.33 ± 0.00	-1.56 ± 0.10	11.01 ± 0.13	1.08
091024	1	-8.192	-1.919	39.0 ± 21.2	-0.33 ± 0.00	-1.68 ± 0.13	1.07 ± 0.16	1.05
091024	2	-1.919	1.710	69.2 ± 44.3	-0.57 ± 0.77	-1.68 ± 0.07	3.10 ± 0.12	1.00
091024	3	1.710	4.819	246.0 ± 103.9	-1.02 ± 0.15	-1.67 ± 0.06	6.74 ± 0.13	1.07
091024	4	4.819	9.079	58.0 ± 26.4	-0.35 ± 0.77	-1.72 ± 0.06	9.17 ± 0.13	1.05
091024	5	9.079	10.905	46.3 ± 21.0	-0.33 ± 0.00	-1.60 ± 0.09	9.90 ± 0.08	0.98
091024	6	10.905	16.384	42.1 ± 26.0	-0.33 ± 0.00	-1.56 ± 0.10	11.01 ± 0.13	1.08
091120	1	0.157	0.651	218.2 ± 81.5	-0.38 ± 0.35	-1.78 ± 0.14	1.46 ± 0.06	1.01
091120	2	1.146	1.430	208.9 ± 48.5	-0.46 ± 0.23	-2.25 ± 0.36	2.95 ± 0.05	0.88
091120	3	1.430	1.714	234.0 ± 60.4	-0.38 ± 0.25	-1.97 ± 0.19	3.84 ± 0.05	0.90
091120	4	1.714	2.106	252.4 ± 65.6	-0.66 ± 0.17	-1.88 ± 0.13	5.19 ± 0.06	0.94
091120	5	2.106	2.506	193.4 ± 53.9	-0.73 ± 0.21	-2.14 ± 0.30	6.05 ± 0.06	0.82
091120	6	2.506	2.907	115.0 ± 99.1	-0.72 ± 0.67	-1.64 ± 0.10	6.64 ± 0.05	0.95
091120	7	4.288	7.323	115.0 ± 27.5	-0.95 ± 0.23	-2.63 ± 0.79	1.23 ± 0.16	0.86
091120	8	7.323	9.373	115.9 ± 31.7	-1.10 ± 0.21	-2.47 ± 0.59	2.35 ± 0.13	0.96
091120	9	9.373	11.498	208.5 ± 47.9	-0.98 ± 0.12	-2.09 ± 0.21	5.08 ± 0.13	0.98

Table 1—Continued

GRB	Slice#	t_{start} (s)	t_{end} (s)	E_p (keV)	α	β	fluence ^a	χ_r^2
091120	10	11.498	13.138	261.4 ± 55.7	-1.00 ± 0.10	-2.25 ± 0.34	7.61 ± 0.12	1.03
091120	11	13.138	15.570	152.0 ± 27.7	-1.05 ± 0.12	-2.56 ± 0.56	9.75 ± 0.15	1.07
091120	12	15.570	19.088	59.5 ± 19.5	-1.08 ± 0.42	-2.29 ± 0.28	10.83 ± 0.13	0.92
091120	13	19.088	21.738	34.5 ± 6.5	0.67 ± 1.40	-2.74 ± 0.41	11.24 ± 0.07	1.02
091120	14	21.738	24.387	35.3 ± 13.8	-1.47 ± 0.66	-2.45 ± 0.50	11.75 ± 0.09	1.02
091120	15	24.387	25.480	103.7 ± 24.8	-0.93 ± 0.23	-2.31 ± 0.30	12.74 ± 0.09	0.98
091120	16	25.480	26.260	128.8 ± 24.8	-1.12 ± 0.15	-2.98 ± 1.41	13.64 ± 0.09	0.97
091120	17	26.260	26.839	198.8 ± 18.4	-0.92 ± 0.08	-3.31 ± 0.00	15.32 ± 0.07	1.00
091120	18	26.839	27.238	111.6 ± 19.7	-0.75 ± 0.20	-2.44 ± 0.31	16.13 ± 0.06	0.92
091120	19	27.238	27.952	92.2 ± 9.4	-0.85 ± 0.17	-3.31 ± 0.00	16.84 ± 0.04	0.95
091120	20	27.952	29.656	60.2 ± 14.4	-0.74 ± 0.42	-2.29 ± 0.22	17.77 ± 0.09	0.89
091120	21	29.632	31.963	62.5 ± 9.3	-0.21 ± 0.43	-2.57 ± 0.29	0.98 ± 0.10	0.93
091120	22	31.963	33.835	72.0 ± 8.1	-0.91 ± 0.23	-3.41 ± 0.00	1.71 ± 0.05	0.91
091120	23	33.835	35.959	100.4 ± 14.2	-0.97 ± 0.15	-2.62 ± 0.40	3.43 ± 0.13	0.93
091120	24	35.959	39.115	78.4 ± 10.3	-0.98 ± 0.23	-3.41 ± 0.00	4.34 ± 0.07	0.81
091120	25	39.115	46.989	33.4 ± 16.3	-1.05 ± 0.00	-2.48 ± 0.73	4.75 ± 0.14	1.02
091120	26	46.989	49.614	71.1 ± 16.5	-1.33 ± 0.29	-3.41 ± 0.00	5.30 ± 0.06	0.87
091120	27	49.614	52.635	81.7 ± 12.9	-0.97 ± 0.19	-2.45 ± 0.27	7.11 ± 0.14	0.99
091120	28	52.635	55.416	75.9 ± 18.4	-1.00 ± 0.31	-2.51 ± 0.48	8.08 ± 0.12	0.99
091127	1	0.274	0.382	47.0 ± 4.1	0.31 ± 0.31	-2.15 ± 0.05	2.49 ± 0.03	0.80
091127	2	0.382	0.489	52.6 ± 5.5	-0.30 ± 0.24	-2.15 ± 0.06	3.50 ± 0.03	0.86
091127	3	0.489	0.749	54.6 ± 4.3	-0.66 ± 0.15	-2.24 ± 0.05	5.32 ± 0.05	0.86
091127	4	0.749	0.950	52.3 ± 5.6	-0.65 ± 0.21	-2.27 ± 0.08	6.24 ± 0.03	0.95
091127	5	0.950	1.087	45.1 ± 8.0	-0.92 ± 0.31	-2.27 ± 0.11	6.69 ± 0.03	1.03
091127	6	1.087	1.224	55.1 ± 13.8	-0.92 ± 0.31	-2.05 ± 0.08	7.27 ± 0.03	0.90
091127	7	1.224	1.304	58.4 ± 16.3	-0.57 ± 0.39	-1.84 ± 0.05	7.92 ± 0.03	0.98
091127	8	1.304	1.439	93.2 ± 18.6	-0.86 ± 0.16	-1.87 ± 0.05	9.28 ± 0.04	0.88
091127	9	1.439	1.495	138.9 ± 24.3	-0.86 ± 0.13	-2.15 ± 0.13	9.98 ± 0.03	0.82
091127	10	1.495	1.652	64.8 ± 20.3	-0.85 ± 0.28	-1.75 ± 0.03	11.35 ± 0.04	0.89
091127	11	1.652	2.014	42.6 ± 15.6	-0.86 ± 0.45	-1.80 ± 0.03	12.77 ± 0.05	0.94
091127	12	2.014	2.650	48.4 ± 16.9	-0.90 ± 0.41	-1.90 ± 0.06	13.73 ± 0.05	0.97
091127	13	2.650	3.456	50.4 ± 14.6	-0.92 ± 0.36	-1.99 ± 0.08	14.63 ± 0.05	1.05
091127	14	3.584	4.096	33.0 ± 2.9	-0.79 ± 0.31	-2.71 ± 0.18	14.85 ± 0.03	0.99
091127	15	4.096	4.608	17.6 ± 3.2	-1.44 ± 0.39	-2.72 ± 0.17	15.26 ± 0.02	0.95
091127	16	4.608	5.120	10.8 ± 9.1	-1.61 ± 0.83	-2.60 ± 0.13	15.59 ± 0.02	0.94
091127	17	5.120	5.632	14.6 ± 2.1	-1.25 ± 0.00	-2.57 ± 0.11	15.94 ± 0.02	1.02
091127	18	5.632	6.144	17.6 ± 2.5	-1.24 ± 0.47	-2.83 ± 0.19	16.29 ± 0.02	0.98
091127	19	6.144	6.912	22.0 ± 1.5	-1.30 ± 0.20	-2.82 ± 0.13	17.22 ± 0.03	0.97
091127	20	6.912	7.168	22.0 ± 2.0	-1.38 ± 0.25	-2.73 ± 0.13	17.79 ± 0.02	1.14
091127	21	7.168	7.680	15.9 ± 2.0	-1.35 ± 0.31	-2.76 ± 0.09	18.59 ± 0.03	0.90
091127	22	7.680	8.192	11.1 ± 4.2	-1.32 ± 0.74	-2.83 ± 0.10	19.06 ± 0.02	0.98
091127	23	8.192	8.704	8.7 ± 2.8	-1.25 ± 0.00	-2.49 ± 0.07	19.43 ± 0.02	0.98
091127	24	8.704	9.216	9.7 ± 2.9	-1.25 ± 0.00	-2.49 ± 0.09	19.71 ± 0.02	1.06
091127	25	9.216	10.240	11.4 ± 2.1	-1.25 ± 0.00	-2.70 ± 0.16	19.98 ± 0.02	1.05
100116A	1	80.384	88.871	494.1 ± 136.3	-1.01 ± 0.08	-2.01 ± 0.25	4.82 ± 0.24	0.96
100116A	2	88.871	90.642	1208.6 ± 206.5	-0.82 ± 0.05	-2.61 ± 0.42	9.27 ± 0.12	0.98
100116A	3	90.642	91.826	1396.4 ± 243.5	-0.85 ± 0.05	-2.52 ± 0.35	13.27 ± 0.11	0.86
100116A	4	91.826	92.621	1632.9 ± 309.6	-0.92 ± 0.04	-2.36 ± 0.27	16.83 ± 0.09	0.96
100116A	5	92.621	93.291	1683.3 ± 335.0	-1.00 ± 0.04	-2.52 ± 0.39	20.04 ± 0.08	0.98
100116A	6	93.291	93.903	2201.0 ± 408.8	-1.00 ± 0.03	-2.61 ± 0.45	23.13 ± 0.08	0.97
100116A	7	93.903	94.626	1577.2 ± 246.6	-0.99 ± 0.03	-2.85 ± 0.00	26.41 ± 0.09	0.85
100116A	8	94.626	96.996	1004.4 ± 185.8	-1.08 ± 0.03	-2.13 ± 0.17	32.44 ± 0.16	0.99
100116A	9	96.996	106.624	667.7 ± 245.9	-1.03 ± 0.09	-2.18 ± 0.52	36.45 ± 0.31	1.01
100122A	1	18.432	19.456	17.8 ± 4.5	-0.93 ± 0.00	-2.18 ± 0.09	0.53 ± 0.05	0.89
100122A	2	19.456	20.480	32.7 ± 3.5	-0.90 ± 0.26	-2.29 ± 0.06	2.47 ± 0.07	1.00
100122A	3	20.480	22.528	53.9 ± 4.1	-0.93 ± 0.12	-2.38 ± 0.07	8.49 ± 0.18	1.08
100122A	4	22.528	23.552	46.1 ± 5.0	-0.70 ± 0.22	-2.28 ± 0.08	10.30 ± 0.08	1.14
100122A	5	23.552	24.576	43.1 ± 6.8	-0.64 ± 0.34	-2.23 ± 0.10	11.46 ± 0.07	1.02
100122A	6	24.576	27.648	29.8 ± 7.3	-0.93 ± 0.00	-2.08 ± 0.13	13.04 ± 0.17	1.02
100206	1	-0.032	0.000	395.2 ± 118.4	-0.34 ± 0.25	-2.54 ± 1.02	0.22 ± 0.02	0.82
100206	2	0.000	0.032	1018.5 ± 227.2	-0.52 ± 0.12	-3.15 ± 1.38	0.71 ± 0.03	0.90
100206	3	0.032	0.064	880.8 ± 241.0	-0.53 ± 0.15	-2.16 ± 0.00	1.11 ± 0.03	0.89
100206	4	0.064	0.096	479.7 ± 131.9	-0.24 ± 0.22	-2.03 ± 0.27	1.44 ± 0.03	0.83
100206	5	0.096	0.128	165.9 ± 95.7	-0.33 ± 0.80	-2.16 ± 0.00	1.48 ± 0.01	0.81
100206	6	0.160	0.192	209.0 ± 132.1	-0.73 ± 0.51	-2.16 ± 0.00	1.56 ± 0.01	0.68
100528A	1	-3.072	3.157	156.0 ± 42.8	-0.89 ± 0.16	-1.81 ± 0.08	3.94 ± 0.15	1.02
100528A	2	3.157	4.822	448.0 ± 147.1	-1.14 ± 0.08	-1.85 ± 0.12	6.67 ± 0.11	0.92

Table 1—Continued

GRB	Slice#	t_{start} (s)	t_{end} (s)	E_p (keV)	α	β	fluence ^a	χ_r^2
100528A	3	4.822	6.170	274.3 ± 58.6	-0.89 ± 0.10	-1.87 ± 0.09	9.30 ± 0.09	1.05
100528A	4	6.170	7.134	490.3 ± 116.6	-1.08 ± 0.06	-2.03 ± 0.16	11.87 ± 0.10	1.00
100528A	5	7.134	7.940	276.7 ± 74.2	-0.92 ± 0.11	-1.72 ± 0.06	14.19 ± 0.07	0.96
100528A	6	7.940	8.830	385.6 ± 93.1	-0.92 ± 0.09	-1.81 ± 0.08	16.68 ± 0.08	0.98
100528A	7	8.830	9.608	434.5 ± 104.6	-1.05 ± 0.07	-1.99 ± 0.14	18.93 ± 0.09	0.99
100528A	8	9.608	10.563	263.0 ± 45.5	-0.91 ± 0.09	-2.12 ± 0.18	21.14 ± 0.08	0.83
100528A	9	10.563	11.578	215.7 ± 76.2	-1.08 ± 0.13	-1.76 ± 0.07	23.14 ± 0.07	0.92
100528A	10	11.578	12.654	203.8 ± 42.6	-0.89 ± 0.11	-1.91 ± 0.10	25.28 ± 0.07	1.08
100528A	11	12.654	14.859	84.6 ± 33.5	-1.03 ± 0.27	-1.84 ± 0.07	27.23 ± 0.09	0.92
100528A	12	14.859	20.559	197.2 ± 100.0	-1.41 ± 0.12	-1.95 ± 0.19	30.00 ± 0.15	1.15
100528A	13	20.559	25.088	46.7 ± 35.0	-1.13 ± 0.83	-2.07 ± 0.23	30.71 ± 0.10	1.04
100612	1	-0.512	1.695	173.1 ± 29.2	-0.43 ± 0.16	-1.89 ± 0.10	3.00 ± 0.13	1.08
100612	2	1.695	2.574	115.4 ± 13.6	0.07 ± 0.21	-1.96 ± 0.08	5.28 ± 0.10	0.83
100612	3	2.574	3.215	117.9 ± 9.7	-0.10 ± 0.15	-2.61 ± 0.23	6.84 ± 0.09	0.95
100612	4	3.215	3.689	109.4 ± 12.5	-0.19 ± 0.18	-2.14 ± 0.11	8.51 ± 0.08	0.99
100612	5	3.689	4.110	101.3 ± 13.3	-0.23 ± 0.20	-2.00 ± 0.08	10.25 ± 0.07	0.96
100612	6	4.110	4.513	131.7 ± 13.3	-0.52 ± 0.13	-2.65 ± 0.31	11.59 ± 0.08	1.02
100612	7	4.513	4.939	84.4 ± 7.9	-0.26 ± 0.19	-2.47 ± 0.17	12.79 ± 0.07	1.01
100612	8	4.939	5.515	84.0 ± 8.8	-0.47 ± 0.18	-2.47 ± 0.18	14.00 ± 0.07	0.99
100612	9	5.515	6.479	79.6 ± 10.7	-0.81 ± 0.18	-2.41 ± 0.21	15.23 ± 0.09	1.02
100612	10	6.479	8.548	60.1 ± 10.1	-0.93 ± 0.24	-2.36 ± 0.20	16.53 ± 0.10	0.88
100612	11	8.548	13.312	30.0 ± 15.3	-0.65 ± 1.20	-1.98 ± 0.11	17.77 ± 0.13	1.00
100625A	1	-0.512	1.695	173.1 ± 29.2	-0.43 ± 0.16	-1.89 ± 0.10	3.00 ± 0.13	1.08
100625A	2	1.695	2.574	115.4 ± 13.6	0.07 ± 0.21	-1.96 ± 0.08	5.28 ± 0.10	0.83
100625A	3	2.574	3.215	117.9 ± 9.7	-0.10 ± 0.15	-2.61 ± 0.23	6.84 ± 0.09	0.95
100625A	4	3.215	3.689	109.4 ± 12.5	-0.19 ± 0.18	-2.14 ± 0.11	8.51 ± 0.08	0.99
100625A	5	3.689	4.110	101.3 ± 13.3	-0.23 ± 0.20	-2.00 ± 0.08	10.25 ± 0.07	0.96
100625A	6	4.110	4.513	131.7 ± 13.3	-0.52 ± 0.13	-2.65 ± 0.31	11.59 ± 0.08	1.02
100625A	7	4.513	4.939	84.4 ± 7.9	-0.26 ± 0.19	-2.47 ± 0.17	12.79 ± 0.07	1.01
100625A	8	4.939	5.515	84.0 ± 8.8	-0.47 ± 0.18	-2.47 ± 0.18	14.00 ± 0.07	0.99
100625A	9	5.515	6.479	79.6 ± 10.7	-0.81 ± 0.18	-2.41 ± 0.21	15.23 ± 0.09	1.02
100625A	10	6.479	8.548	60.1 ± 10.1	-0.93 ± 0.24	-2.36 ± 0.20	16.53 ± 0.10	0.88
100625A	11	8.548	13.312	30.0 ± 15.3	-0.65 ± 1.20	-1.98 ± 0.11	17.77 ± 0.13	1.00
100701B	1	0.002	1.952	2588.4 ± 834.8	-0.94 ± 0.07	-2.27 ± 0.40	3.78 ± 0.20	1.01
100701B	2	1.952	4.000	1586.6 ± 140.6	-0.58 ± 0.04	-2.35 ± 0.11	19.84 ± 0.34	0.91
100701B	3	4.000	5.024	1157.9 ± 133.1	-0.65 ± 0.05	-2.59 ± 0.24	25.31 ± 0.14	1.01
100701B	4	5.024	7.072	829.4 ± 207.1	-0.75 ± 0.10	-2.31 ± 0.35	29.57 ± 0.24	0.90
100701B	5	7.072	9.120	574.3 ± 232.7	-0.88 ± 0.18	-2.54 ± 0.00	31.35 ± 0.21	0.89
100701B	6	9.120	10.144	751.5 ± 301.6	-0.66 ± 0.20	-2.49 ± 0.95	32.42 ± 0.11	0.86
100701B	7	10.144	12.192	591.8 ± 149.3	-0.54 ± 0.15	-2.04 ± 0.20	36.08 ± 0.24	1.04
100701B	8	12.192	13.216	168.4 ± 163.0	-0.77 ± 0.00	-1.44 ± 0.13	36.41 ± 0.05	0.96
100707	1	-0.960	1.088	577.6 ± 32.5	0.47 ± 0.10	-2.35 ± 0.08	26.10 ± 0.57	1.01
100707	2	1.088	2.112	417.8 ± 15.8	0.35 ± 0.06	-2.39 ± 0.06	45.47 ± 0.30	1.13
100707	3	2.112	3.136	277.3 ± 11.8	0.26 ± 0.07	-2.41 ± 0.08	57.85 ± 0.22	1.02
100707	4	3.136	4.160	177.1 ± 9.2	0.29 ± 0.10	-2.36 ± 0.09	65.89 ± 0.18	1.01
100707	5	4.160	5.184	139.6 ± 8.5	0.08 ± 0.11	-2.39 ± 0.10	71.41 ± 0.16	1.00
100707	6	5.184	7.232	130.4 ± 10.8	-0.06 ± 0.13	-2.28 ± 0.11	79.19 ± 0.29	1.14
100707	7	7.232	10.304	96.0 ± 10.1	0.35 ± 0.26	-2.12 ± 0.10	86.85 ± 0.38	1.01
100707	8	10.304	13.376	62.9 ± 6.8	0.84 ± 0.44	-2.26 ± 0.12	91.57 ± 0.32	1.10
100707	9	13.376	18.496	59.2 ± 6.5	0.04 ± 0.38	-2.54 ± 0.00	95.84 ± 0.23	0.97
100707	10	18.496	24.640	48.1 ± 13.7	-0.68 ± 0.58	-2.44 ± 0.38	98.68 ± 0.46	1.03
100724B	1	8.714	11.355	429.9 ± 54.2	-0.56 ± 0.07	-1.75 ± 0.04	20.45 ± 0.19	1.07
100724B	2	11.355	13.963	434.1 ± 54.9	-0.61 ± 0.07	-1.81 ± 0.05	27.63 ± 0.18	0.98
100724B	3	13.963	16.008	553.5 ± 72.6	-0.68 ± 0.06	-1.79 ± 0.05	34.98 ± 0.19	0.94
100724B	4	16.008	17.907	686.4 ± 91.9	-0.69 ± 0.05	-1.78 ± 0.05	42.54 ± 0.19	1.09
100724B	5	17.907	20.276	567.6 ± 79.4	-0.73 ± 0.06	-1.79 ± 0.05	49.98 ± 0.19	0.94
100724B	6	20.276	25.444	418.3 ± 38.7	-0.67 ± 0.05	-1.89 ± 0.05	62.99 ± 0.26	0.95
100724B	7	25.444	30.914	374.7 ± 63.6	-0.81 ± 0.08	-1.85 ± 0.08	70.06 ± 0.22	1.04
100724B	8	30.914	35.328	198.3 ± 56.3	-0.64 ± 0.19	-1.71 ± 0.07	73.60 ± 0.15	0.95
100724B	9	35.328	36.888	221.2 ± 97.3	-0.58 ± 0.31	-1.71 ± 0.12	1.29 ± 0.09	1.01
100724B	10	36.888	38.448	364.4 ± 128.5	-0.84 ± 0.15	-1.82 ± 0.14	3.11 ± 0.11	0.96
100724B	11	38.448	39.323	489.1 ± 89.0	-0.75 ± 0.09	-2.13 ± 0.19	5.65 ± 0.12	0.85
100724B	12	39.323	40.239	263.5 ± 60.9	-0.63 ± 0.14	-1.73 ± 0.07	8.01 ± 0.09	0.99
100724B	13	40.239	41.505	231.7 ± 50.8	-0.55 ± 0.16	-1.78 ± 0.08	10.42 ± 0.10	0.92
100724B	14	41.505	43.526	246.7 ± 48.6	-0.66 ± 0.14	-2.06 ± 0.19	12.79 ± 0.12	0.95
100724B	15	43.526	45.335	330.7 ± 64.6	-0.78 ± 0.11	-2.22 ± 0.31	15.25 ± 0.13	1.01
100724B	16	45.335	47.650	262.1 ± 38.8	-0.56 ± 0.11	-1.84 ± 0.07	19.80 ± 0.14	1.25

Table 1—Continued

GRB	Slice#	t_{start} (s)	t_{end} (s)	E_p (keV)	α	β	fluence ^a	χ_r^2
100724B	17	47.650	49.576	228.0 ± 68.4	-0.74 ± 0.17	-1.77 ± 0.09	22.10 ± 0.11	1.07
100724B	18	49.576	52.117	218.1 ± 45.1	-0.58 ± 0.16	-1.94 ± 0.13	24.77 ± 0.13	1.15
100724B	19	52.096	55.221	402.4 ± 56.7	-0.80 ± 0.07	-2.10 ± 0.15	5.54 ± 0.18	0.98
100724B	20	55.221	58.347	445.0 ± 33.3	-0.70 ± 0.04	-2.41 ± 0.18	15.41 ± 0.23	0.96
100724B	21	58.347	59.866	396.2 ± 37.4	-0.65 ± 0.06	-2.03 ± 0.08	22.26 ± 0.16	0.99
100724B	22	59.866	61.263	407.9 ± 35.9	-0.70 ± 0.05	-2.24 ± 0.13	28.68 ± 0.16	1.06
100724B	23	61.263	62.698	436.6 ± 45.9	-0.68 ± 0.05	-1.91 ± 0.06	35.78 ± 0.16	1.02
100724B	24	62.698	65.421	426.3 ± 28.9	-0.66 ± 0.04	-2.03 ± 0.05	49.40 ± 0.22	1.06
100724B	25	65.421	66.958	480.0 ± 42.1	-0.68 ± 0.05	-2.18 ± 0.11	56.75 ± 0.18	0.91
100724B	26	66.958	68.499	452.1 ± 39.9	-0.71 ± 0.05	-2.23 ± 0.12	63.76 ± 0.17	0.99
100724B	27	68.499	70.249	530.5 ± 52.7	-0.82 ± 0.04	-2.19 ± 0.12	71.18 ± 0.19	1.02
100724B	28	70.249	72.000	360.1 ± 45.2	-0.70 ± 0.07	-1.95 ± 0.08	76.43 ± 0.14	1.06
100724B	29	71.936	73.263	313.9 ± 54.7	-0.69 ± 0.10	-1.88 ± 0.09	3.20 ± 0.11	0.96
100724B	30	73.263	74.063	394.3 ± 51.5	-0.55 ± 0.09	-1.98 ± 0.09	6.72 ± 0.11	0.83
100724B	31	74.063	75.232	419.0 ± 40.3	-0.57 ± 0.06	-1.99 ± 0.07	13.01 ± 0.15	1.03
100724B	32	75.232	76.421	440.1 ± 43.2	-0.64 ± 0.06	-1.99 ± 0.07	19.51 ± 0.15	1.03
100724B	33	76.421	77.303	425.0 ± 63.7	-0.82 ± 0.07	-2.25 ± 0.23	22.45 ± 0.12	0.87
100724B	34	77.303	80.388	337.6 ± 42.7	-0.79 ± 0.07	-2.00 ± 0.09	28.78 ± 0.17	1.05
100724B	35	80.388	86.175	268.4 ± 70.7	-0.78 ± 0.14	-1.79 ± 0.09	33.06 ± 0.18	1.05
100724B	36	86.175	90.543	141.3 ± 59.5	-0.18 ± 0.52	-1.59 ± 0.07	35.27 ± 0.13	1.05
100724B	37	90.543	94.912	145.1 ± 47.1	-0.01 ± 0.51	-1.80 ± 0.14	37.05 ± 0.14	1.03
100724B	38	94.976	107.261	169.6 ± 49.5	-0.23 ± 0.35	-1.73 ± 0.10	4.12 ± 0.24	1.07
100724B	39	114.308	118.608	166.6 ± 36.6	-1.00 ± 0.17	-13.20 ± 0.00	8.03 ± 0.14	0.95
100724B	40	118.608	122.908	187.6 ± 25.6	-1.02 ± 0.10	-13.20 ± 0.00	10.17 ± 0.16	0.95
100724B	41	122.908	127.219	198.5 ± 33.7	-1.05 ± 0.11	-13.20 ± 0.00	12.01 ± 0.16	0.96
100724B	42	127.219	128.615	184.3 ± 24.2	-0.99 ± 0.10	-13.20 ± 0.00	13.29 ± 0.09	1.00
100724B	43	128.615	130.268	176.6 ± 22.3	-0.97 ± 0.10	-13.20 ± 0.00	14.64 ± 0.10	1.05
100724B	44	130.268	132.863	170.4 ± 31.0	-1.22 ± 0.11	-13.20 ± 0.00	16.03 ± 0.12	0.89
100728A	1	-3.072	7.932	520.0 ± 103.4	-0.34 ± 0.21	-6.07 ± 0.00	4.81 ± 0.41	1.20
100728A	2	7.932	15.886	448.2 ± 129.3	-0.47 ± 0.20	-2.08 ± 0.37	8.95 ± 0.31	1.05
100728A	3	15.886	19.506	291.2 ± 94.4	-0.45 ± 0.26	-1.95 ± 0.29	11.04 ± 0.15	1.03
100728A	4	19.506	27.788	286.4 ± 56.8	-0.58 ± 0.20	-6.07 ± 0.00	13.47 ± 0.29	0.87
100728A	5	27.788	32.448	333.8 ± 108.2	-0.88 ± 0.20	-6.07 ± 0.00	14.94 ± 0.21	0.92
100728A	6	32.448	42.334	295.5 ± 75.4	-0.83 ± 0.18	-6.07 ± 0.00	17.41 ± 0.32	1.13
100728A	7	49.005	55.530	417.2 ± 47.5	-0.55 ± 0.08	-3.14 ± 1.45	6.71 ± 0.32	1.11
100728A	8	55.530	59.938	397.2 ± 50.9	-0.53 ± 0.09	-2.44 ± 0.39	12.46 ± 0.23	1.15
100728A	9	59.938	65.481	422.3 ± 61.0	-0.58 ± 0.09	-2.30 ± 0.32	18.72 ± 0.26	0.97
100728A	10	65.481	70.701	505.8 ± 49.5	-0.61 ± 0.07	-3.29 ± 0.00	25.82 ± 0.27	0.97
100728A	11	70.701	75.361	548.5 ± 49.4	-0.55 ± 0.07	-3.29 ± 0.00	33.45 ± 0.26	1.03
100728A	12	75.361	79.109	604.8 ± 62.8	-0.65 ± 0.06	-2.69 ± 0.49	41.41 ± 0.28	1.14
100728A	13	79.109	89.998	456.2 ± 20.7	-0.57 ± 0.03	-3.31 ± 0.72	66.30 ± 0.51	1.23
100728A	14	89.998	98.633	333.3 ± 32.9	-0.75 ± 0.06	-2.76 ± 0.61	75.64 ± 0.30	1.06
100728A	15	98.633	107.065	204.9 ± 46.4	-0.80 ± 0.14	-2.03 ± 0.20	80.25 ± 0.23	1.06
100728A	16	107.840	110.764	324.7 ± 37.4	-0.60 ± 0.10	-3.49 ± 0.00	2.90 ± 0.17	1.18
100728A	17	110.764	112.219	327.7 ± 82.4	-0.80 ± 0.12	-1.94 ± 0.18	5.19 ± 0.10	0.89
100728A	18	112.219	119.001	193.1 ± 39.9	-1.04 ± 0.14	-3.49 ± 0.00	7.11 ± 0.18	1.11
100728A	19	119.001	123.930	255.4 ± 35.3	-0.76 ± 0.12	-3.49 ± 0.00	9.76 ± 0.18	1.08
100728A	20	123.930	126.140	318.0 ± 48.0	-0.51 ± 0.12	-2.50 ± 0.51	12.60 ± 0.14	1.10
100728A	21	126.140	131.854	275.0 ± 27.3	-0.75 ± 0.08	-3.49 ± 0.00	16.96 ± 0.22	1.00
100728A	22	131.854	135.559	370.0 ± 59.9	-0.84 ± 0.10	-3.49 ± 0.00	19.84 ± 0.20	1.04
100728A	23	135.559	139.264	204.3 ± 44.3	-0.75 ± 0.16	-2.43 ± 0.59	21.93 ± 0.17	0.93
100728A	24	139.264	145.092	50.1 ± 24.3	-0.71 ± 0.76	-1.96 ± 0.14	23.32 ± 0.15	0.96
100728A	25	145.092	150.921	27.0 ± 16.0	-0.97 ± 0.00	-2.01 ± 0.20	23.90 ± 0.12	1.01
100728A	26	150.921	162.015	142.6 ± 53.7	-1.08 ± 0.24	-2.55 ± 1.21	25.73 ± 0.30	1.13
100728A	27	162.015	167.972	250.8 ± 50.2	-0.95 ± 0.13	-3.49 ± 0.00	27.92 ± 0.20	0.89
100728A	28	167.972	174.503	107.5 ± 35.9	-0.81 ± 0.31	-2.07 ± 0.24	29.75 ± 0.19	0.90
100728A	29	174.503	180.545	255.0 ± 58.0	-1.10 ± 0.09	-2.40 ± 0.59	33.51 ± 0.21	1.01
100728A	30	180.545	182.481	254.2 ± 91.6	-0.52 ± 0.27	-1.82 ± 0.19	35.04 ± 0.10	1.09
100728A	31	182.481	184.416	193.4 ± 78.2	-0.60 ± 0.33	-2.05 ± 0.40	36.02 ± 0.10	0.90
100728A	32	184.416	188.288	258.6 ± 0.0	-1.36 ± 0.20	-1.69 ± 0.28	36.73 ± 0.11	0.94
100814A	1	-0.343	1.362	258.9 ± 55.8	0.28 ± 0.37	-2.12 ± 0.33	1.68 ± 0.13	1.00
100814A	2	1.362	4.189	136.1 ± 22.0	0.96 ± 0.53	-1.78 ± 0.08	4.37 ± 0.13	1.25
100814A	3	4.189	7.411	116.7 ± 14.8	1.59 ± 0.64	-1.98 ± 0.13	6.88 ± 0.16	1.07
100814A	4	7.411	8.858	117.8 ± 26.8	1.16 ± 0.83	-1.66 ± 0.07	8.42 ± 0.09	0.88
100814A	5	8.858	10.958	108.9 ± 24.7	0.72 ± 0.69	-1.88 ± 0.15	9.75 ± 0.12	0.90
100814A	6	10.958	13.061	103.8 ± 22.0	0.50 ± 0.60	-2.15 ± 0.29	10.73 ± 0.13	0.85
100814A	7	13.061	17.266	82.2 ± 14.4	0.15 ± 0.00	-1.62 ± 0.09	12.35 ± 0.13	1.16

Table 1—Continued

GRB	Slice#	t_{start} (s)	t_{end} (s)	E_p (keV)	α	β	fluence ^a	χ_r^2
100814A	8	17.266	22.801	52.6 ± 16.7	0.15 ± 0.00	-1.47 ± 0.07	13.92 ± 0.13	1.19
100814A	9	22.801	30.484	57.0 ± 11.0	0.27 ± 0.83	-3.25 ± 1.44	14.49 ± 0.14	1.10
100814A	10	30.484	42.819	24.1 ± 14.7	0.15 ± 0.00	-1.88 ± 0.00	15.04 ± 0.12	1.15
100814A	11	43.072	55.092	18.7 ± 13.2	2.18 ± 0.00	-1.94 ± 0.00	0.30 ± 0.10	1.04
100814A	12	55.092	67.113	20.6 ± 8.5	2.18 ± 0.00	-1.61 ± 0.12	1.51 ± 0.22	0.99
100814A	13	67.113	73.239	26.5 ± 5.4	2.18 ± 0.00	-1.66 ± 0.10	2.71 ± 0.15	1.02
100814A	14	73.239	80.843	33.7 ± 5.5	2.18 ± 0.00	-1.73 ± 0.12	4.06 ± 0.18	1.03
100814A	15	80.843	88.156	32.9 ± 6.6	2.18 ± 0.00	-1.93 ± 0.22	4.78 ± 0.16	1.14
100814A	16	88.156	108.047	29.1 ± 9.7	2.18 ± 0.00	-1.80 ± 0.25	5.77 ± 0.29	1.09
100814A	17	112.049	122.146	56.9 ± 18.0	1.93 ± 0	-2.44 ± 1.04	1.11 ± 0.18	1.05
100814A	18	122.146	142.339	21.1 ± 17.2	1.93 ± 0	-1.63 ± 0.25	1.86 ± 0.27	1.06
100814A	19	142.339	149.070	31.8 ± 7.2	1.93 ± 0.00	-1.89 ± 0.22	2.52 ± 0.15	0.97
100814A	20	149.070	152.791	13.9 ± 11.6	1.93 ± 0.00	-1.62 ± 0.09	3.24 ± 0.11	0.87
100814A	21	152.791	161.452	25.2 ± 10.1	1.93 ± 0.00	-2.10 ± 0.48	3.53 ± 0.14	0.99
100906A	1	-0.256	1.744	494.2 ± 154.7	-0.90 ± 0.13	-2.02 ± 0.20	3.35 ± 0.19	1.01
100906A	2	1.744	3.096	80.0 ± 24.0	0.37 ± 0.81	-1.71 ± 0.06	5.61 ± 0.10	0.91
100906A	3	3.096	4.905	126.8 ± 47.2	-0.58 ± 0.39	-1.82 ± 0.10	7.81 ± 0.12	0.90
100906A	4	4.905	5.839	148.2 ± 33.4	-0.87 ± 0.00	-1.74 ± 0.09	9.26 ± 0.09	1.07
100906A	5	5.839	8.104	112.6 ± 44.7	-0.70 ± 0.37	-1.75 ± 0.06	12.37 ± 0.13	1.04
100906A	6	8.104	9.885	181.9 ± 39.0	-0.71 ± 0.17	-1.95 ± 0.11	16.05 ± 0.14	0.89
100906A	7	9.885	11.503	181.0 ± 48.9	-0.86 ± 0.18	-1.92 ± 0.11	19.22 ± 0.13	0.87
100906A	8	11.503	12.285	100.2 ± 45.2	-0.44 ± 0.65	-1.94 ± 0.18	20.11 ± 0.08	0.96
100906A	9	12.285	14.067	44.0 ± 22.0	-0.87 ± 0.00	-1.70 ± 0.07	21.52 ± 0.11	1.03
100906A	10	14.067	15.849	38.9 ± 25.8	-0.87 ± 0.00	-1.73 ± 0.09	22.57 ± 0.10	0.99
100906A	11	15.849	18.741	30.3 ± 27.0	-0.87 ± 0.00	-1.86 ± 0.16	23.31 ± 0.13	0.84
101014A	1	0.003	1.536	260.6 ± 11.3	-0.47 ± 0.05	-2.65 ± 0.13	11.89 ± 0.21	1.07
101014A	2	1.536	2.560	286.5 ± 15.1	-0.70 ± 0.04	-2.81 ± 0.22	20.59 ± 0.18	0.93
101014A	3	2.560	4.608	200.2 ± 16.2	-0.99 ± 0.07	-2.97 ± 0.00	27.10 ± 0.24	1.18
101014A	4	4.608	5.632	100.8 ± 7.9	-0.97 ± 0.10	-2.97 ± 0.00	29.26 ± 0.08	0.95
101014A	5	5.632	6.656	120.4 ± 12.4	-0.89 ± 0.10	-2.61 ± 0.22	32.30 ± 0.12	0.88
101014A	6	6.656	7.680	196.7 ± 15.1	-0.68 ± 0.07	-2.53 ± 0.16	37.48 ± 0.14	0.98
101014A	7	7.680	8.704	114.5 ± 7.8	-0.70 ± 0.09	-3.08 ± 0.34	40.73 ± 0.12	1.10
101014A	8	8.704	9.728	86.0 ± 5.3	-0.82 ± 0.10	-2.97 ± 0.00	43.17 ± 0.08	1.06
101014A	9	9.728	10.752	86.7 ± 9.8	-0.93 ± 0.14	-2.73 ± 0.30	44.95 ± 0.10	0.84
101014A	10	10.752	14.848	29.1 ± 5.6	0.28 ± 1.19	-2.61 ± 0.30	46.53 ± 0.22	0.95
101014A	11	14.848	20.992	27.9 ± 10.4	-1.14 ± 0.00	-2.97 ± 0.00	47.28 ± 0.15	0.82
101014A	12	20.992	23.040	42.9 ± 8.6	0.04 ± 0.57	-1.90 ± 0.05	51.52 ± 0.20	1.02
101014A	13	23.040	25.088	42.9 ± 10.9	-0.40 ± 0.64	-2.20 ± 0.16	53.14 ± 0.16	1.04
101014A	14	25.088	26.112	190.7 ± 22.7	-1.00 ± 0.08	-2.72 ± 0.43	56.00 ± 0.12	0.86
101014A	15	26.112	27.136	223.8 ± 25.6	-0.81 ± 0.08	-2.22 ± 0.12	60.45 ± 0.13	1.10
101014A	16	27.136	28.160	279.3 ± 24.6	-0.90 ± 0.05	-2.60 ± 0.26	65.68 ± 0.14	1.00
101014A	17	28.160	29.184	63.7 ± 12.3	-0.68 ± 0.35	-2.51 ± 0.32	66.47 ± 0.09	0.95
101014A	18	29.184	31.233	28.7 ± 10.6	-0.42 ± 1.37	-2.24 ± 0.20	67.41 ± 0.14	0.87
101014A	19	31.233	33.281	56.2 ± 9.6	-1.56 ± 0.17	-2.97 ± 0.00	68.98 ± 0.11	1.01
101014A	20	33.281	34.304	114.2 ± 21.8	-1.22 ± 0.12	-2.42 ± 0.26	70.95 ± 0.11	1.05
101014A	21	34.304	35.328	99.8 ± 9.2	-0.82 ± 0.11	-2.75 ± 0.25	73.44 ± 0.11	1.21
101014A	22	35.328	36.352	79.5 ± 6.2	-0.98 ± 0.11	-3.37 ± 0.69	75.28 ± 0.10	1.00
101014A	23	36.352	38.401	30.5 ± 8.4	-1.12 ± 0.90	-2.97 ± 0.00	75.64 ± 0.06	1.00
101023A	1	3.045	9.065	87.4 ± 25.5	-0.78 ± 0.37	-2.06 ± 0.14	2.80 ± 0.20	1.07
101023A	2	9.065	13.468	58.4 ± 14.8	-0.44 ± 0.55	-2.04 ± 0.10	5.37 ± 0.16	0.99
101023A	3	13.468	19.637	55.3 ± 14.2	-1.23 ± 0.39	-2.45 ± 0.33	7.06 ± 0.18	1.18
101023A	4	19.637	25.807	34.0 ± 9.8	-1.25 ± 0.92	-2.45 ± 0.00	7.95 ± 0.09	0.91
101023A	5	44.234	55.806	56.7 ± 9.2	-1.57 ± 0.19	-2.45 ± 0.00	13.74 ± 0.16	1.15
101023A	6	55.806	61.765	174.1 ± 48.0	-1.28 ± 0.11	-2.11 ± 0.18	18.50 ± 0.20	1.05
101023A	7	61.765	62.335	239.0 ± 34.2	-0.80 ± 0.10	-2.09 ± 0.10	21.58 ± 0.09	0.98
101023A	8	62.335	63.202	214.3 ± 25.3	-0.84 ± 0.09	-2.37 ± 0.20	24.79 ± 0.10	1.05
101023A	9	63.202	63.952	181.5 ± 26.0	-0.79 ± 0.11	-2.15 ± 0.12	27.66 ± 0.09	1.02
101023A	10	63.952	64.630	239.5 ± 28.0	-0.81 ± 0.08	-2.37 ± 0.19	30.74 ± 0.10	0.95
101023A	11	64.630	65.161	242.2 ± 35.5	-0.88 ± 0.09	-2.13 ± 0.12	33.66 ± 0.09	0.96
101023A	12	65.161	65.583	270.3 ± 27.6	-0.75 ± 0.08	-2.46 ± 0.21	36.68 ± 0.09	0.93
101023A	13	65.583	66.058	267.4 ± 34.8	-0.91 ± 0.08	-2.26 ± 0.16	39.64 ± 0.09	0.93
101023A	14	66.058	66.633	212.6 ± 44.3	-0.94 ± 0.11	-1.90 ± 0.07	42.61 ± 0.09	0.98
101023A	15	66.633	67.338	146.8 ± 26.9	-0.87 ± 0.14	-1.99 ± 0.07	45.37 ± 0.09	0.89
101023A	16	67.338	68.436	121.1 ± 20.3	-0.77 ± 0.16	-2.02 ± 0.08	48.29 ± 0.10	1.02
101023A	17	68.436	69.692	146.4 ± 24.7	-0.79 ± 0.14	-2.02 ± 0.08	51.45 ± 0.10	1.05
101023A	18	69.692	70.720	200.9 ± 34.7	-0.98 ± 0.10	-2.09 ± 0.11	54.72 ± 0.10	1.16
101023A	19	70.720	71.831	160.2 ± 26.9	-1.00 ± 0.11	-2.16 ± 0.13	57.68 ± 0.10	0.93

Table 1—Continued

GRB	Slice#	t_{start} (s)	t_{end} (s)	E_p (keV)	α	β	fluence ^a	χ_r^2
101023A	20	71.831	73.528	103.2 ± 16.7	-0.91 ± 0.16	-2.15 ± 0.10	60.58 ± 0.12	1.14
101023A	21	73.528	76.693	93.3 ± 20.3	-1.12 ± 0.18	-2.11 ± 0.11	63.84 ± 0.15	1.16
101023A	22	76.693	81.754	95.5 ± 24.1	-1.38 ± 0.15	-2.21 ± 0.17	67.30 ± 0.19	1.04
101023A	23	81.754	101.376	44.1 ± 11.9	-1.73 ± 0.23	-2.41 ± 0.39	71.05 ± 0.37	1.18
101123A	1	48.129	49.153	364.3 ± 43.9	-0.80 ± 0.06	-1.98 ± 0.08	5.54 ± 0.14	0.89
101123A	2	49.153	50.177	380.9 ± 29.9	-0.69 ± 0.05	-2.38 ± 0.16	12.36 ± 0.17	1.19
101123A	3	50.177	51.201	397.3 ± 33.3	-0.77 ± 0.04	-2.09 ± 0.07	20.67 ± 0.17	1.12
101123A	4	51.201	52.225	459.4 ± 29.8	-0.80 ± 0.03	-2.73 ± 0.29	29.73 ± 0.20	1.10
101123A	5	52.225	53.249	521.8 ± 32.9	-0.79 ± 0.03	-2.62 ± 0.20	40.22 ± 0.22	1.30
101123A	6	53.249	54.273	381.0 ± 34.1	-0.80 ± 0.05	-2.16 ± 0.10	47.29 ± 0.16	1.17
101123A	7	54.273	56.321	108.9 ± 45.4	-0.76 ± 0.32	-1.69 ± 0.06	50.86 ± 0.17	1.10
101208	1	-1.536	0.164	39.2 ± 15.8	-0.94 ± 0.64	-2.06 ± 0.12	0.95 ± 0.09	0.95
101208	2	0.164	0.282	137.6 ± 41.3	-0.85 ± 0.21	-1.95 ± 0.13	1.68 ± 0.04	0.86
101208	3	0.282	0.376	150.5 ± 37.5	-0.61 ± 0.21	-1.91 ± 0.11	2.49 ± 0.04	0.83
101208	4	0.376	0.479	172.3 ± 24.8	-0.83 ± 0.12	-3.03 ± 1.13	3.17 ± 0.05	1.00
101208	5	0.479	0.604	141.2 ± 20.5	-0.83 ± 0.14	-3.14 ± 1.34	3.75 ± 0.05	0.99
101208	6	0.604	0.786	81.7 ± 16.7	-0.77 ± 0.26	-2.29 ± 0.22	4.32 ± 0.05	0.87
101208	7	0.786	1.260	50.4 ± 25.7	-1.06 ± 0.51	-1.94 ± 0.10	5.09 ± 0.06	1.06
101208	8	1.260	2.560	35.8 ± 18.8	-1.35 ± 0.81	-2.34 ± 0.46	5.41 ± 0.07	0.94
110123A	1	-1.792	0.555	153.2 ± 53.3	-0.66 ± 0.00	-1.47 ± 0.07	1.21 ± 0.09	0.98
110123A	2	0.555	2.903	199.5 ± 53.4	-0.47 ± 0.23	-1.72 ± 0.08	3.69 ± 0.12	0.96
110123A	3	2.903	4.602	239.5 ± 49.2	-0.55 ± 0.15	-1.85 ± 0.10	6.29 ± 0.11	1.01
110123A	4	4.602	8.699	291.0 ± 28.6	-0.59 ± 0.07	-2.10 ± 0.12	13.84 ± 0.21	1.00
110123A	5	8.699	11.672	321.1 ± 41.9	-0.64 ± 0.08	-2.02 ± 0.12	19.15 ± 0.17	1.04
110123A	6	11.672	16.372	304.8 ± 40.3	-0.68 ± 0.08	-2.08 ± 0.15	25.21 ± 0.21	0.90
110123A	7	16.372	19.159	172.5 ± 53.4	-0.49 ± 0.28	-1.75 ± 0.10	27.29 ± 0.12	1.01
110123A	8	19.159	24.960	103.3 ± 46.7	-0.66 ± 0.00	-1.53 ± 0.10	28.59 ± 0.14	1.10
110213A	1	-1.792	0.555	153.2 ± 53.3	-0.66 ± 0.00	-1.47 ± 0.07	1.21 ± 0.09	0.98
110213A	2	0.555	2.903	199.5 ± 53.4	-0.47 ± 0.23	-1.72 ± 0.08	3.69 ± 0.12	0.96
110213A	3	2.903	4.602	239.5 ± 49.2	-0.55 ± 0.15	-1.85 ± 0.10	6.29 ± 0.11	1.01
110213A	4	4.602	8.699	291.0 ± 28.6	-0.59 ± 0.07	-2.10 ± 0.12	13.84 ± 0.21	1.00
110213A	5	8.699	11.672	321.1 ± 41.9	-0.64 ± 0.08	-2.02 ± 0.12	19.15 ± 0.17	1.04
110213A	6	11.672	16.372	304.8 ± 40.3	-0.68 ± 0.08	-2.08 ± 0.15	25.21 ± 0.21	0.90
110213A	7	16.372	19.159	172.5 ± 53.4	-0.49 ± 0.28	-1.75 ± 0.10	27.29 ± 0.12	1.01
110213A	8	19.159	24.960	103.3 ± 46.7	-0.66 ± 0.00	-1.53 ± 0.10	28.59 ± 0.14	1.10
110301A	1	-0.128	0.663	82.9 ± 13.9	-0.16 ± 0.26	-1.71 ± 0.04	4.24 ± 0.13	0.91
110301A	2	0.663	1.512	100.1 ± 7.1	-0.45 ± 0.10	-2.20 ± 0.07	9.76 ± 0.17	1.15
110301A	3	1.512	1.818	109.4 ± 9.7	-0.71 ± 0.10	-2.12 ± 0.05	12.39 ± 0.05	-27.42
110301A	4	1.818	2.057	110.0 ± 10.3	-0.71 ± 0.10	-2.08 ± 0.03	15.08 ± 0.05	-2.17
110301A	5	2.057	2.248	110.4 ± 9.6	-0.71 ± 0.10	-2.13 ± 0.03	17.72 ± 0.05	-9.06
110301A	6	2.248	2.432	95.4 ± 9.9	-0.61 ± 0.13	-1.93 ± 0.03	20.62 ± 0.05	0.68
110301A	7	2.432	2.615	98.1 ± 12.9	-0.64 ± 0.14	-1.89 ± 0.04	23.58 ± 0.07	1.03
110301A	8	2.615	2.863	84.5 ± 12.2	-0.59 ± 0.16	-1.85 ± 0.03	26.69 ± 0.08	1.06
110301A	9	2.863	3.110	78.5 ± 13.0	-0.68 ± 0.18	-1.87 ± 0.04	29.30 ± 0.07	0.93
110301A	10	3.110	3.520	59.9 ± 7.7	-0.44 ± 0.21	-1.91 ± 0.04	32.59 ± 0.10	1.11
110301A	11	3.456	3.738	48.1 ± 7.7	-0.11 ± 0.36	-1.81 ± 0.03	2.38 ± 0.07	1.28
110301A	12	3.738	3.882	61.8 ± 13.1	-0.46 ± 0.31	-1.77 ± 0.03	4.32 ± 0.06	1.00
110301A	13	3.882	4.027	81.7 ± 10.0	-0.32 ± 0.18	-1.86 ± 0.03	7.05 ± 0.07	1.25
110301A	14	4.169	4.339	55.7 ± 8.7	-0.51 ± 0.27	-1.88 ± 0.01	11.39 ± 0.04	-0.65
110301A	15	4.584	4.926	27.6 ± 7.2	-0.05 ± 0.94	-1.83 ± 0.03	15.47 ± 0.07	1.06
110301A	16	4.926	5.250	42.4 ± 11.0	-0.67 ± 0.41	-1.84 ± 0.04	17.55 ± 0.07	1.16
110301A	17	5.250	5.795	37.7 ± 8.3	-0.50 ± 0.47	-1.93 ± 0.05	19.56 ± 0.09	1.20
110301A	18	5.795	7.014	32.0 ± 10.5	-0.33 ± 0.88	-1.88 ± 0.06	22.07 ± 0.16	1.21
110301A	19	7.014	8.563	29.2 ± 6.3	-0.52 ± 0.00	-1.83 ± 0.07	24.07 ± 0.18	1.13
110301A	20	8.563	10.112	26.1 ± 22.5	-0.52 ± 0.00	-1.54 ± 0.06	25.80 ± 0.18	1.18
110529A	1	-0.064	0.000	507.1 ± 376.3	-0.48 ± 0.45	-1.91 ± 0.44	0.16 ± 0.03	0.89
110529A	2	0.000	0.064	1282.1 ± 320.7	-0.80 ± 0.07	-2.14 ± 0.21	1.26 ± 0.05	0.92
110529A	3	0.064	0.128	904.9 ± 224.1	-0.64 ± 0.11	-2.33 ± 0.33	2.03 ± 0.05	0.92
110529A	4	0.128	0.312	642.3 ± 356.7	-0.77 ± 0.18	-1.68 ± 0.14	2.62 ± 0.05	0.85
110529A	5	0.312	0.384	380.3 ± 263.2	-0.36 ± 0.48	-1.65 ± 0.18	2.83 ± 0.03	0.68
110705A	1	-0.064	-0.048	195.7 ± 134.8	-0.10 ± 1.21	-2.90 ± 0.00	0.02 ± 0.01	0.74
110705A	2	-0.048	-0.032	260.9 ± 249.7	-0.59 ± 0.87	-2.90 ± 0.00	0.05 ± 0.01	0.69
110705A	3	-0.032	-0.016	463.8 ± 209.3	-0.00 ± 0.60	-2.90 ± 0.00	0.14 ± 0.02	0.72
110705A	4	-0.016	0.032	1374.1 ± 207.9	-0.40 ± 0.09	-2.90 ± 0.00	1.23 ± 0.05	0.96
110705A	5	0.032	0.064	1189.7 ± 259.6	-0.40 ± 0.12	-2.60 ± 0.43	1.99 ± 0.04	0.80
110705A	6	0.064	0.096	1008.4 ± 296.2	-0.34 ± 0.17	-2.04 ± 0.21	2.57 ± 0.04	0.87
110705A	7	0.096	0.128	793.3 ± 202.6	-0.24 ± 0.21	-2.90 ± 0.00	2.98 ± 0.03	0.70

Table 1—Continued

GRB	Slice#	t_{start} (s)	t_{end} (s)	E_{p} (keV)	α	β	fluence ^a	χ_r^2
110705A	8	0.128	0.160	725.7 ± 115.1	-0.13 ± 0.16	-2.90 ± 0.00	3.68 ± 0.04	0.82
110705A	9	0.160	0.192	1374.1 ± 218.7	-0.22 ± 0.12	-2.90 ± 0.00	4.50 ± 0.05	0.87
110705A	10	0.192	0.208	848.8 ± 299.8	-0.50 ± 0.21	-2.90 ± 0.00	4.74 ± 0.02	0.74
110705A	11	0.208	0.224	260.9 ± 161.5	-0.99 ± 0.35	-2.90 ± 0.00	4.80 ± 0.01	0.85
110721A	1	0.020	0.616	5093.1 ± 640.7	-0.95 ± 0.02	-2.24 ± 0.19	5.59 ± 0.11	0.98
110721A	2	0.616	0.995	2449.3 ± 358.1	-0.92 ± 0.03	-2.21 ± 0.16	9.48 ± 0.10	1.05
110721A	3	0.995	1.426	1113.2 ± 177.3	-0.81 ± 0.05	-1.98 ± 0.09	13.24 ± 0.10	0.99
110721A	4	1.426	1.887	898.3 ± 125.7	-0.91 ± 0.04	-2.34 ± 0.19	16.85 ± 0.10	1.10
110721A	5	1.887	2.259	403.4 ± 50.4	-0.76 ± 0.06	-2.18 ± 0.14	19.59 ± 0.09	0.94
110721A	6	2.259	2.623	267.3 ± 41.2	-0.72 ± 0.09	-1.88 ± 0.06	22.15 ± 0.07	1.01
110721A	7	2.623	3.007	218.2 ± 40.4	-0.81 ± 0.10	-1.87 ± 0.07	24.36 ± 0.07	0.90
110721A	8	3.007	3.429	278.4 ± 58.8	-1.04 ± 0.08	-1.98 ± 0.11	26.32 ± 0.07	0.83
110721A	9	3.429	4.029	543.5 ± 132.5	-1.27 ± 0.05	-2.26 ± 0.31	28.59 ± 0.10	0.95
110721A	10	4.029	4.805	270.4 ± 119.8	-1.19 ± 0.11	-1.71 ± 0.06	30.84 ± 0.07	0.92
110721A	11	4.805	6.109	381.2 ± 138.7	-1.20 ± 0.08	-1.78 ± 0.08	33.60 ± 0.10	0.95
110721A	12	6.109	8.385	313.4 ± 109.8	-1.15 ± 0.09	-1.78 ± 0.08	36.76 ± 0.11	1.10
110721A	13	8.385	14.474	405.8 ± 124.6	-1.17 ± 0.08	-2.02 ± 0.23	40.99 ± 0.20	0.95
110721A	14	14.474	19.712	534.8 ± 354.7	-1.16 ± 0.15	-2.06 ± 0.60	42.78 ± 0.20	1.00
110731A	1	-0.512	-0.173	139.4 ± 84.3	-0.99 ± 0.58	-2.52 ± 0.00	0.16 ± 0.03	0.89
110731A	2	-0.173	0.393	178.1 ± 75.7	-1.19 ± 0.18	-1.97 ± 0.14	1.34 ± 0.06	0.98
110731A	3	0.393	0.643	229.5 ± 69.8	-1.06 ± 0.14	-2.01 ± 0.14	2.43 ± 0.05	0.90
110731A	4	0.643	1.017	133.6 ± 28.2	-0.56 ± 0.23	-2.05 ± 0.11	3.60 ± 0.05	0.86
110731A	5	1.017	1.427	133.6 ± 41.5	-0.78 ± 0.26	-1.93 ± 0.10	4.66 ± 0.05	0.98
110731A	6	1.427	1.844	178.1 ± 40.6	-0.57 ± 0.21	-1.98 ± 0.11	5.96 ± 0.06	0.89
110731A	7	1.844	2.385	217.7 ± 56.2	-0.76 ± 0.18	-1.97 ± 0.12	7.36 ± 0.06	1.04
110731A	8	2.385	3.445	282.0 ± 50.8	-0.80 ± 0.11	-1.98 ± 0.10	10.21 ± 0.09	1.04
110731A	9	3.445	3.961	386.3 ± 76.7	-0.65 ± 0.13	-2.03 ± 0.13	12.04 ± 0.08	0.98
110731A	10	3.961	4.421	398.3 ± 60.9	-0.55 ± 0.12	-2.35 ± 0.25	13.92 ± 0.08	0.96
110731A	11	4.421	4.868	371.7 ± 47.3	-0.17 ± 0.15	-2.13 ± 0.12	16.24 ± 0.08	0.87
110731A	12	4.868	5.311	246.9 ± 66.3	-0.64 ± 0.20	-1.94 ± 0.13	17.41 ± 0.06	0.84
110731A	13	5.311	5.755	380.8 ± 86.7	-0.90 ± 0.11	-1.96 ± 0.10	19.29 ± 0.07	1.00
110731A	14	5.755	6.217	348.2 ± 81.8	-0.78 ± 0.13	-1.96 ± 0.12	20.90 ± 0.07	0.92
110731A	15	6.217	6.679	320.4 ± 71.1	-0.71 ± 0.14	-1.98 ± 0.12	22.43 ± 0.07	1.06
110731A	16	6.679	7.442	388.2 ± 67.0	-0.69 ± 0.11	-2.10 ± 0.15	24.74 ± 0.09	0.99
110817	1	0.000	0.790	315.7 ± 52.8	-0.24 ± 0.17	-1.81 ± 0.08	2.70 ± 0.09	0.98
110817	2	0.790	1.080	277.8 ± 46.7	-0.40 ± 0.14	-1.88 ± 0.09	4.44 ± 0.06	1.02
110817	3	1.080	1.369	245.7 ± 34.5	-0.41 ± 0.13	-2.04 ± 0.12	6.16 ± 0.06	0.89
110817	4	1.369	1.681	142.6 ± 18.4	-0.07 ± 0.20	-2.00 ± 0.09	7.68 ± 0.06	0.89
110817	5	1.681	1.989	153.5 ± 20.9	-0.25 ± 0.19	-2.11 ± 0.13	8.98 ± 0.06	0.88
110817	6	1.989	2.398	117.5 ± 24.1	-0.28 ± 0.27	-1.80 ± 0.07	10.43 ± 0.06	0.97
110817	7	2.398	2.811	99.7 ± 18.0	-0.23 ± 0.27	-1.87 ± 0.07	11.90 ± 0.06	1.13
110817	8	2.811	3.462	48.0 ± 10.9	0.49 ± 0.76	-1.76 ± 0.05	13.35 ± 0.06	0.94
110817	9	3.462	4.407	45.9 ± 16.8	0.18 ± 0.99	-1.68 ± 0.05	14.88 ± 0.07	1.18
110817	10	4.407	7.184	38.7 ± 12.2	-0.73 ± 0.00	-1.76 ± 0.08	16.80 ± 0.15	1.09

^aIn units of 10^{-6} erg cm^{-2}